10-31-1993

Experimental investigation of submerged, turbulent, axisymmetric air jet impinging on a flat plate

Lan Xiao
New Jersey Institute of Technology

Copyright Warning & Restrictions

The copyright law of the United States (Title 17, United States Code) governs the making of photocopies or other reproductions of copyrighted material.

Under certain conditions specified in the law, libraries and archives are authorized to furnish a photocopy or other reproduction. One of these specified conditions is that the photocopy or reproduction is not to be "used for any purpose other than private study, scholarship, or research." If a, user makes a request for, or later uses, a photocopy or reproduction for purposes in excess of "fair use" that user may be liable for copyright infringement,

This institution reserves the right to refuse to accept a copying order if, in its judgment, fulfillment of the order would involve violation of copyright law.

Please Note: The author retains the copyright while the New Jersey Institute of Technology reserves the right to distribute this thesis or dissertation

Printing note: If you do not wish to print this page, then select "Pages from: first page # to: last page #" on the print dialog screen

ABSTRACT

Experimental Investigation of Submerged, Turbulent, Axisymmetric Air Jet Impinging on a Flat Plate

by
Lan Xiao

Experimental investigation was carried out on the flow characteristics of a circular, submerged, turbulent, axisymmetric air jet impinging normally on a smooth, flat, square, Lucite plate and a sand paper covered plate. Jet issuing from a circular nozzle of 0.5 inch diameter while the Reynolds Number varying from 10,000 to 85,000 was investigated. The flow can be considered incompressible since the pressure and the velocity of the jet were not too high, with Mach Number of the order of 0.3.

Various flow parameters were measured to obtain the velocity and pressure distributions at the surface of the flat Lucite plate, along the centerline and on the cross section of the normal impinging jet.

In particular, it is shown that the potential core length of free jet a weak function of the Reynolds Number. It has also been demonstrated that impinging jets have very similar characteristics as free jets, except at the vicinity of the target plate. The flow profile in the deflection zone and the wall jet zone were analyzed experimentally and most of the results found to conform with the works of previous investigators. Some of the results come opposite to the results obtained by the previous investigators.

Recommendations are made at the end of this thesis. They give other and future investigators some suggestions to further this experiment.

EXPERIMENTAL INVESTIGATION OF SUBMERGED, TURBULENT, AXISYMMETRIC AIR JET IMPINGING ON A FLAT PLATE

by
Lan Xiao

A Thesis
Submitted to the Faculty of
New Jersey Institute of Technology
in Partial Fulfillment of the Requirements for the Degree of
Master of Science in Mechanical Engineering

Department of Mechanical and Industrial Engineering

May 1993

APPROVAL PAGE

Experimental Investigation of
Submerged, Turbulent, Axisymmetric Air Jet
Impinging on a Flat Plate

Lan Xiao

5.17.1993

Dr. Peter Hrycak, P. E., Thesis Advisor (Date)
Professor of Mechanical Engineering
New Jersey Institute of Technology

May 17 93

Dr. Avraham Harnoy, Committee Member (Date)
Associate Professor of Mechanical Engineering
New Jersey Institute of Technology

05/17/93

Dr. Ernest S. Geskin, Committee Member (Date)
Professor of Mechanical Engineering
New Jersey Institute of Technology

BIOGRAPHICAL SKETCH

Author: Lan Xiao

Degree: Master of Science in Mechanical Engineering

Date: May 1993

Date of Birth:

Place of Birth:

Undergraduate and Graduate Education:

- Master of Science in Mechanical Engineering
  New Jersey Institute of Technology, Newark, New Jersey, 1993
- Bachelor of Science
  Department of Energy & Power Engineering
  Xi'an Jiaotong University
  Xi'an, Shaanxi, People's Republic of China, 1991

Major: Mechanical Engineering

This thesis is dedicated to
my parents

ACKNOWLEDGMENT

The author wishes to thank and express his sincere, utmost appreciation to his advisor, Dr. Peter Hrycak, P. E., for his instruction, inspiration, friendship, moral support, and professional attitude throughout this research.

Thanks are due to Dr. Avraham Harnoy and Dr. Ernest S. Geskin for reviewing this thesis and serving as members of the committee.

The author appreciates the timely help and suggestions from Mr. Dongyang Chen and Ph.D. candidate Ping Meng in the experimental work.

Acknowledgment is also due to the staff of the Mechanical Engineering Department of New Jersey Institute of Technology for their help rendered during the experimental stages.

The author is indebted to his brother, uncles and aunts for their strong support and guidance during his study in New Jersey Institute of Technology.

Special thanks to the author's grandfather for his encouragement and concern.

Finally, the author is grateful to his girl friend, Yuanyuan, for her patience, understanding and love.

TABLE OF CONTENTS

Chapter **Page**

LIST OF FIGURES

LIST OF SYMBOLS

a = Coefficient in Equation (13)

a^* = Defined in Equation (32)

A = Defined in Equation (36)

b = Width of jet

B = Defined in Equation (36)

C = Potential Core Length, defined in Figure 4-1 or in Equation (8)

D, d = Nozzle diameter

L = Lip of the nozzle defined in Figure 4-1

m = Defined in Equation (33)

m' = Defined in Equation (34)

n = Defined in Equation (35)

P,p = Pressure

P_∞ = Atmosphere pressure

P_c = Static Pressure

r = Radial distance

$r_{\frac{1}{2}}$ = r -location where $U = 1/2U_m$

Re_d = Reynolds Number based on nozzle diameter and air properties at exit of nozzle

u,U = Velocity in x direction

U_∞ = Velocity at center of nozzle exit

U_m = Maximum axial velocity of the jet

v,V = Velocity in r - direction

V_m = Maximum velocity along flat plate

w,W = Velocity in z - direction

x = Axial distance from the nozzle, Figure 1-1

y,Y = Defined in Figure 1-1

$Y_{\frac{1}{2}}$ = y - location where $U = 1/2U_m$

z,Z = Defined in Figure 1-1

$Z_{\frac{1}{2}}$ = z - location where $V = 1/2V_m$

Z_n = Normal distance between target plate and nozzle

δ = Boundary layer thickness in wall jet region

μ = Dyramic viscosity

τ = Shear stress

ξ = $(z - \delta) / b$

α = Power of r in Equation (28)

ρ = Density of air

CHAPTER 1
INTRODUCTION

1.1 Historical Background

Jets have been investigated intensively since Prandtl published his mixing length theory in 1925. Tollmien is one of the first persons to apply Prandtl's old theory of free turbulence when he applied Prandtl's mixing length hypothesis to solve the problem of axially symmetric jet issuing from a small opening theoretically [1]*. In 1932, another theory of free turbulence was developed by Taylor. Prandtl published his second theory based on viscous friction in 1942 [17]. With the help of this theory, Goertler solved governing equations for a free circular turbulent jet in closed form [1]. Later on, other investigators like Reichardt, Abramovich and Schlichting made important advances in this topic. Reichardt [17] substantiated the problem of the mixing zone at the boundary of parallel jets. Glauert [7] in 1956 investigated the flow spreading radially outward along the flat plate, called the "wall jet". Bakke [2] later on carried out interesting experiments with wall jets. Thereafter, Poreh and Cermak[16], Hrycak[10], Lee[14], Jachna[13], and T. Tanaka and E. Tanaka [22], also investigated experimentally and analytically various aspects of impinging jets and extended our practical knowledge of wall jets.

---

*Many original papers are not easily available today. Since they have been reviewed by Schlichting, his monograph is used in the direct citations.

1.2 Experimental Introduction

The impinging air jet is of increasing importance today because of the many practical engineering applications of jets. Particularly a vertical take-off or landing aircraft, rocket take-off, arc welding, paints spraying, blast drying where impinging jets occur naturally. Impinging jet can also be produced for surface cooling of vital machinery components such as gas turbine blades in high performance engines. Since conventional convective cooling methods and alternatives like uses of porous surfaces have inherent disadvantages, cooling by means of impinging jets seems to be very suitable. The glass industry has been using jets for cooling intricate molds for quite a long time. Impinging jets also find applications in cooling of strip steel and for various other cooling and heating purposes.

A jet is a quantity of fluid being discharged from a nozzle or orifice into a medium. Two main classes of jets are defined. A jet of fluid issuing from a slot, is called a two-dimensional plane jet. The jet issuing from a circular nozzle or orifice is classified as an axisymmetric radial jet.

The flow field for a circular jet has been divided into three main regions, namely, free jet zone, impinging jet zone and wall jet zone by previous investigators (Figure 1-1). The "free jet zone" is defined as the portion of the jet from the exit plane of the nozzle to approximately $4/5Z_n$ where Z_n is the perpendicular distance between the plane of the target plate and the plane of the nozzle exit. Brady and Ludwig [4] have found that if the normal distance between the flat plate and the nozzle exit is smaller than 1.5 D to 2.0 D, the flat plate will affect the readings at the nozzle exit. Therefore, whenever the measurements are taken in the region where $Z_n > 2.0$ D, the effect of the impinging plate is disregarded.

The second region is called the deflection zone since in this zone the flow changes its direction from vertical to radial.

After the "deflection zone" the flow spreads radially outward along the flat plate. This region is termed the "wall jet" zone, and the parameters in this region are the most complicated in the research.

The primary objective of this experimental investigation is to find the flow characteristics of axisymmetric, turbulent, submerged air jets impinging from circular nozzles onto a flat, smooth, Lucite plate, The flow can be considered incompressible because the velocity of the jet was not very high, with a maximum Mach Number of the order of 0.3 to 0.5.

Important phenomena relating to free jets have been studied by previous investigators. Impinging jets have also been studied recently, though not as much as free jets. This study will concentrate on nozzle Reynolds Number ranging from 10,000 to 85,000 and different normal distances between the exit plane of the nozzle and the target plate from four to twenty of nozzle diameter, to observe the effect of varying Reynolds Number and normal vertical distances on the flow characteristics.

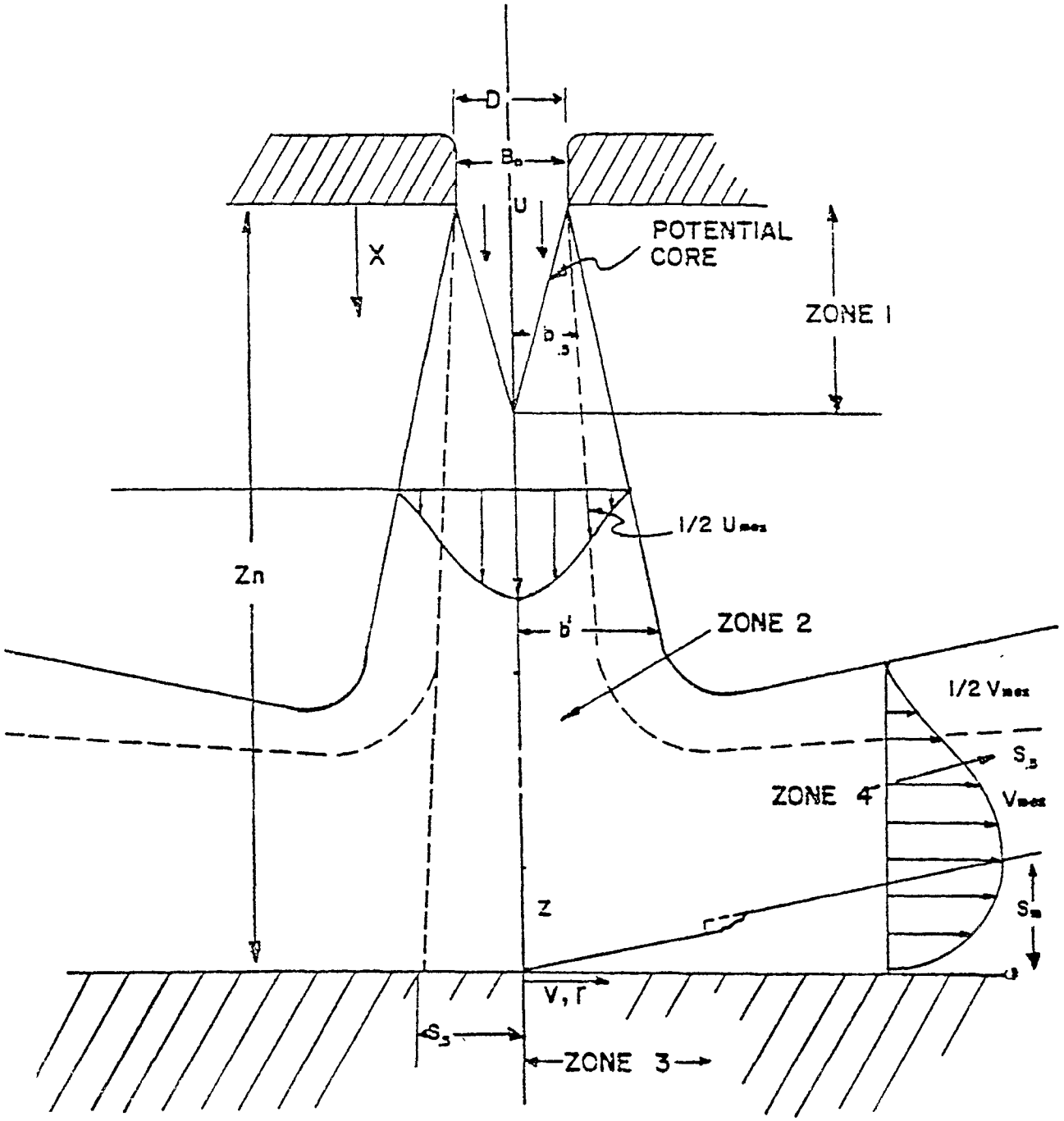

Figure 1-1 Flow pattern and coordinate system for
circular, submerged, turbulent, axisymmetric air jet impinging on a flat plate

CHAPTER 2

OBJECT OF INVESTIGATION

This investigation was carried out experimentally on a turbulent, axisymmetric, submerged, circular air jet issuing from a nozzle and impinging normally on a flat, smooth Lucite plate and a sand paper covered plate. The impinging jet consists of three main jet zones. This investigation can be divided into the following parts:

I. Velocity profile of free jets along the axis of flow of the jet.
II. Static pressure distribution of free jets both along and across the axis of flow of jet.
III. Velocity distribution in the Deflection Zone of the jet.
IV. Pressure distribution in the Deflection Zone of the jet.
V. Velocity profile in the wall jet region both along and across the axis of the jet.
VI. Measurement of full valued and half valued jet width in the free jet zone.
VII. Measurement of boundary layer thickness along the flat plate at the stagnation point and some distance away from it.

Reynolds number was varied from 10,000 to 85,000. On the basis of the finding of Hrycak [12], Reynolds number over 4,000 resulted in fully turbulent flow in the jet. The effects of compressibility were neglected since the pressure and velocity is not very high.

The technique adhered to during the course of the investigation was similar to that of Lee [14], Jachna[13], and Basu [3], the present equipment and the probes

are of the same kind as they used themselves, with some slight improvements in positioning of probes and in indication of stagnation point location.

CHAPTER 3

EXPERIMENTAL APPARATUS AND PROCEDURE

3.1 Experimental Apparatus

3.1.1 Piping System and Air Supply

Figure 3-1 shows a sketch of the piping system that was installed. Compressed air at over 35 psig was supplied by compressing the intake ambient air by means of a reciprocating air compressor. To ensure steady flow, the air is then stored in a large storage tank to maintain pressure and flow rate of air. The air mass flow rate is controlled by valves and measured by a pair of rotameters with a calibrated accuracy of better than 1% of full deflection. At the rotameter inlet, the pressure was measured by a Bourdon pressure gauge. The rotameter measures accurately the rate of flow of air to the nozzle. The flow goes though the controlled section and then enters a 1.5 inch pipe. An orifice flow meter is installed between two pressure tapes that might be used to calculate the flow rate. Three manometers (one with mercury, one with pure water and the other with 0.797 specific gravity colored fluid) were used to record the pressure. The air then enters a plenum chamber that is 2.5 inches in diameter and 3.5 inches in length. The plenum chamber is connected to 1.5 inches pipe by a 90 degree 1.5 to 2.5 inch's reducer. At the end of the plenum chamber an end plate is welded onto which one size nozzle (0.5 inch diameter) is to be screwed in. A rubber ring seal was placed at the threaded end of the nozzle to prevent air leakage. The plenum chamber is fixed vertically and its exact alignment can be adjusted by varying the length of the three supporting guide wires.

3.1.2 Manometer

Two large vertical column manometers, one with pure water and the other with mercury as the fluid were used. For measuring small pressures, such as the static pressure of the wall jet, a micro-manometer with 0.797 specific gravity blue fluid was used. Readings were obtained by turning the circular dial that is divided into 0.001 inch by bringing the meniscus level back to zero; this procedure indicated also the best possible accuracy in pressure measurements.

3.1.3 Transversing Carriage

Figure 3.2 shows by the pressure probes mounted on the transversing carriage by means of a slide. The three dimensional movements of the slide-carriage combined system helps to take pressure measurements at all points. In the Z-direction (vertically) the slide travels to a maximum of 2 ft., while in the x and y direction s (horizontal plane) it moves 6 inches. In addition, the probe can be rotated about the longitudinal axis of the tubing to enable it to follow the jet flow patterns.

3.1.4 Pressure Measuring Probes

Figure 3.3 shows the details of the probes. One static pressure probe and three total pressure probes are used. In addition, many micro-tubing pressure taps of 1/64 inch diameter were used. The measurements of each probe conform to the design recommended by NASA. to obtain very precise pressure measurements, the nozzles were equipped with a unique lip feature to produce a reasonably flat velocity profile and to generate the least interference in the flow field.

3.1.5 Impinging Plate

A smooth, flat Lucite plate 10 inches square and 1/4 inch thick was provided with 39 holes, 1/64 inch diameter for pressure taps to measure the pressure distribution

along the plate. The plate shown in Figure 3.4 is supported so that it can be freely rotated and raised or lowered. The two rows of 1/64 inch diameter holes are at right angles to each other.

3.2 Experimental Procedure

Using the experimental set-up and the instruments described in the last section (Figure 3-1 to 3-4) the total pressure and the static pressures were measured to study the velocity and pressure distribution. Nozzle of only one size is studied- 1/2 inch diameter. The turbulent, circular jets issuing from one nozzle were allowed to strike the smooth, flat Lucite plate. The Lucite plate was kept horizontal by means of a level gauge. The nozzle was set up in such a manner that it was exactly perpendicular to the impinging plate and parallel to the vertical direction of the traveling carriage. The motion of the probes should be along the centerline of the jet, i. e., along the line connecting the center of the nozzle with the stagnation point.

To obtain the stagnation point, the method recommended by Snedeker [20] was followed. A drop of colored grease was applied at the approximate stagnation point, the grease would spread out radially showing clearly the exact stagnation point, as well as the flow lines. As the Reynolds Number increases, the grease was found to spread more and more radially outward from the center. Close inspection of the grease on the transparency reveals a dot of grease just at the stagnation point with streak line radiating outward towards the circumference. Near the circumference, the grease accumulates in the form of waves, one on top of the other, in the form of a circle around the stagnation point.

The transversing carriage holding the probe was then so aligned so that when the probe was lowered down from the center of the nozzle it coincided exactly with the stagnation point. During this investigation, the Reynolds Number

based on nozzle diameter and air properties at nozzle exit were varied from 10,000 to 85,000 with Z_n / D (impingement distance to nozzle diameter ratio) varied at 4, 7, 10, and 20. The velocity and pressure distribution of the jet were measured with the total and static probes shown in Figure 3-3. For each particular measurement the probe was rotated so that it was tangential to the streamlines of the spreading jet and the measure value was taken. This technique ensures true measurement of velocity and pressure profiles and was employed by Lee [14] and Jachna [13] and was suggested by Hrycak.

To analyze the length of the potential core with varying Z_n / D, the velocity decay along the centerline and the velocity and pressure distribution was measured in the free jet zone. The velocity profile and the maximum velocity decay along the surface of the plate in the wall jet zone the pressure distribution was measured by a series of 1/64" tubes (Figure 3-4) which acted as pressure taps. For different locations and for Z_n / D values from the stagnation point, the velocity distribution was measured. The flow patterns and the system of coordinates used is shown in Figure 1-1. The growth of full valued jet width at 0.99 value of maximum velocity and half-valued jet width in the free jet zone was measured. The boundary layer thickness at and some distance away from the stagnation point was also observed.

In order to compare the difference of the boundary layer between a smooth Lucite plate and a rough surface, some kinds of sand papers were used to cover on the smooth plate to establish the rough surface.

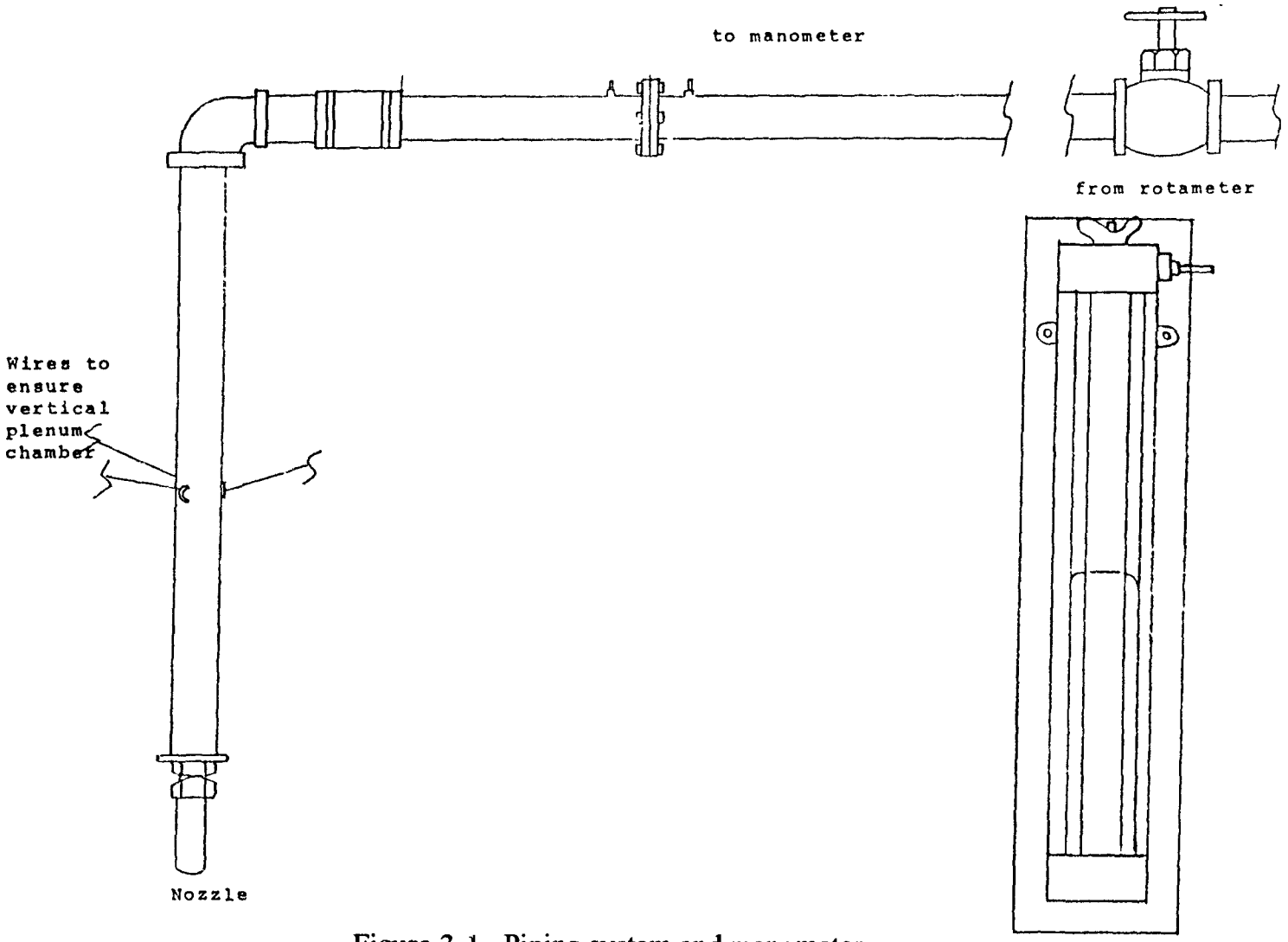

Figure 3-1 Piping system and manometer

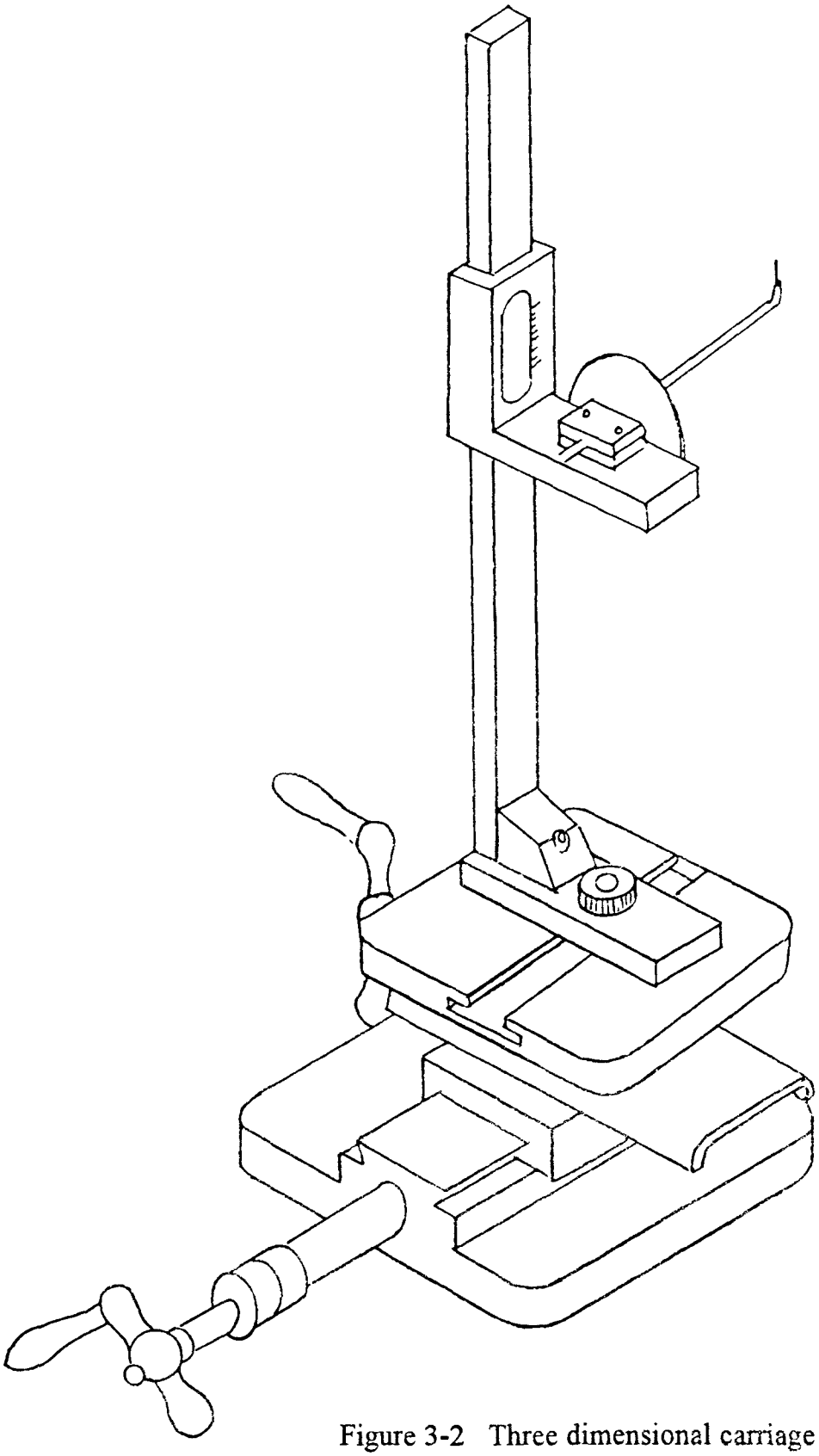

Figure 3-2 Three dimensional carriage

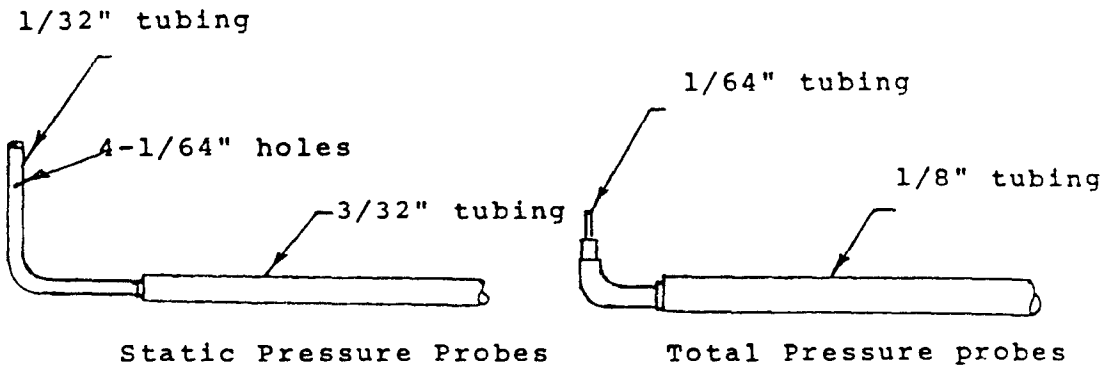

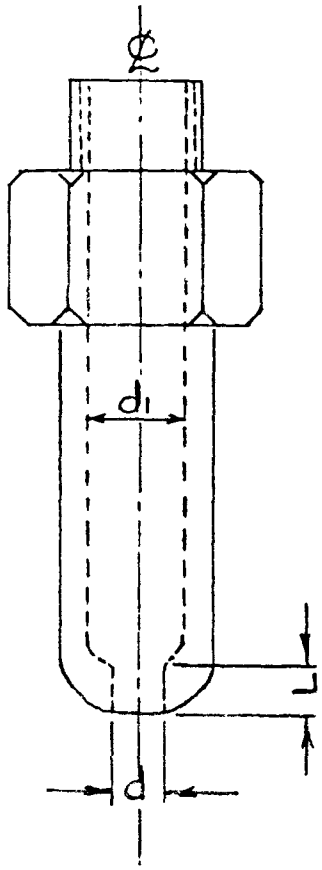

$d_1 > 2d$

$d = L$

Nozzle

Figure 3-3 Experimental instruments

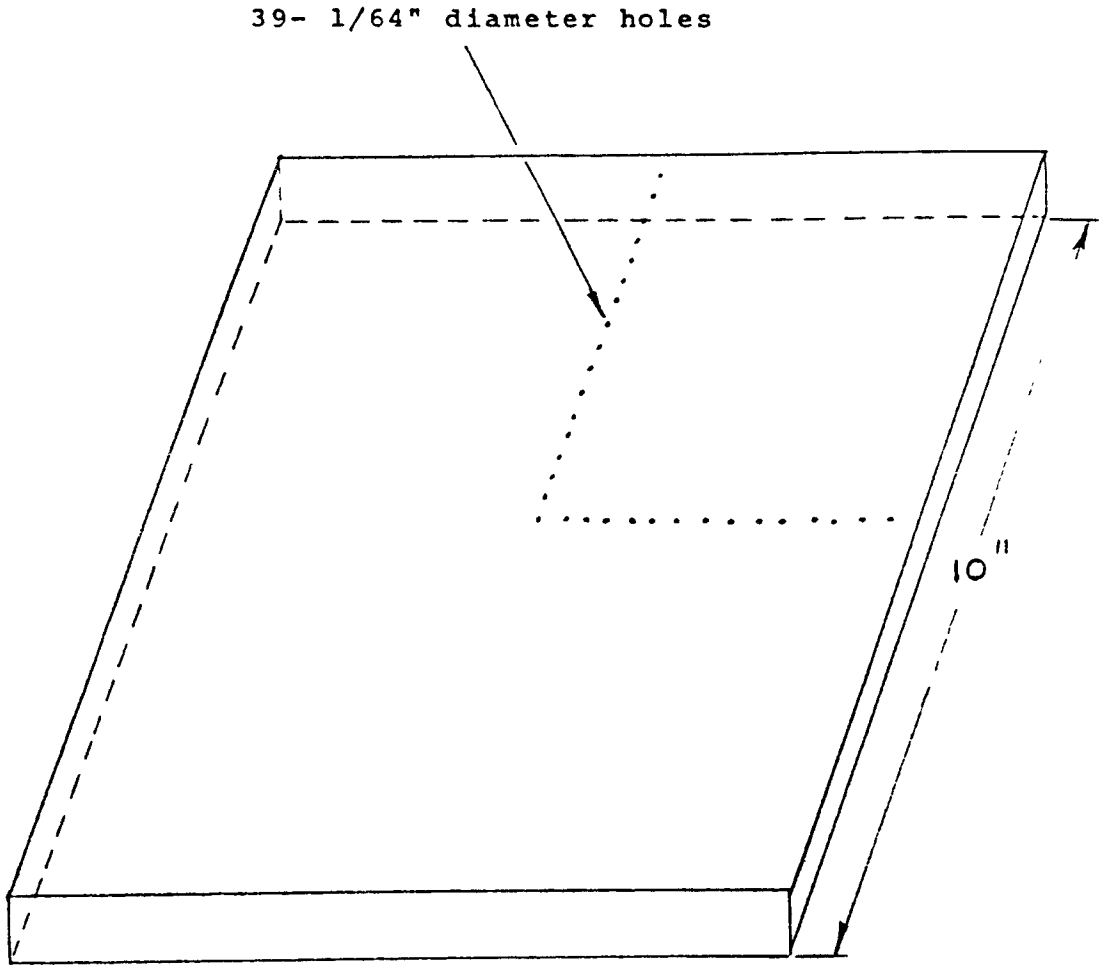

Figure 3-4 Impinging plate

CHAPTER 4

THEORETICAL BACKGROUND

4.1 Free Jet Zone

When a jet issuing from a nozzle strikes a target plate, the free jet zone has been defined as eight-tenths (8/10) of the perpendicular distance between the plane of the nozzle exit and the impinging plate. This has been determined by previous investigators such as Poreh, Cermak [16] and was verified by Tani, Komatsu [23], and by Lee [14], also by the present experiment, in which the flow properties remain the same as in a free jet. The free jet zone can be considered to consist of two regions. The first is called potential core region where the center line velocity still remains constant and the fully developed region where the flow velocity begins to decay according to a certain equation given later and develops a typical velocity profile. The theoretical analysis of a free jet is based on Prandtl's theory. The very famous Prandtl's mixing length theory is written as,

$$\tau = \rho \cdot l^2 \cdot \left|\frac{\partial v}{\partial z}\right| \cdot \frac{\partial v}{\partial z} \qquad (1)$$

Where, τ = shearing stress

z = radial distance

l = length of the fluid element

and,

$$\tau = \rho \cdot l^2 \cdot \frac{\partial v}{\partial z} \cdot \sqrt{\left(\frac{\partial v}{\partial z}\right)^2 + l_1^2 \cdot \left(\frac{\partial^2 v}{\partial z^2}\right)^2} \qquad (2)$$

Where 1 and l_1 are mixing lengths and are purely local functions. Thereafter, Prandtl presented a hypothesis that,

$$\tau = \varepsilon \cdot \rho \cdot \frac{\partial v}{\partial z} = \rho \cdot A \cdot b \cdot (U_{max} - U_{min}) \cdot \frac{\partial v}{\partial z} \quad (3)$$

Where, ε = virtual kinematics viscosity

b = width of mixing zone

A = empirical constant

From equation (3) we get,

$$\varepsilon = A \cdot b \cdot (U_{max} - U_{min}) \quad (4)$$

And, according to the theory given by Schlichting [19], the variation of the width of the jet with respect to the distance from jet source, x, is constant.

$$\frac{db}{dx} = \text{const.} \quad (5)$$

or

$$b = \text{const. } x \quad (5)$$

Where, b = Width of the jet

x = Distance from jet source

And the momentum of a circular jet can be obtained by conservation of momentum.

$$J = \rho \int u^2 \cdot dA = \text{const.} = \text{const.} \rho \cdot u^2 \cdot b^2 \quad (6)$$

Substituting Eq. (6) into Eq. (7), we have,

$$J = \text{const} \cdot \rho \cdot U_m^2 (B^2 \cdot x^2)$$

or, $$J = K \cdot \rho \cdot U_m^2 \cdot x^2$$

Where, $K = CB^2$ = Another constant

U_m = Maximum axial velocity

From the above expression,

$$U_m^2 = J/(K \cdot \rho \cdot x^2)$$

or $$U_m = \frac{J^{\frac{1}{2}}}{(K \cdot \rho)^{\frac{1}{2}} x}$$

By conservation of momentum, the momentum of an axisymmetric jet, J = constant.

Since the flow in this experiment is considered to be incompressible,

$$\rho = \text{constant}$$

Therefor, from the above equation, it gives,

$$U_m = \frac{K_1}{x}$$

Where, $$K_1 = \frac{J^{\frac{1}{2}}}{(K \cdot \rho)^{\frac{1}{2}}} \qquad (7)$$

$$\frac{U_m}{U_{oc}} = \frac{K}{x \cdot U_{oc}}$$

Where, U_{oc} = Velocity at the center of the nozzle during exit.

Now we have,

$$U_\infty = \frac{Re_d \cdot \mu}{d\rho}$$

So $$\frac{U_m}{U_\infty} = \frac{K}{Re_d \cdot \mu \cdot \left(\frac{x}{d}\right)}$$

For a particular measurement series, ρ, Re_d and μ are constant.

So we have, $$\frac{U_m}{U_\infty} = \frac{K}{constant \cdot \frac{x}{d}}$$ or

$$\frac{U_m}{U_\infty} = \frac{C}{\frac{x}{d}} \qquad (8)$$

Where $$C = \frac{K \cdot \rho}{Re_d \cdot \mu}$$

The above equation is only applicable in the fully developed region and gives the maximum centerline velocity decay of the jet. The coefficient "C" in the above equation has been found to be independent of the Reynolds Number for $20{,}000 < Re_d < 400{,}000$ according to Abramovich [1]. Lee [14] found the coefficient "C" to be a weak function of Reynolds Number for Reynolds Number less than 20,000. The definition of "C" is shown in Figure 4-1 that is detailed in Chapter 5.

The static pressure for a submerged, incompressible, low speed jet has been found to be a function of Reynolds Number By Lee [14] and Jachna [13]. For

high velocity jets, the static pressure distribution is dependent on the Mach Number according to Snedecker and Donaldson [20].

Schlichting [19] found that for a circular jet the kinematic momentum is,

$$K = 2\pi \int_0^\infty u^2 \cdot y \cdot dy = \frac{J}{\rho} \tag{9}$$

The velocity is given by,

$$U = \frac{3K}{8\pi \cdot \varepsilon_0 \cdot x \cdot (1 + 0.25\eta^2)^2} \tag{10}$$

$$V = \frac{1}{4} \cdot \sqrt{\frac{3}{\pi}} \cdot \sqrt{\frac{K}{x}} \frac{\eta - 0.25\eta^2}{(1 + 0.25\eta^2)^2} \tag{11}$$

and $$V = \frac{1}{4} \cdot \sqrt{\frac{3}{\pi}} \cdot \frac{\sqrt{K}}{\varepsilon_0} \cdot \frac{y}{x} \tag{12}$$

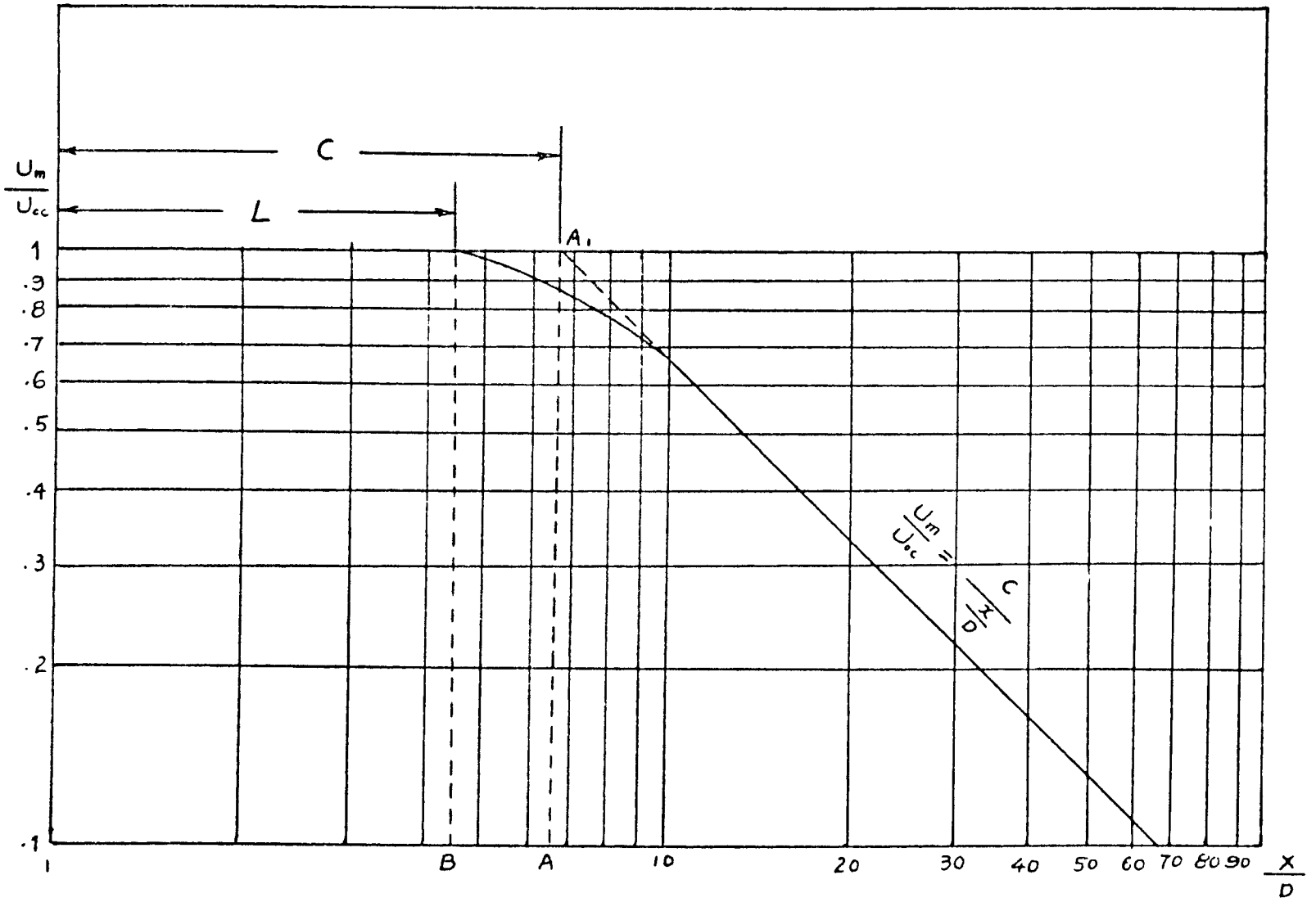

Figure 4-1 Definition of "C" and "L"

4.2 Deflection Zone

For a non- viscous fluid, the three dimensional flow equation in stagnant flow was investigated and reported by Homann [9] and by Schlichting [19], by considering a fluid stream impinging perpendicularly to a flat plate and blowing radially outwards.

According to the Navier- Stokes Equation in cylindrical coordinates for steady incompressible flow,

$$v\frac{\partial v}{\partial r}+w\frac{\partial v}{\partial z}=-\frac{1}{\rho}\frac{\partial p}{\partial r}+\nu\cdot\left(\frac{\partial^2 v}{\partial r^2}+\frac{1}{r}\frac{\partial v}{\partial r}-\frac{v}{r^2}+\frac{\partial^2 v}{\partial z^2}\right)$$

$$v\frac{\partial w}{\partial r}+w\frac{\partial w}{\partial z}=-\frac{1}{\rho}\frac{\partial p}{\partial r}+\nu\cdot\left(\frac{\partial^2 w}{\partial r^2}+\frac{1}{r}\frac{\partial w}{\partial r}+\frac{\partial^2 w}{\partial z^2}\right)$$

$$\frac{\partial v}{\partial r}+\frac{v}{r}+\frac{\partial w}{\partial z}=0$$

Where, v = Velocity in the r- direction

w = Velocity in the z- direction

Assuming the stagnation point is at the origin point, the flow is downward (in the direction of the negative z-axis), and at the wall (target plate), z=0, we then have, with "a" being a free constant,

$$v = ar \tag{13}$$

$$w = -2az \tag{14}$$

and $$p_0 - p = \frac{1}{2}\rho\cdot\left(v^2+w^2\right)=\frac{1}{2}\rho\cdot a^2\cdot\left(r^2+4z^2\right) \tag{15}$$

Where, r is the radial distance

These three equations describe the velocities in z and r directions and pressure distribution within the region near the stagnation point. Because the deflection zone in the present experiment is not large, and the plate is very smooth, the viscous effect is not important at the stagnation point. The Schlichting's equation (Equation 13) is quite satisfactory to describe the flow and is supported by the present experiment. By observation of Equation (13), the radial velocity increased linearly from zero at the stagnation point (where r = 0, z = 0). When the flow reaches some place farther from the stagnation point, the viscous dissipation is predominant, and the flow is no longer governed by Equation (13). The rate of velocity increase is reduced and finally reaches zero value. Then velocity starts to decrease. Equation (14) shows the axially velocity of flow is linearly decreased to zero at the stagnation point on the flat plate. The pressure varies parabolically along the flat plate and jet centerline as given by Equation (15).

If in the case of viscous flow, the equations for the velocities and pressure distribution are,

$$V = r\,f'(z) \tag{16}$$

$$W = -2\,f(z) \tag{17}$$

and

$$p_0 - p = \frac{1}{2}\rho \cdot a^2 \cdot \left[r^2 + F(z)\right] \tag{18}$$

Homann [9] solved these equations in the form of a power series. Later on, contributions have also been made by Schach [18], Strand [21], Tani and Komatsu [23], Lee [14], and Hrycak [11].

4.3 Wall Jet Zone

Farther out from the stagnation point, where the effect of viscous friction predominates, there begins the region of radial wall jet. Poreh and Cermak [16] assumed that the effect of the wall on the wall jet would be confined to the boundary layer near the wall and found it is useful to define in the wall jet region a reference boundary velocity, V_{RB}, which can be extrapolated from the velocity profile near the plate as

$$V_{RB} = 2\varepsilon_1 \cdot \frac{\alpha^2}{r} = \frac{\text{const.}}{r} \tag{19}$$

whereas the velocity distribution in dimensionless form is given by,

$$\frac{V}{V_{RB}} = 1 - \tanh^2 \alpha\eta$$

$$\eta = \frac{z}{r} \tag{20}$$

According to the result, the reference boundary velocity is expected to decay inversely proportionally to r, and the velocity distribution is expected to follow Equation (20), which was obtained from the integration of the momentum equation according to Prandtl's second hypotheses. This equation is similar to the valid for a plane free jet.

The velocity of a fan jet as developed by Abramovich [1] can be used to describe the velocity distribution of a wall jet. According to his theory,

$$\rho_0^2 \cdot v_0^2 \cdot b_0^2 \cdot r_0 \cdot \cos\phi \cdot d\phi = r \cdot \cos\phi \cdot d\phi \int_0^b v^2 \rho dz$$

Where, $d\phi$ is a sectoral element.

Since the velocity v at any radius r depends only on distance z,

$$\rho_0 \cdot v_0^2 \cdot b_0 \cdot r_0 = r \cdot \int_0^b \rho v^2 dz = \rho_0 \cdot r \cdot b \cdot V_m^2 \cdot \int_0^1 \left(\frac{v}{V_m}\right)^2 \frac{\rho}{\rho_0} d\xi$$

Where, $\xi = (z - \delta)/b$

For an isothermal jet,

$$\int_0^1 \frac{\rho}{\rho_0} \cdot \left(\frac{v}{V_m}\right)^2 \cdot d\xi = 0.316$$

Substituting the above equation into the previous one,

$$\left(\frac{v_0}{V_m}\right)^2 = \frac{0.316 r \cdot b}{r_0 \cdot b_0} \qquad (21)$$

According to the growth law of a submerged jet,

$$\frac{db}{dr} = K = 0.22$$

Let, $x = (r - r_0)$

So $b = K \cdot (r - r_0 - x_0) = K \cdot (x - x_0)$

Substituting the above equation into Equation (19), one gets,

$$\left(\frac{U_m}{U_0}\right)^2 = \frac{b_0 \cdot r_0}{0.316 \cdot K \cdot (x - x_0) \cdot (x + r_0)}$$

If the distance from the nozzle is very large, i. e., $x \geq r_0$ and $x_0 \approx 0$, since $x = (r - r_0)$,

$$\frac{U_m}{U} = \frac{1}{x}\cdot\sqrt{\frac{r_0 \cdot b_0}{0.316 \cdot K}}$$
$$\approx \frac{3.8 \cdot b_0}{x}\cdot\frac{r_0}{b_0}$$

For the special application of wall jets,

$$\frac{V_m}{U_\infty} = \frac{3.8 \cdot b_0}{S}\cdot\sqrt{\frac{S_0}{b_0}}$$

or, $$V_m = \frac{Constant}{S} \qquad (22)$$

Where, r has been replaced by S, the circumferential distance.

This equation is similar to Equation (19); the radial wall jet can be handled as half of the fan jet except for a thin layer near the wall.

A theory for the radial wall jet was developed by Poreh, Tsuei, and Cermak [16]. They used the conservation of mean momentum in the radial and vertical direction and the continuity equation to establish a relation between the skin friction T_w and the velocity field as,

$$\frac{T_w}{\rho} = \frac{1}{r}\cdot\frac{\partial}{\partial r}\cdot\left(r^2 \cdot \int_0^\infty v^2 dz\right)$$

and further assumed that except for a very thin layer near the wall, the velocity of the wall jet is similar and can be described as,

$$v = V_m \cdot f(\xi)$$

Where $\xi = z/z_{\frac{1}{2}}$, V_m are functions of r only.

Furthermore, an equation for the actual maximum velocity decay for the radial wall jet is derived herein. We proceed to analyze it in a way similar to that used for analysis of two dimensional wall jets by Abramovich [1]. In order to set up the momentum balance equation, a control volume with cross section ABCD in Figure 4-2 is established. Writing the equation of conservation of momentum for the control volume ABCD:

MOMENTUM IN - MOMENTUM OUT = MOMENTUM STORED

or,

$$E - F + G - H = I$$

Where, E = Momentum in through surface AB

F = Momentum out through surface AD

G = Momentum in through surface BC

H = Momentum out through surface DC

I = Momentum stored in control volume ABCD

This equation is true only if,

$$\tau \propto \frac{dv}{dz} = 0 \qquad \text{at} \qquad v = V_m$$

Assuming the fluid density, ρ, is constant, the fluid to be stationary and to be steady, the momentum balance equation becomes,

$$2\pi \cdot r_0 \cdot b_0 \cdot \rho \cdot V_0^2 - \int_{r_0}^{r} \rho \cdot V_m \cdot \frac{\partial}{\partial r}\left(\int_0^{\delta} v \cdot 2\pi r \cdot dz\right) dr = \int_{\delta}^{\delta+b} \rho \cdot v^2 \cdot 2\pi r \cdot dz$$

Since, $\rho = \text{constant}$, it becomes,

$$V_0^2 \cdot b_0 \cdot r_0 - \int_{r_0}^{r} V_m \cdot \frac{\partial}{\partial r}\left(\int_0^{\delta} v \cdot r dz\right) dr = \int_{\delta}^{\delta+b} r \cdot v^2 dz$$

To make parameters dimensionless, let us introduce the following notations:

$$\bar{v} = \frac{v}{V_0} \quad ; \quad \overline{V_m} = \frac{V_m}{V_0}$$

$$\bar{z} = \frac{z}{\delta} \quad ; \quad \xi = \frac{z-\delta}{b}$$

$$d\bar{z} = \frac{1 \cdot dz}{\delta} \quad ; \quad d\xi = \frac{dz}{b}$$

Near the wall, the normalized dimensionless velocity distribution for the turbulent boundary is given by the well known Prandtl's Power Law as,

$$\overline{V} = \overline{V_m} \cdot (\bar{z})^{\frac{1}{n}} \tag{23}$$

The above equation is valid for $0 \le z < \delta$, i. e. $0 \le z \le 1$. The index "n", a positive number, has been found to be a function of the Reynolds Number, may vary from 7 to 15 as determined by Hrycak and Lee [10]. For the dimensionless velocity distribution beyond the boundary layer one can use the relation,

$$\overline{V} = \overline{V_m} \cdot \left(1 - \xi^{\frac{3}{2}}\right)^2 \tag{24}$$

Originally proposed by Schlichting [19] and valid for the region where z varies from δ to $\delta + b$ or $\bar{z}$ from 0 to 1. The use of Equation of (24) is satisfactory by observation of Poreh and Cermak [16], Lee [14] and Jachna's [13] experiment results. The approximate relations for the thickness of radial wall jet and for the thickness of the boundary layer are taken as,

$$b = 0.22(r - r_0) \tag{25}$$

and $\delta = 0.1b$ (26)

we have,

$$\overline{V_m} = \frac{C_2}{r^{\alpha} \cdot \left(1 - \frac{r_0}{r}\right)^{\frac{\alpha}{2}}} \tag{27}$$

Where, C_2 = a constant

In equation (27), α varies with n, while n is a function of Reynolds Number as indicated above, and varies from 7 to 15. The table below based on Lee [14] shows the variation of α for corresponding values of n:

n	α
7	1.1217
9	1.1247
11	1.1268
13	1.1283
15	1.1294

Thus, α is shown to be a weak function of the Reynolds Number. Furthermore, far from the virtual source, where $r >> r_0$, Equation (27) reduces to a simple form,

$$V_m = \frac{C_2}{r^{\alpha}} \tag{28}$$

Which is very suited to an experiment verification. Here the above derivation shows that the maximum velocity decay in a radial wall jet is inversely proportional to r^{α}. An alternate analysis of the similar phenomena related to wall jets was given by Glauert [7], who obtained useful results likewise assuming $\tau = 0$ at $v = V_m$.

The present result gives a new relationship among several experimental facts. It shows how the local energy dissipation in the wall jet boundary layer formation and velocity profiles, (through the variation of "n") relates to the original nozzle Reynolds Number.

The boundary layer thickness near the stagnation point on the wall can be calculated for three-dimensional flow according to Schlichting's monograph [19] as follows,

$$\delta = \frac{1.98}{\sqrt{\frac{V_m \cdot r}{r^2 \cdot \nu}}} = \frac{1.98 \cdot r^{\frac{1}{2}}}{\sqrt{\frac{V_m}{\nu}}} \tag{29}$$

at the stagnation point, where $z = \delta$ at $\frac{v}{V_m} = 1$.

since $V_m = a \cdot r$, from equation (29), by substitution, we have,

$$\delta = \frac{1.98}{\sqrt{\frac{a}{\nu}}} \tag{30}$$

In the dimensionless form, V_m can be written as,

$$\frac{V_m}{U_\infty} = a^* \cdot \frac{r}{D}$$

Therefore

$$a = \frac{a^* \cdot U_\infty}{D}$$

Substituting the above equation in Equation (30) gives,

$$\delta = \frac{1.98}{\sqrt{\frac{a^* \cdot U_\infty}{D \cdot \nu}}} \tag{31}$$

or,

$$\frac{\delta}{D} = \frac{1.98}{\sqrt{a^* \cdot Re_d}} \tag{32}$$

at the stagnation point.

Since, however, a^* is a function of Z_n / D, δ is a function of Z_n / D and Re_d. For larger a^* or smaller Z_n / D and larger Re_d, the boundary layer will be thinner. In the present experiments, δ / D has been calculated and shown in Figure 5-56 to Figure 5-60.

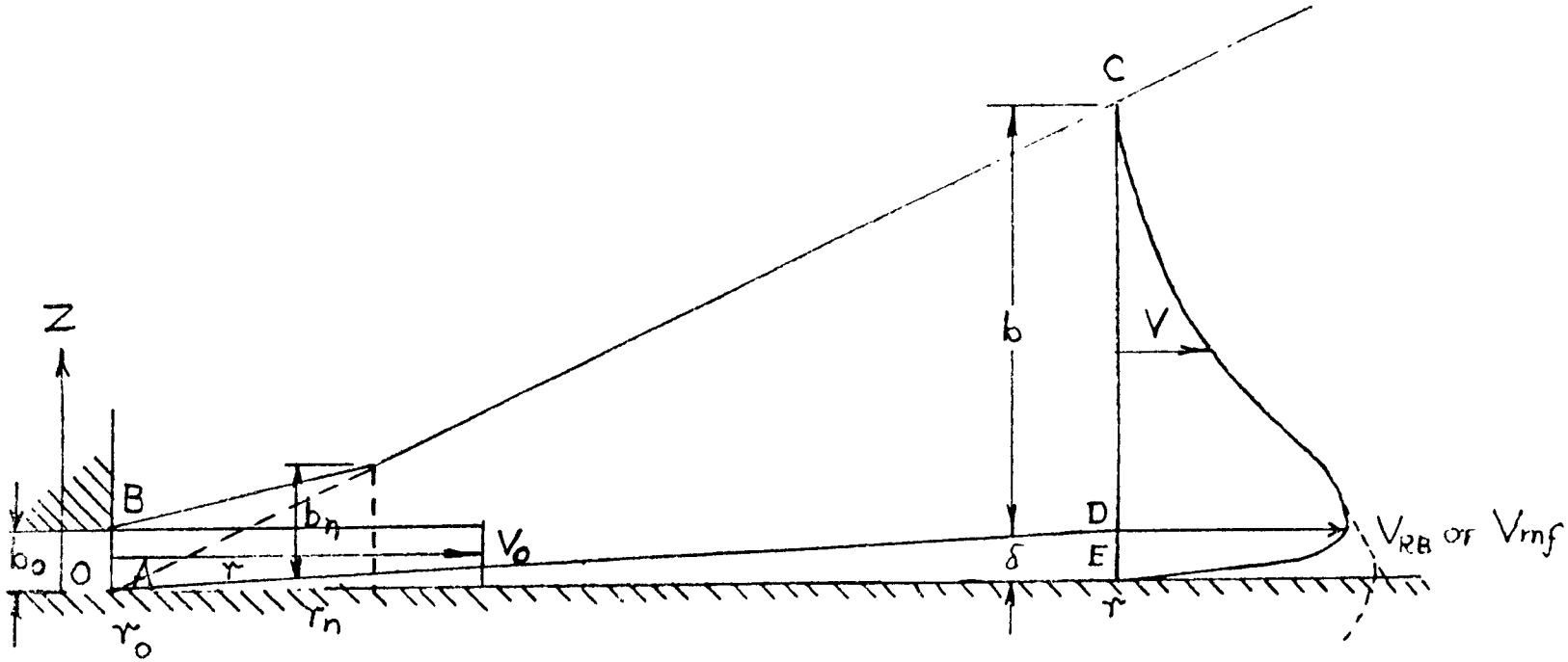

Figure 4-2 Coordinate system of a wall jet

CHAPTER 5

ANALYSIS OF THE EXPERIMENTAL RESULTS

5.1 Free Jet Zone

5.1.1 The Theoretical Dimensionless Length of the Potential Core in the Free Jet Zone

At first, a definition is given for the "theoretical dimensionless length of the potential core" which is labeled C. C is the dimensionless length x/D at point A as shown in the Figure 4-1. A_1 is the intersection of the tangent from the plot of the centerline velocity decay in the fully developed region, i. e.,

$$\frac{U_m}{U_\infty} = \frac{C}{\frac{x}{D}}$$

With the line $U_m / U_\infty = 1$ that describes the condition that the centerline velocity remains constant. That is to suppose that the Figure 4-1 shows that centerline velocity of the jet remains constant within $C \times D$ and then begins to decay. Actually, the centerline velocity begins to decrease at a distance somewhat closer to the nozzle exit than the location of the intercept, A_1.

To find the effect of Reynolds Number on C is one of the primary purposes of these experiments. The variation of C as a function of the Re_d is clearly shown in Figure 5-5. Generally, for only one nozzle investigated, C is smaller corresponding to larger Reynolds Number. The result is listed in the following table (next page).

Re_d	C
48,000	6.08
52,000	6.15
56,000	6.25
63,000	6.40

The results show, in general, C is a monotonic function of the Reynolds Number for the same diameter nozzle for a specific interval of Reynolds Number. Lee [14] reported in his thesis that C is not a monotonic function of Reynolds Number but is a function of the nozzle diameter. The recorded variation of C observed by previous investigators is from 5.2 (Tani and Komatsu [23]) to 7.7 (Poreh and Cermak [16]) and the mean value of C is taken as 7 by Trentacoste and Sforza. Lee [14] and Basu [3] got different values on C since they use different diameter nozzles to do the experiments. Lee's values are from 4.8 to 6.8 as well as Basu's.

5.1.2. Actual Dimensionless Length of Potential Core

It is defined that the actual dimensionless length, L, (Figure 4-1) is to extend over that axial dimensionless length where the centerline velocity of jet remains constant, i. e. $\frac{U_m}{U_\infty}$ near 1, (0.97-1.00), actually in the experiment $\frac{U_m}{U_\infty}$ can not always equal one since there exist errors, then we consider that $\frac{U_m}{U_\infty}$ >0.97 as 1 for the convenience of analysis. It is found that L is a very weak function of Reynolds Number in the turbulent flow. The value of L is around 3 when the Reynolds Number increases from 48,000 to 63,000. The difference between each L which

corresponding to different Reynolds Number is so small that can be surely neglected. Lee [14] found that L is also dependent on the Reynolds Number since he did the experiment in the laminar flow condition (Reynolds Number is less than 4,000). And he also found that when the flow becomes a turbulent flow, the value of L remains constant for a certain distance: L equals 4. In other words, at the center of the free jet, the velocity keeps constant in the distance of 3 (present experiment) or 4 (Lee) times the diameter of the nozzle, D, and then decays according to the curve shown in Figure 5-1 to Figure 5-4.

5.1.3 Pressure Variation along Jet Centerline

The static pressure according to the simplified Boundary Layer Theory should be identical with the ambient pressure. It is found, however, to be actually lower than the surrounding atmospheric pressure and varies with the axial distance from the nozzle, verifying the well-known Navier-Stokes Equation. Figure 5-6 gives a plot of the variation of static gauge pressure, p_c , along the centerline of the jet. "p_c" is a function of x / D for a specific nozzle size. The static pressure reaches a minimum at about x / D = 6 and then increases to the ambient pressure at the farther position along the jet centerline.

Different from the previous investigators Lee [14] and Basu [3], the author finds that when x / D < 2, the dimensionless static pressure does not go up monotonically, on the contrary it drops off sharply to the point near the minimum point. So according to the fact appeared in the experiment, it is not true to expect the dimensionless static pressure, $\frac{p_c - p_\infty}{\rho U_\infty^2}$, going to zero when x / D decreases. This may be caused by the sudden expansion of pressurized air at the exit of the

nozzle. The author repeated this experiment several times, and got the same results.

5.1.4 Static Pressure Variation on the Cross Section of Free Jet

The pressure variation on the different cross section of free jet for x / D = 4 to x / D = 16 is shown in Figure 5-7 through 5-11. It is found also that the minimum pressure is in the center of the jet that approaches the ambient pressure at the outer portion of the jet. This type of pressure variation was also investigated by Lee [14], Basu [3], and Snedeker [20]. Their results were quite similar to the results obtained here. Snedeker found the static pressure distribution also to be a function of the Mach Number. Lee's results have been plotted for comparison in Figure 5-12 for x / D = 4 through x / D = 16. It is found that the minimum pressure at the center of the jet increases with increasing x / D. There is no big difference between the present experiment and Lee's result.

5.1.5 Spread of Jet in the Free Jet Zone

Previous investigators have found that the jet width is proportional to the axial distance. Hence, the jet spreads linearly in the main region. Figures 5-13 through 5-15 show the variation of the free jet width, and the variation of the half-valued jet width is shown in Figures 5-16 to 5-18. The value of x / D is varied from 0 to 14. It is found that the variation of jet width is governed by the equation,

$$y / D = m \cdot x / D \qquad (33)$$

The m values are listed in the following table for different values of the Reynolds Number. The Reynolds Number was varied between 66,000 and 74,000 for three curves drawn.

Re_d	m
66,000	0.261
70,000	0.265
74,000	0.269

The variation of the half-valued width was also observed. The half-valued jet width was found to follow the equation, similar to Equation (33),

$$y_{\frac{1}{2}}/D = m' \cdot x/D \tag{34}$$

Where m' is between 0.098 and 0.103 for Reynolds Number between 66,000 and 74,000 for three curves drawn.

Re_d	m'
66,000	0.098
70,000	0.101
74,000	0.103

The above two equations are valid only in the main region of the free jet zone where unmodified flow characteristics of the jet are presented. It should be mentioned that as the Reynolds Number was increased, m and m' was also to increase. This increase was however very small. Abramovich [1] obtained a value of 0.097 for m'. Lee [14] reported a value for m' to be 0.0926. The value of m as found by Lee [14] was 0.271.

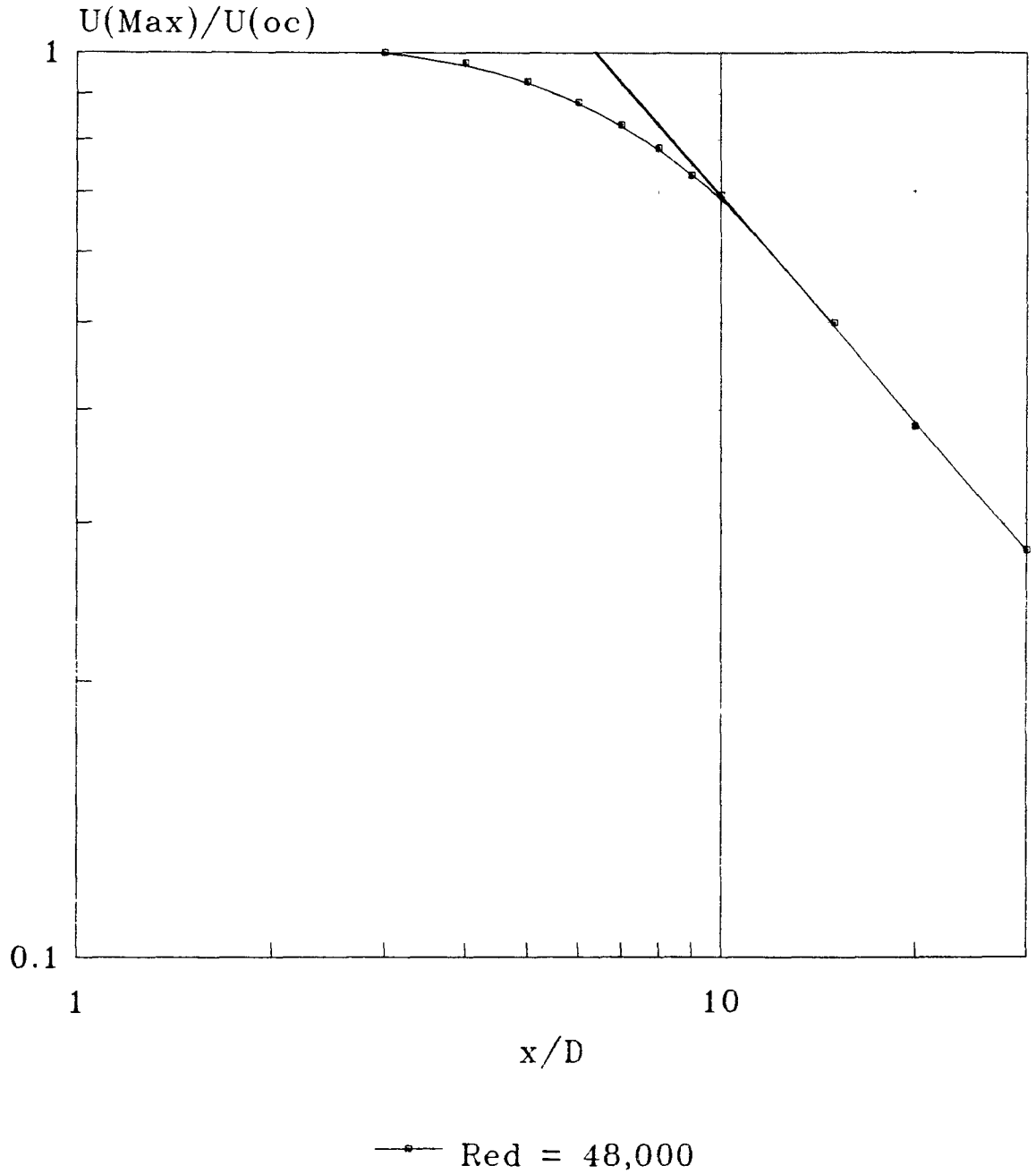

Figure 5-1 Centerline velocity decay of free jet
Re_d = 48,000, D = 0.5 in.

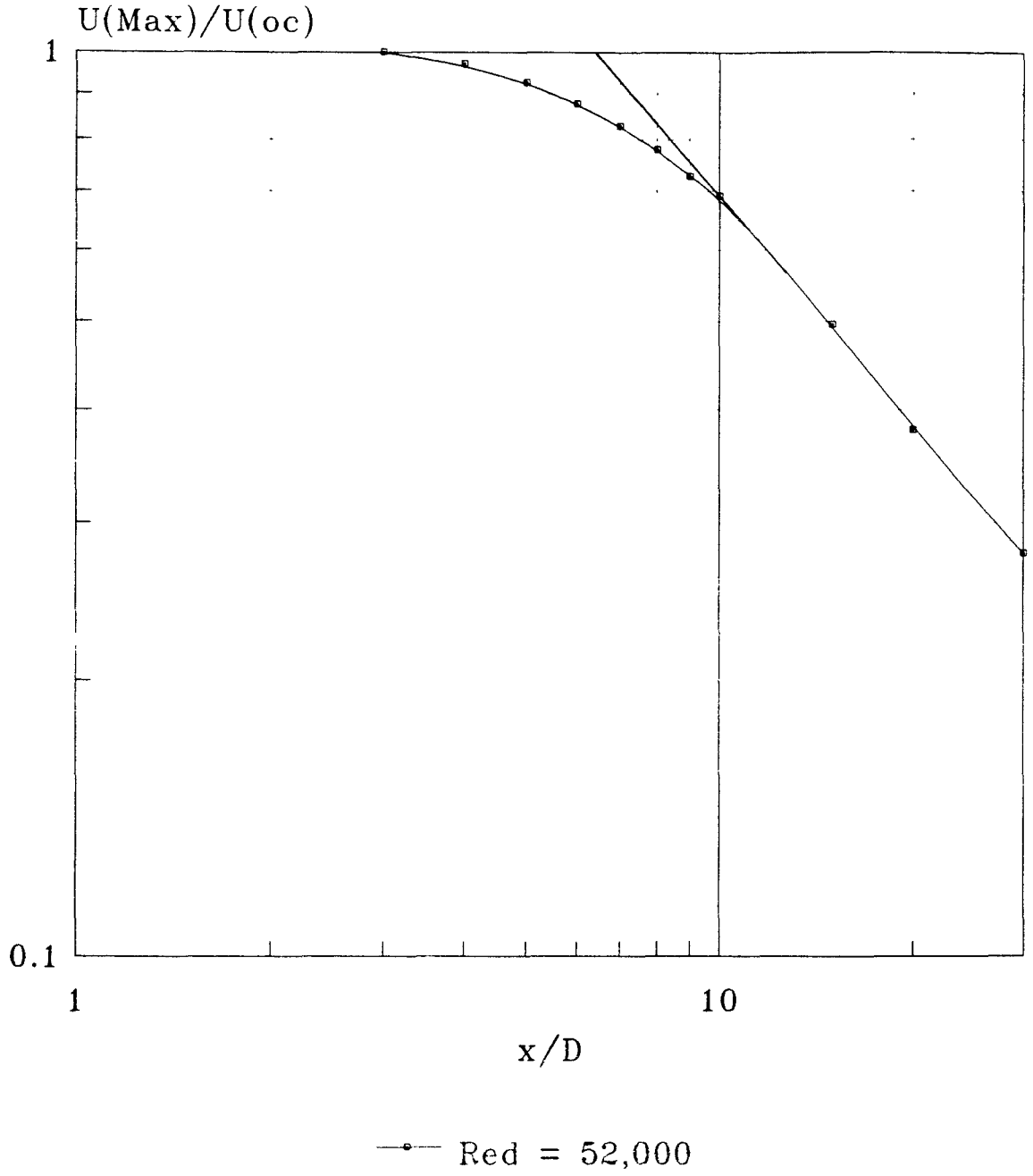

Figure 5-2 Centerline velocity decay of free jet
Re_d = 52,000, D = 0.5 in.

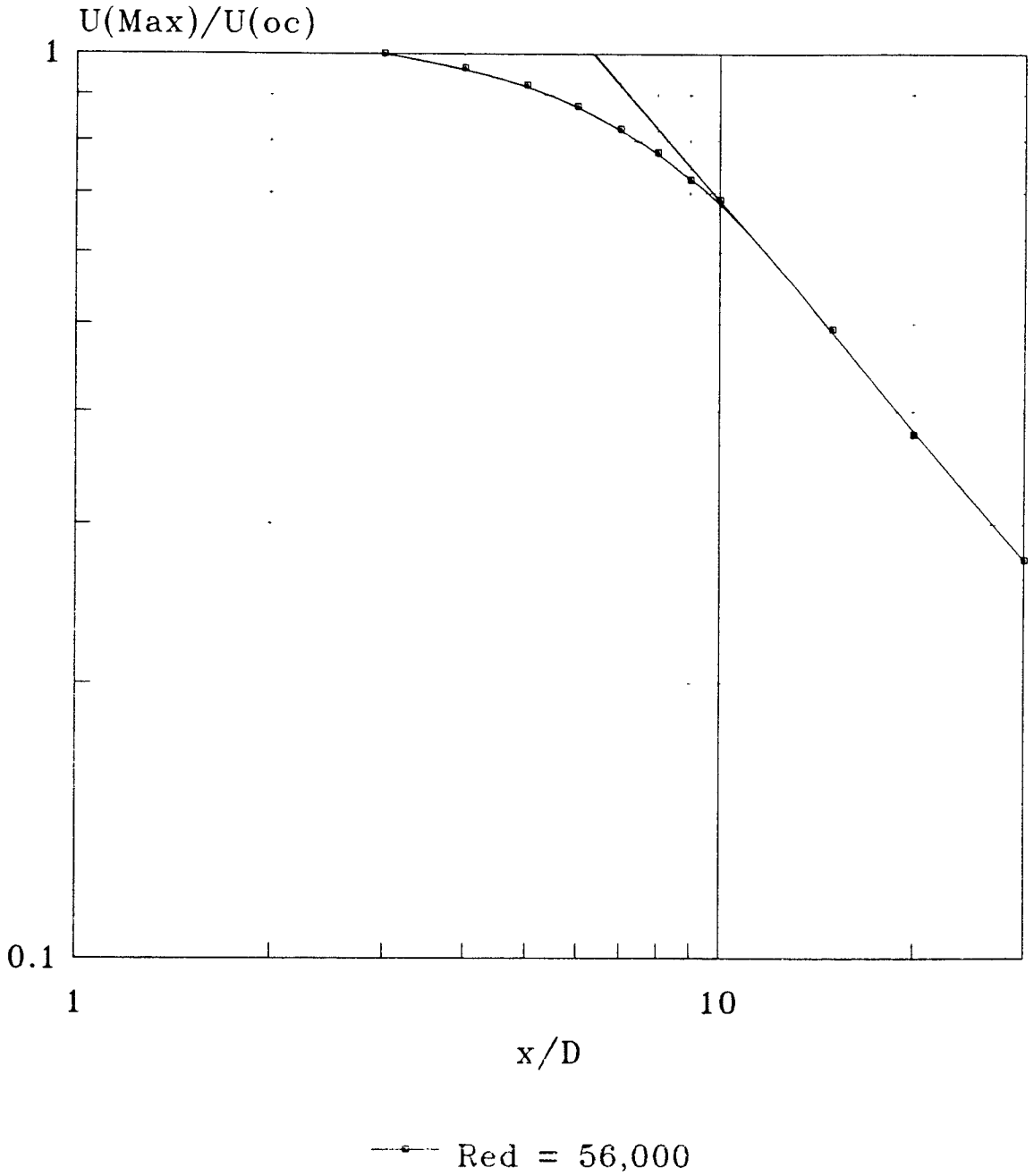

Figure 5-3 Centerline velocity decay of free jet
Re_d = 56,000, D = 0.5 in.

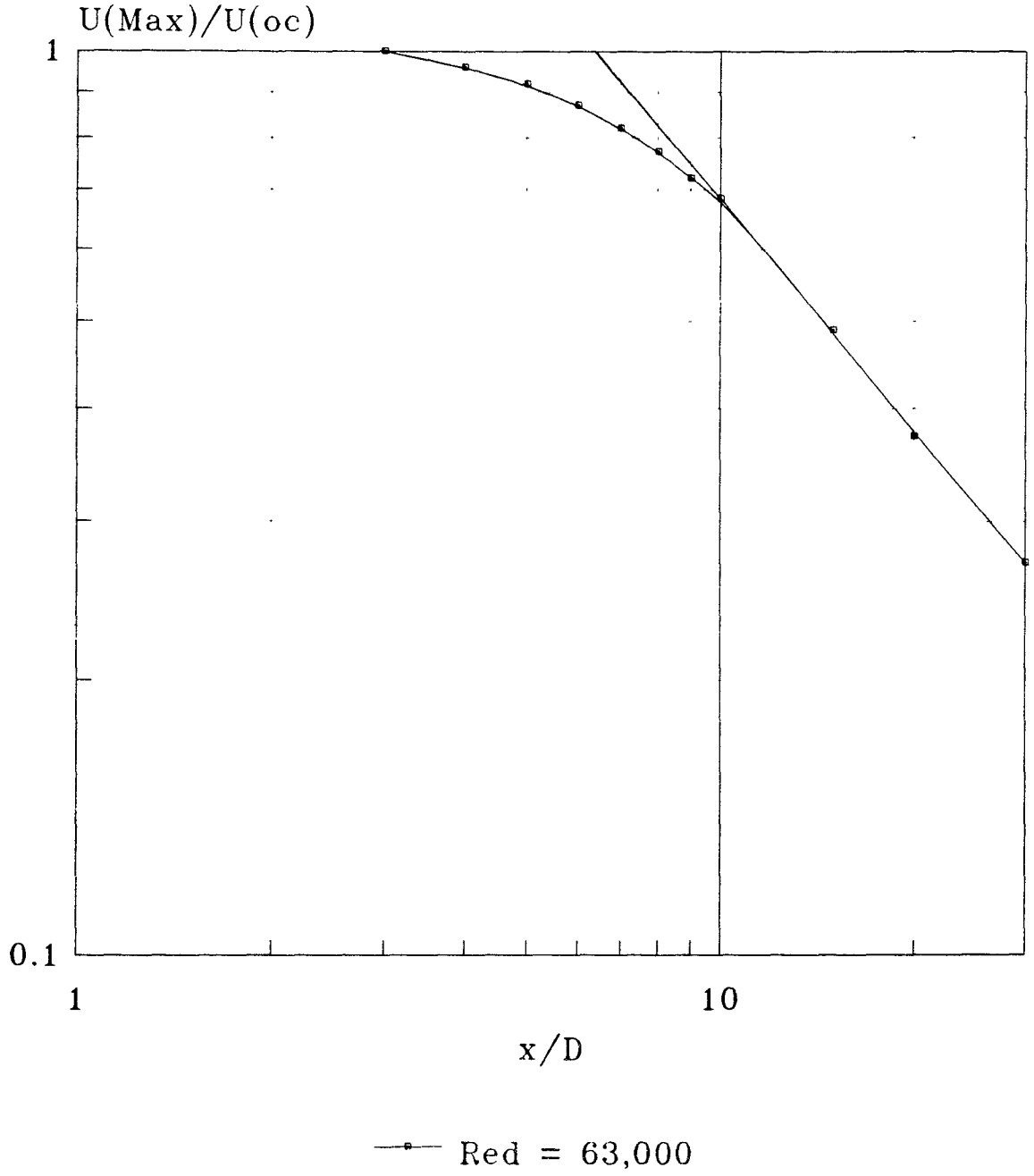

Figure 5-4 Centerline velocity decay of free jet
Re_d = 63,000, D = 0.5 in.

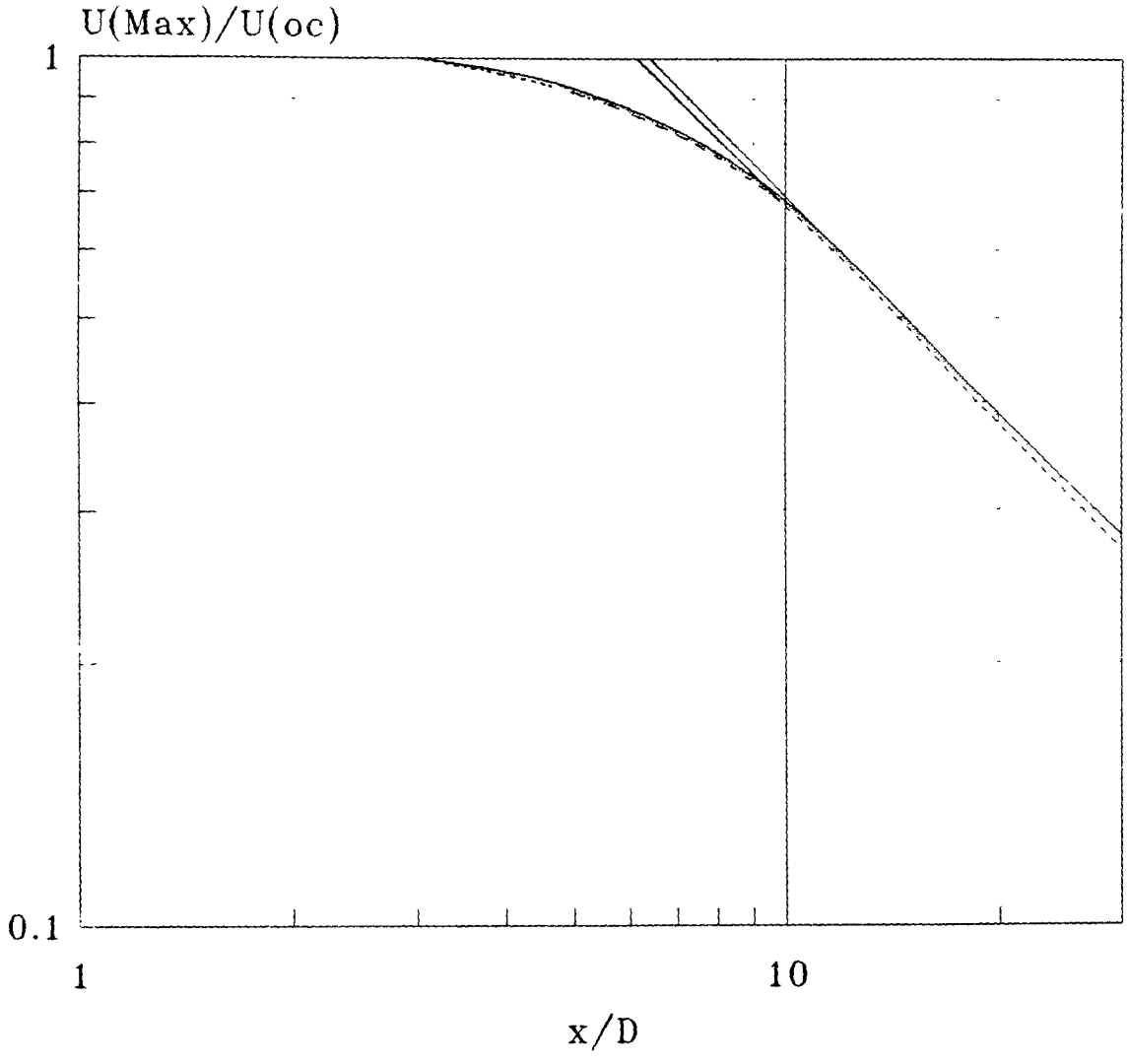

Figure 5-5 Centerline velocity decay of free jet
for varied Reynolds Number, D = 0.5 in.

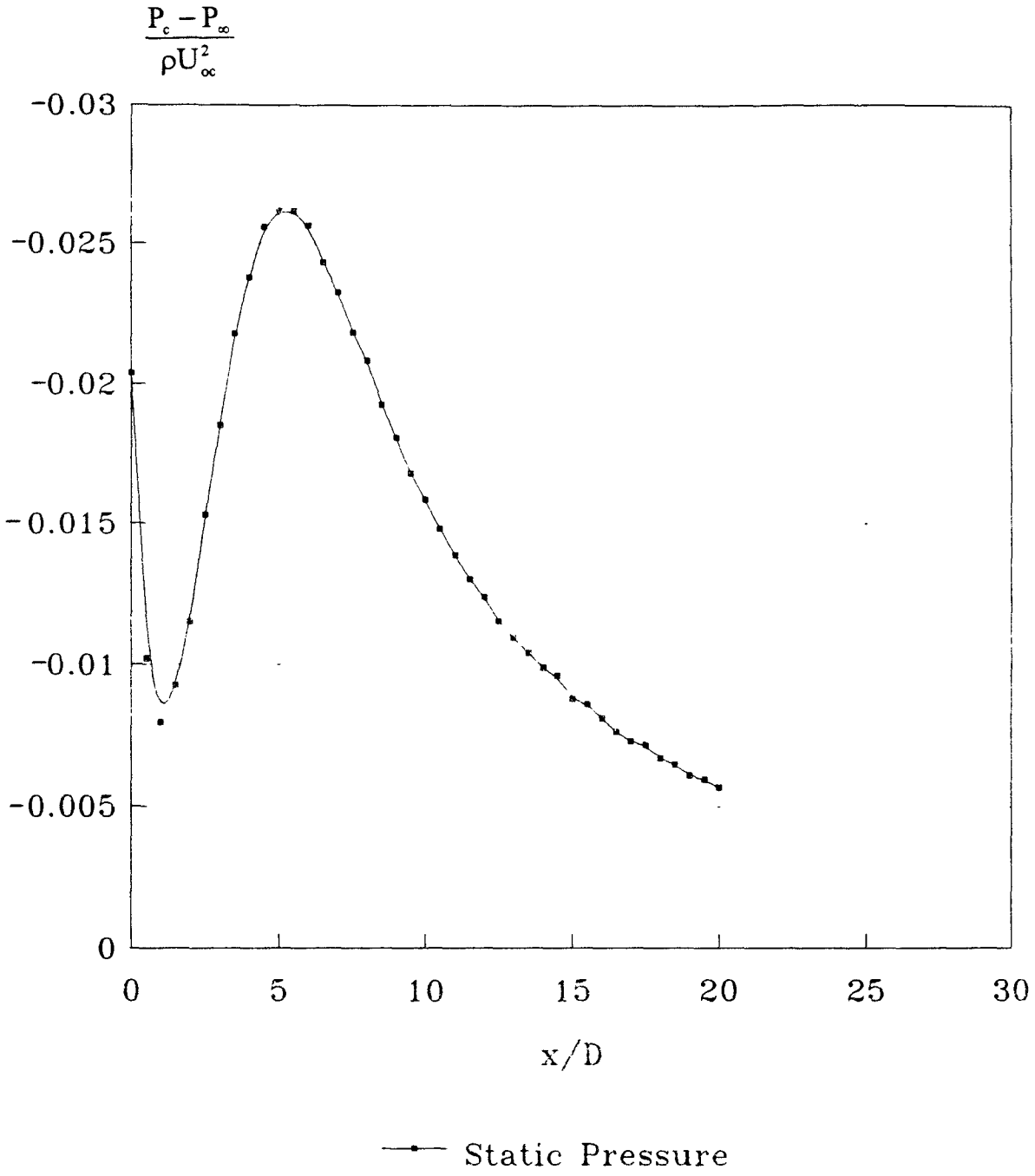

Figure 5-6 Static pressure distribution along centerline of free jet
Re_d = 64,000, D = 0.5 in.

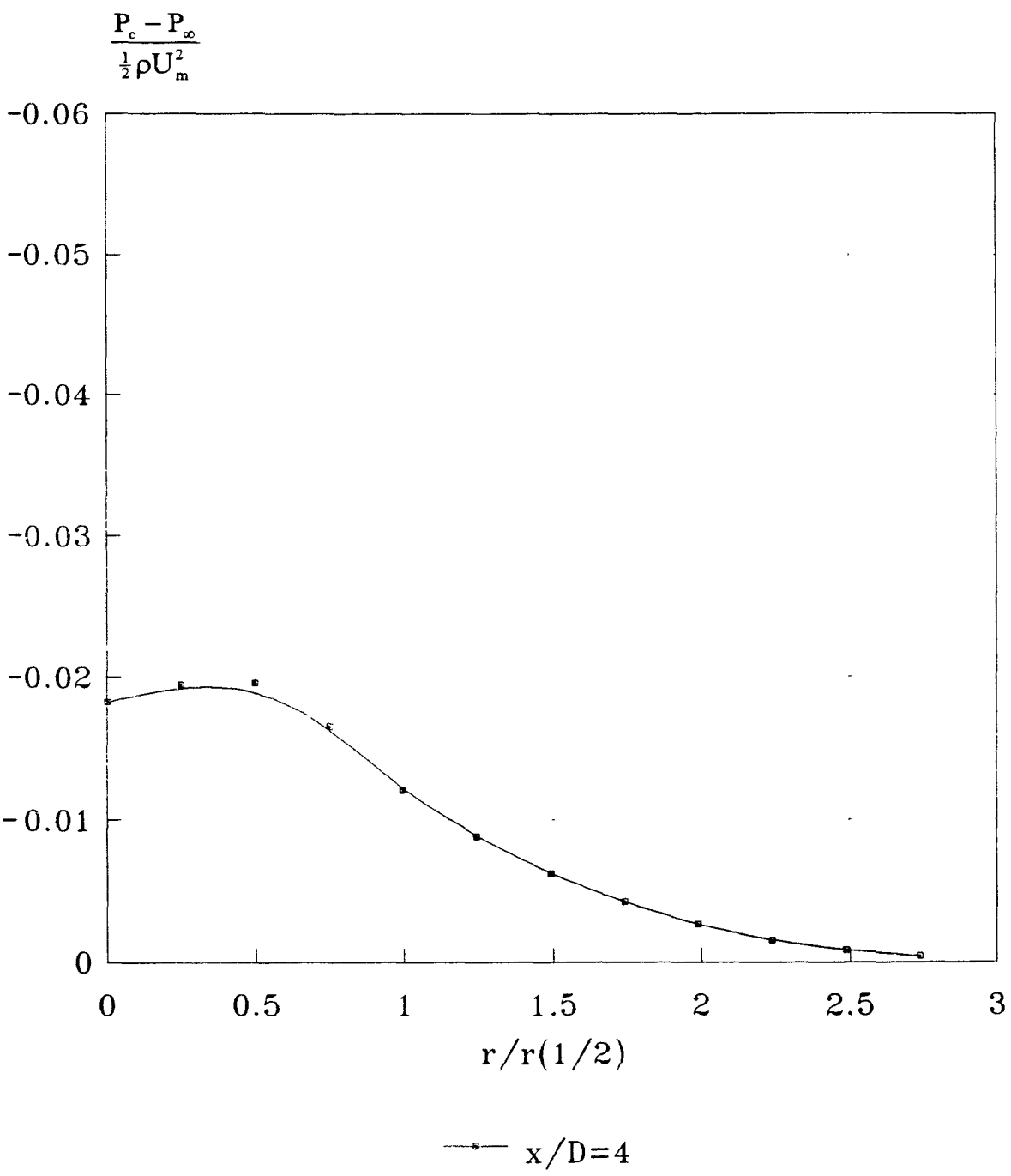

Figure 5-7 Static pressure distribution on the cross section of free jet
Re_d = 66,000, x/D = 4, D = 0.5 in.

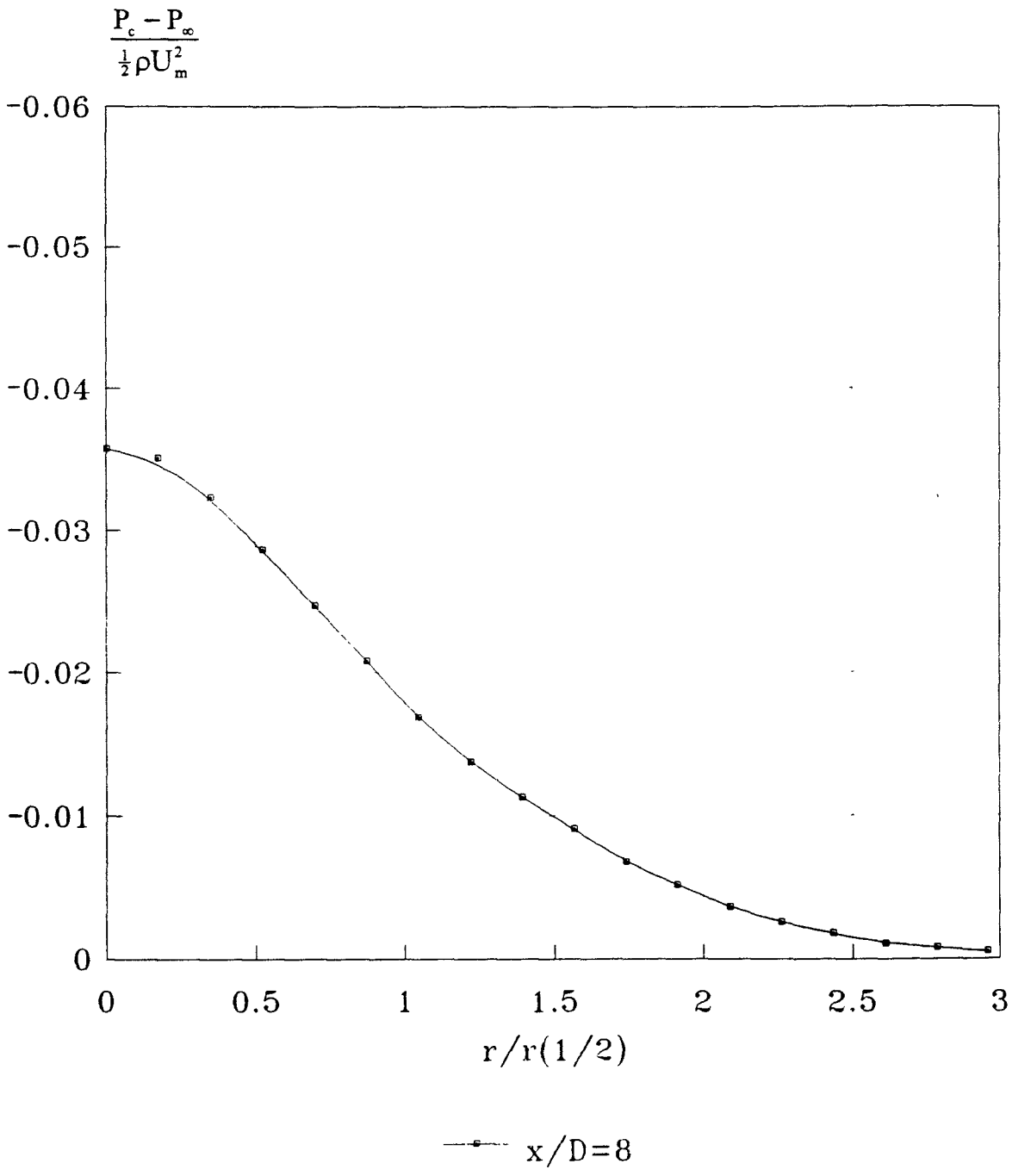

Figure 5-8 Static pressure distribution on the cross section of free jet
Re_d = 66,000, x/D = 8, D = 0.5 in.

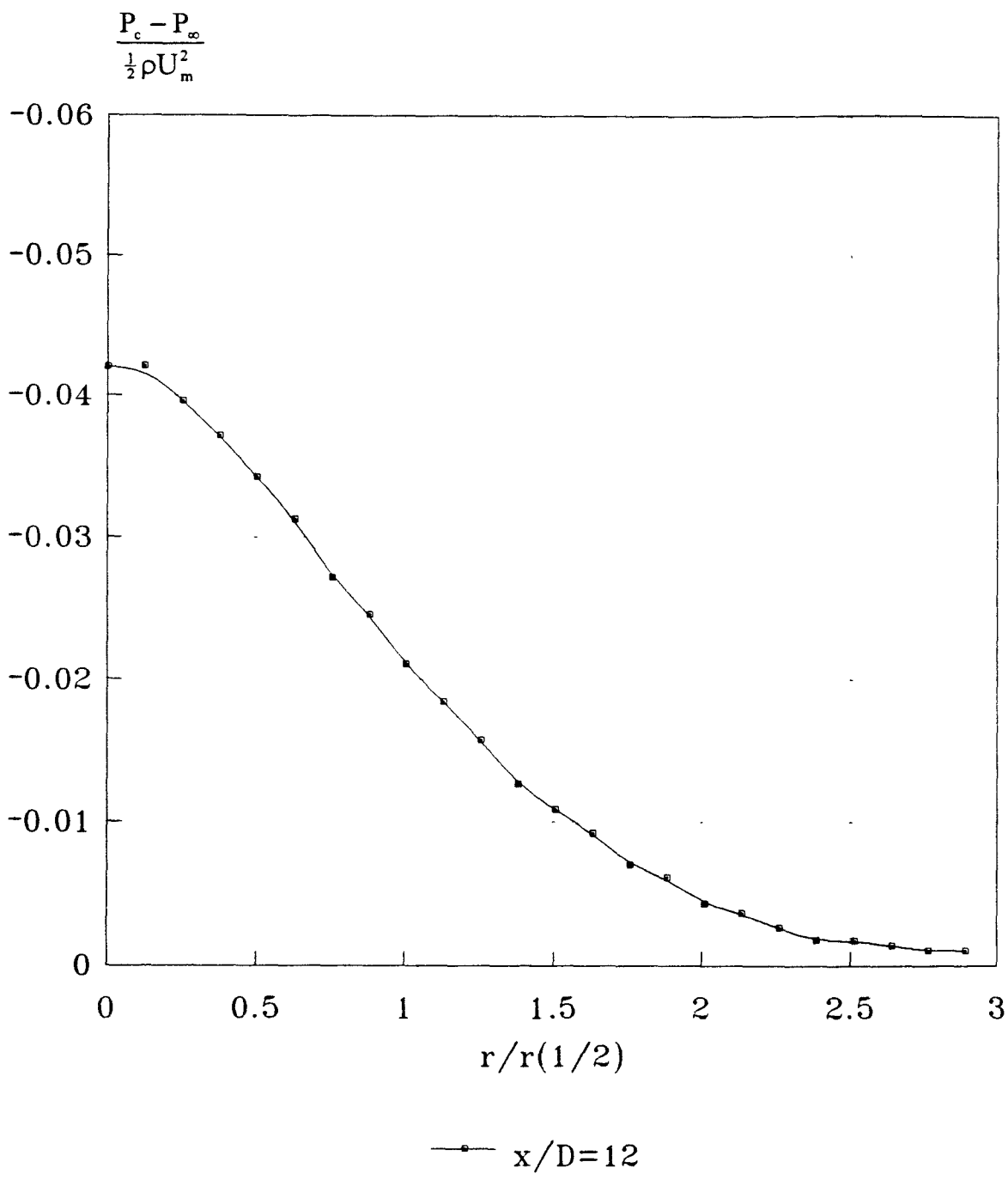

Figure 5-9 Static pressure distribution on the cross section of free jet
Re_d = 66,000, x/D = 12, D = 0.5 in.

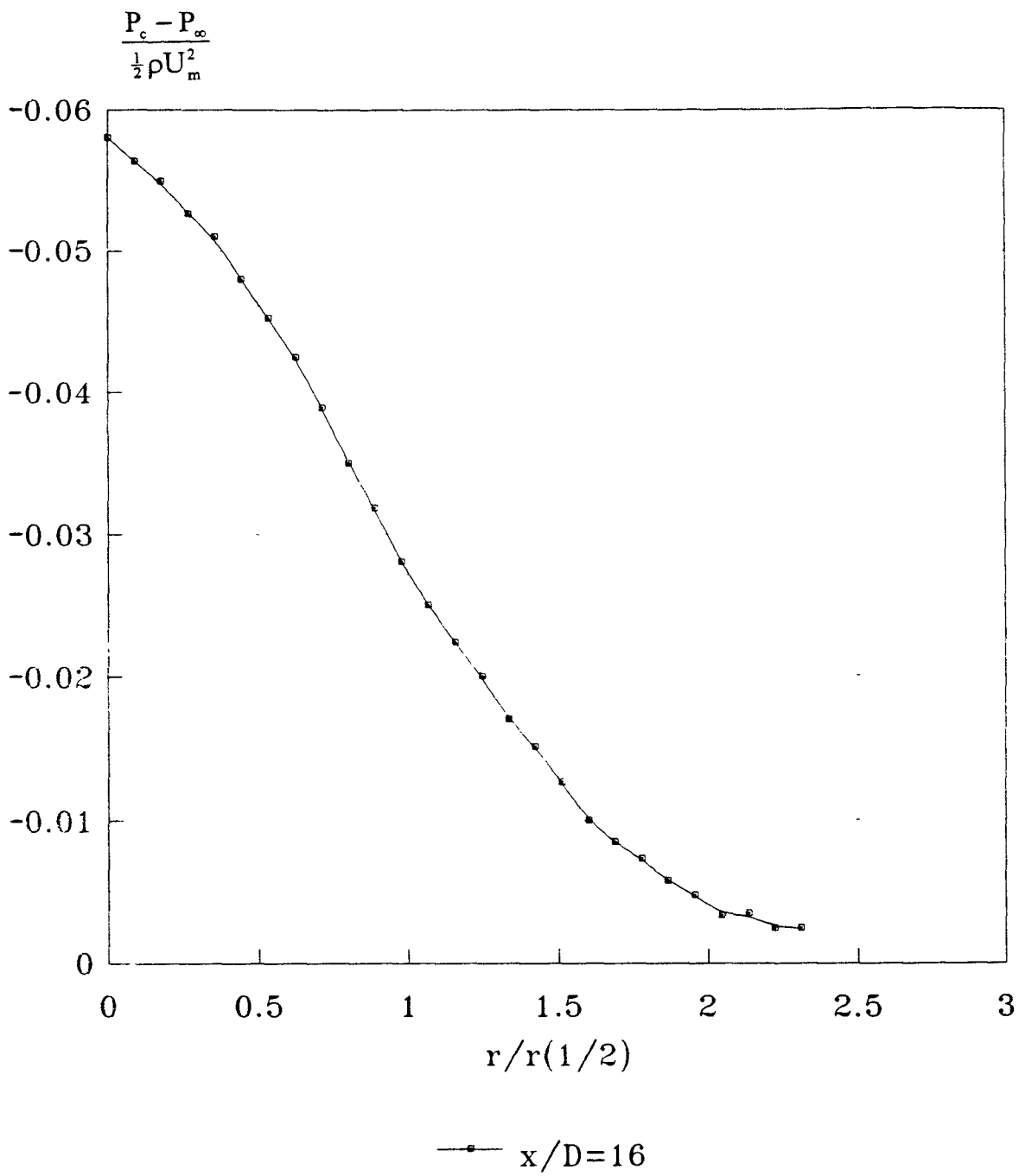

Figure 5-10 Static pressure distribution on the cross section of free jet
Re_d = 66,000, x/D = 16, D = 0.5 in.

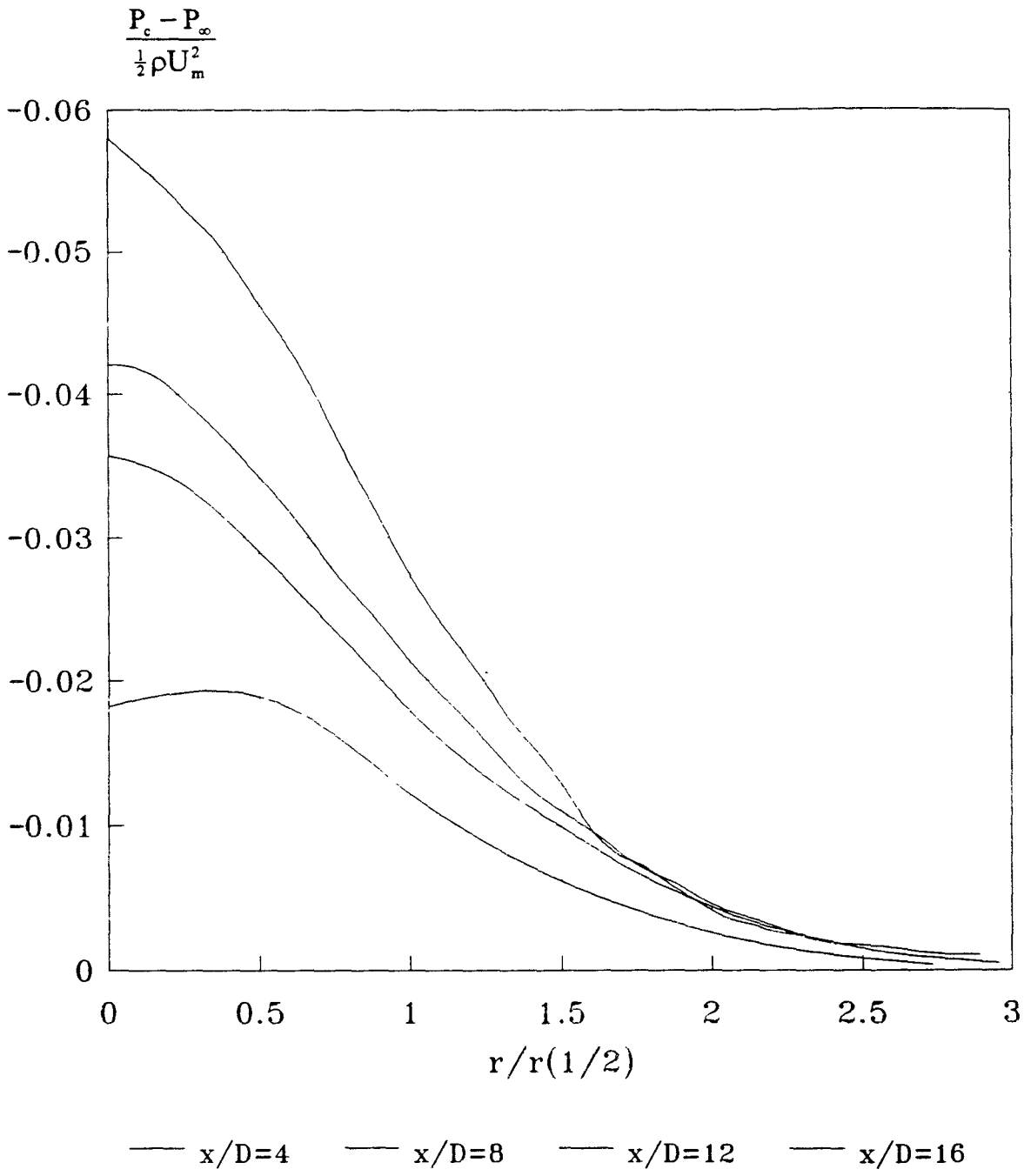

Figure 5-11 Static pressure distribution on the cross section of free jet for varied x/D, Re_d = 66,000, D = 0.5 in.

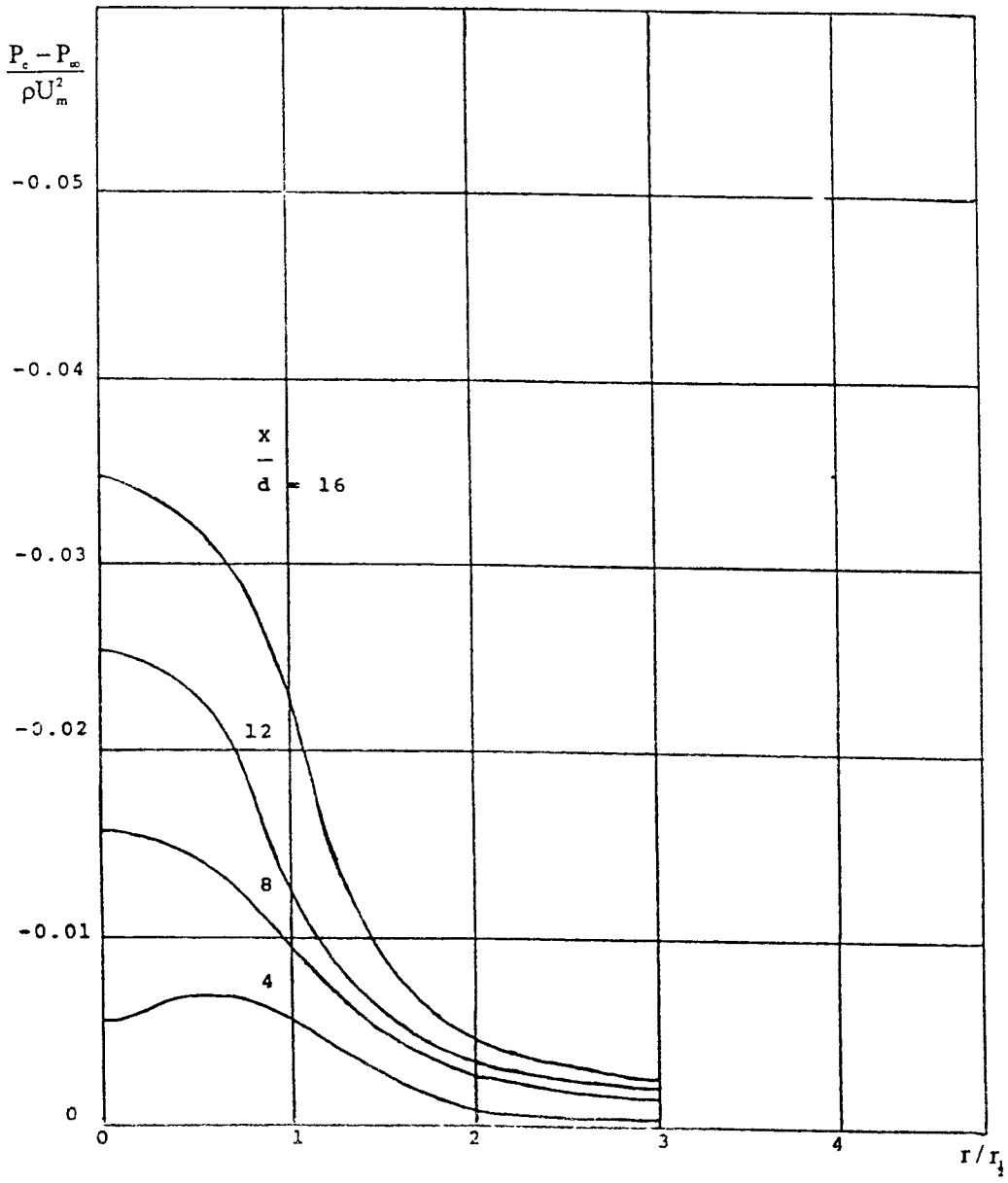

Figure 5-12 Static pressure distribution on the cross section of free jet for varied x/D obtained by Lee [14]

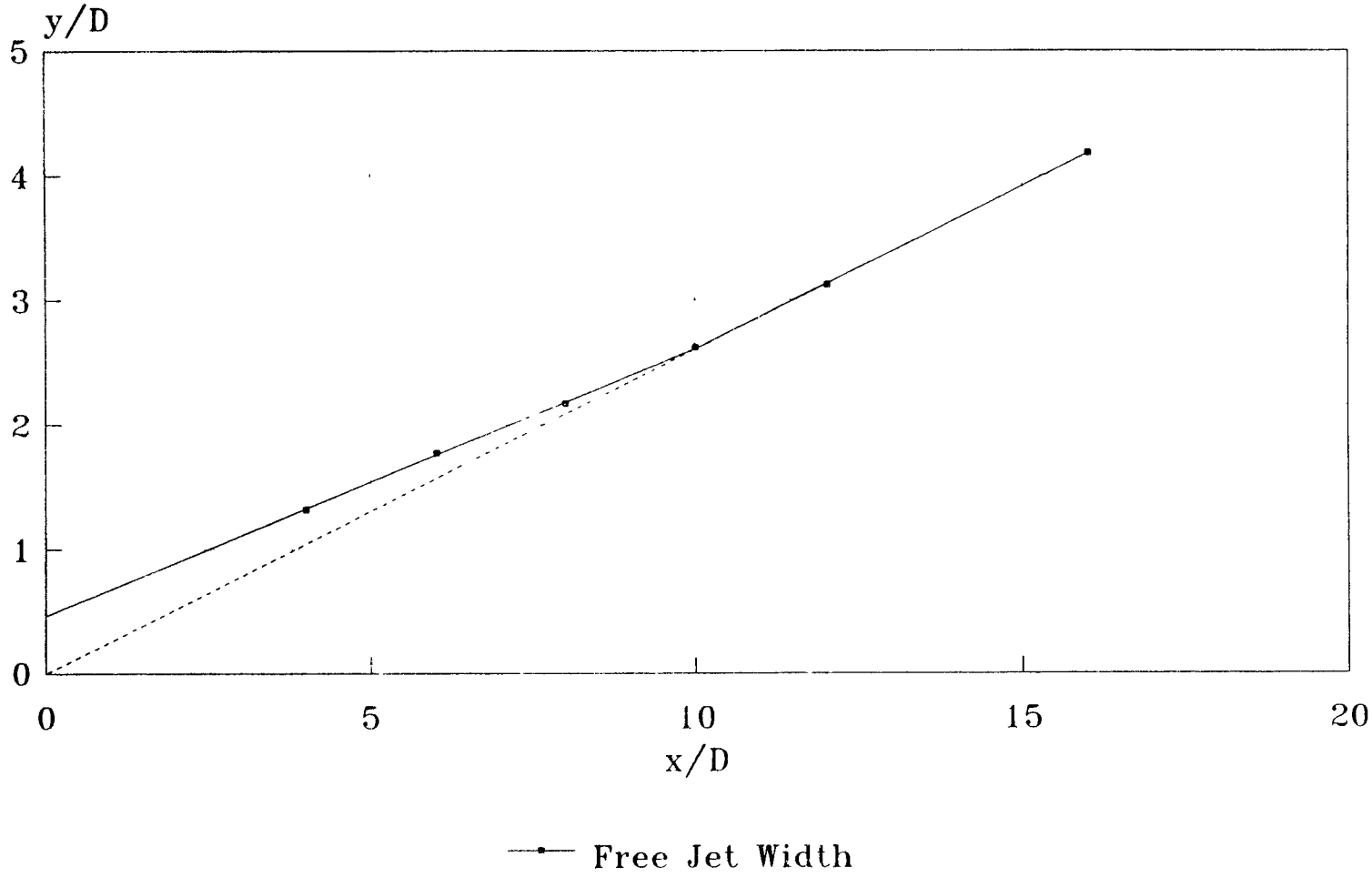

Figure 5-13 Variation of free jet width
Re_d = 66,000, D = 0.5 in.

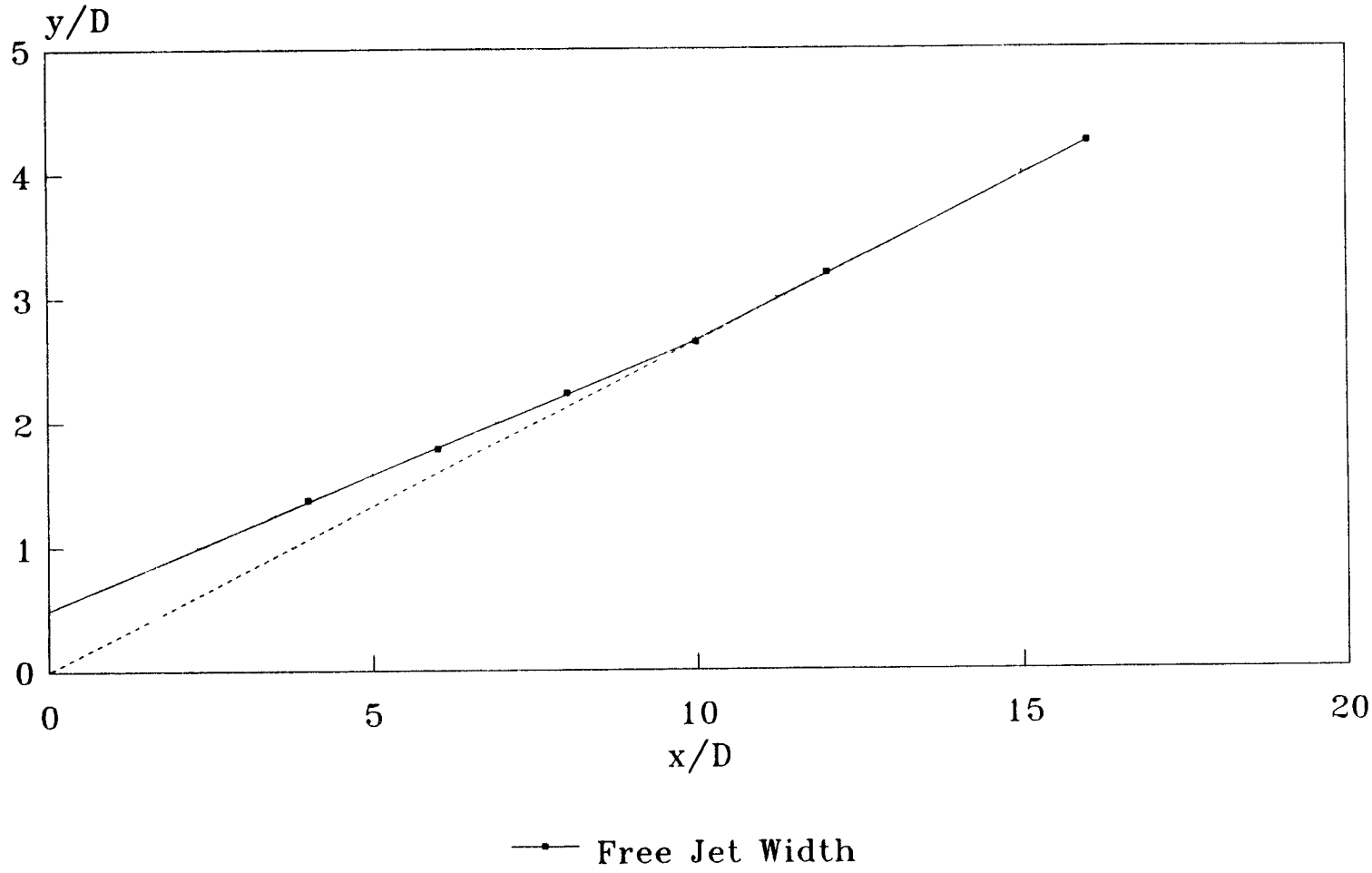

Figure 5-14 Variation of free jet width
Re_d = 70,000, D = 0.5 in.

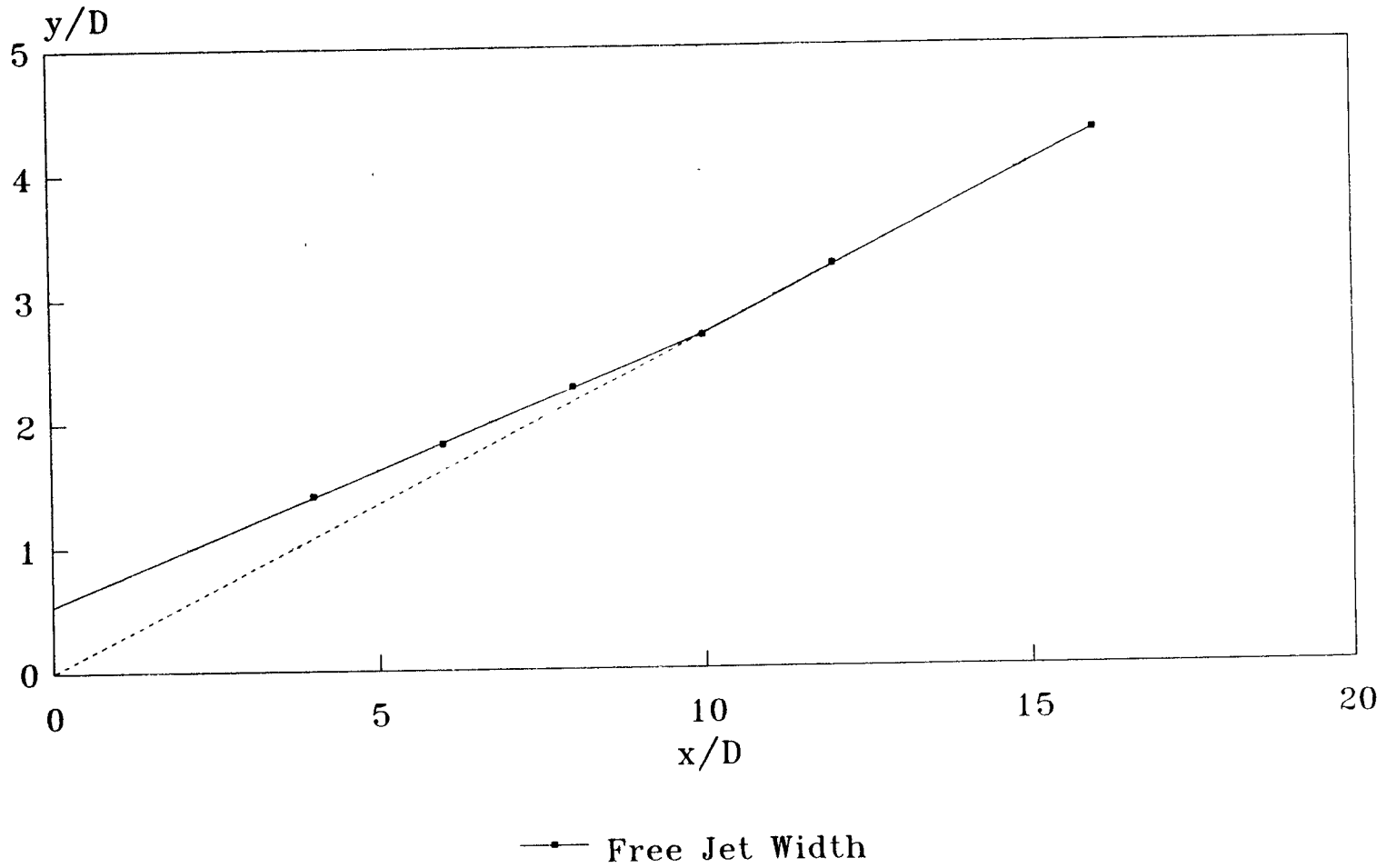

Figure 5-15 Variation of free jet width
Re_d = 74,000, D = 0.5 in.

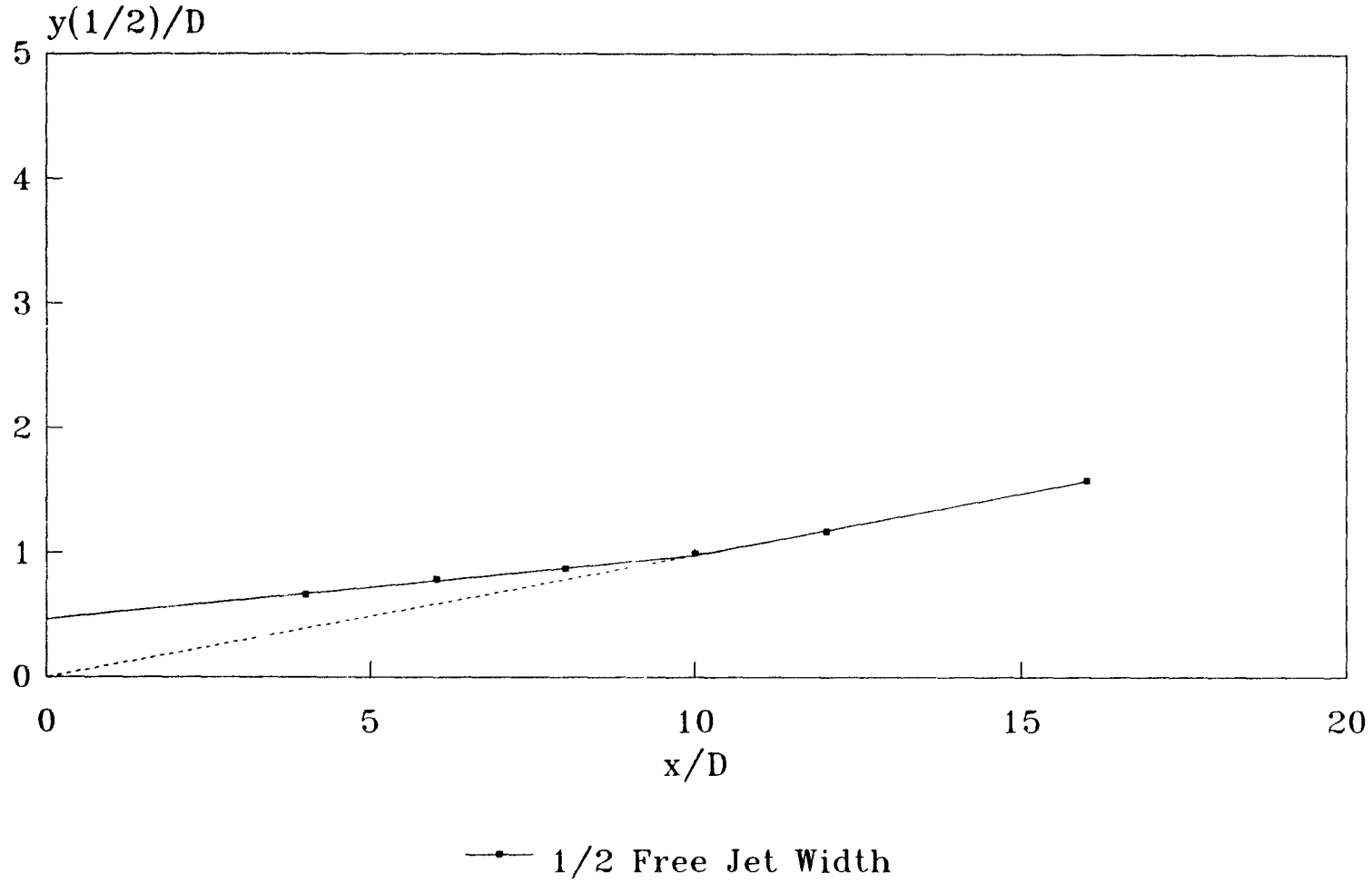

Figure 5-16 Variation of half- valued free jet width
Re_d = 66,000, D = 0.5 in.

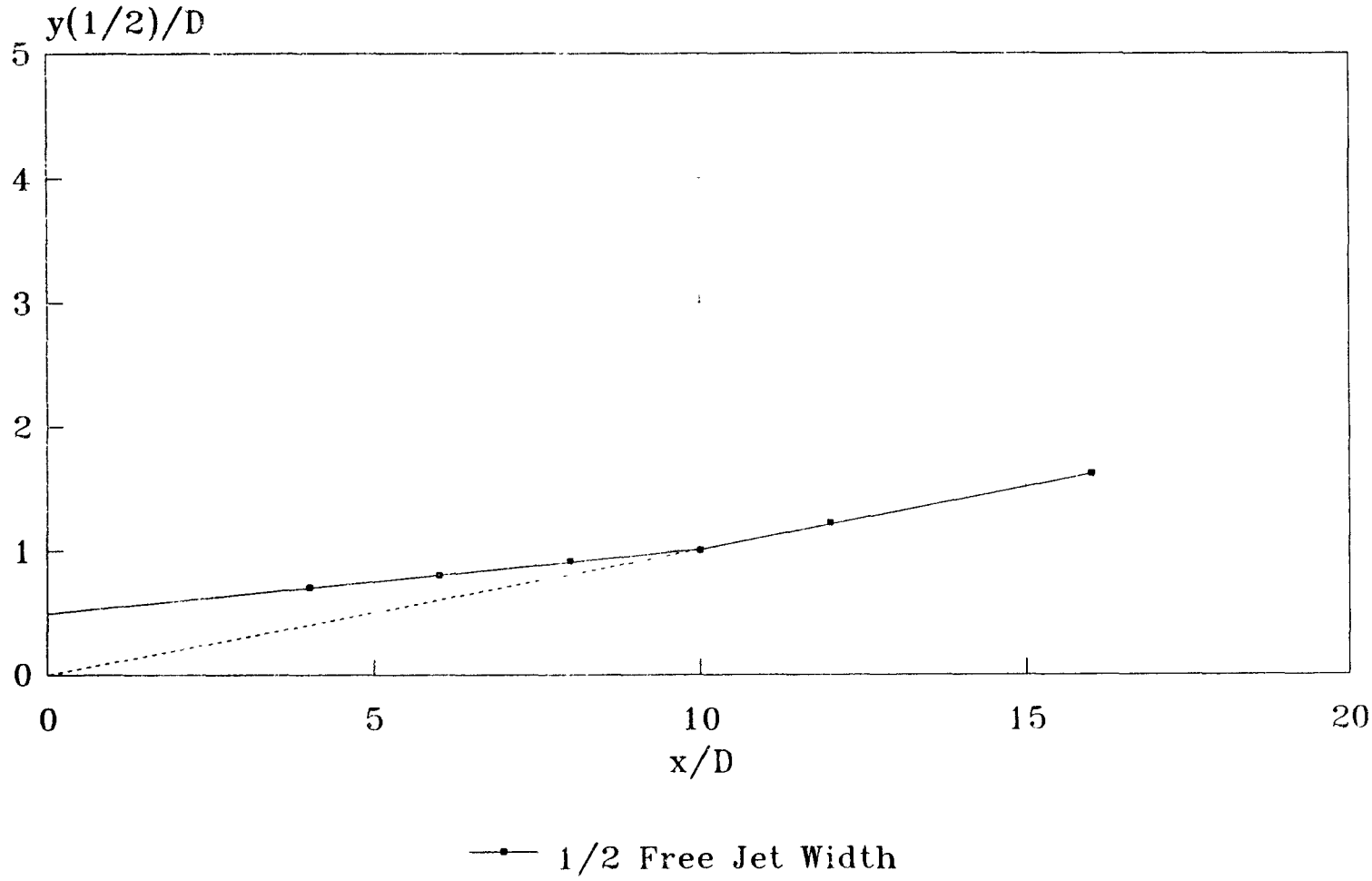

Figure 5-17 Variation of half- valued free jet width
Re_d = 70,000, D = 0.5 in.

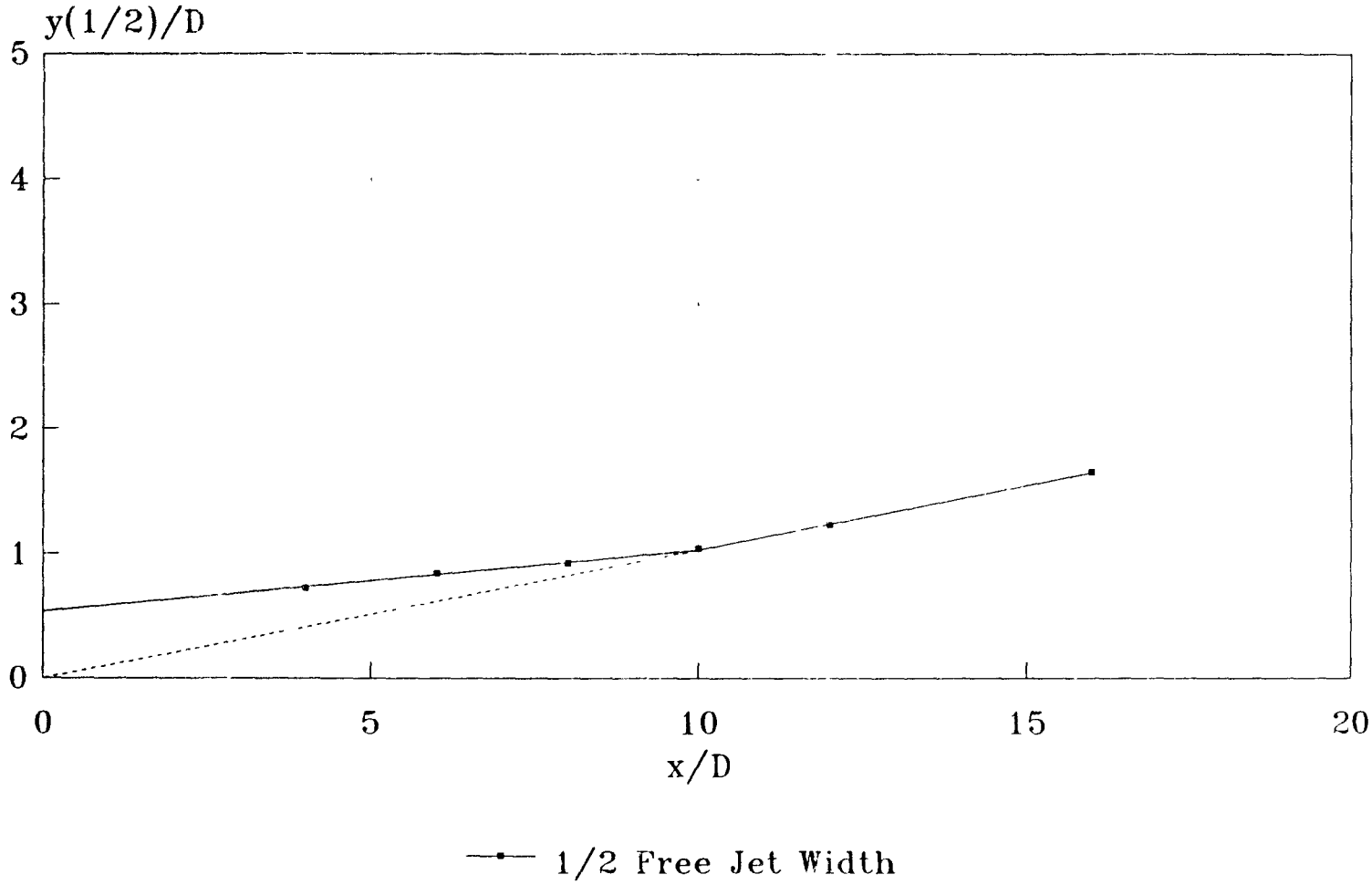

Figure 5-18 Variation of half- valued free jet width
Re_d = 74,000, D = 0.5 in.

5.2 Deflection Zone

5.2.1 Pressure Variation along the Flat Plate

Figure 5-19 through 5-24 shows a comparison of the dimensionless pressure $\frac{p_c - p_\infty}{\frac{1}{2}\rho U_\infty^2}$ distribution along the flat plate, where p_∞ is the ambient pressure. The surplus pressure $p - p_\infty$ decreases from the maximum at the stagnation point ($r / D = 0$) to about zero at r / D larger than 4, however, the static pressure can be neglected at the locations farther than 2.5D. These figures also show that the pressure distribution is steeper and higher for small Z_n / D values. The value of the surplus pressure at $r / D = 0$, increases from 0.235 for $Z_n / D = 20$ to 0.594 for $Z_n / D = 4$.

Since the limitation of the present experimental equipment, the pressure distribution measurement points are not enough when r / D is less than 1.

5.2.2 Velocity Distribution along the Flat Plate

The variation of velocity along the flat plate in the deflection zone is shown in 5-25 through 5-29. The radial velocity, v, is increasing from zero to a maximum. The maximum velocity, V_m, increases linearly for r / D from 0.75 (Z_n / D less than 20) to 0.80 ($Z_n / D = 20$). After this region, the velocity begins to decay by dissipation of energy. Maximum velocity distribution is the same as that obtained from pressure distribution for $r / D = 0$ up to $r / D = 0.75$ to 0.80, depending on Z_n / D. The maximum velocity increase and the pressure distribution in the deflection zone have also been presented by Lee [14], Basu [3], Tani and Komatsu [23]. Present experiment shows that depending on Z_n / D, in the region from $r / D = 0$ up to $r / D = 0.75$ to 0.80 the maximum velocity increase is coincident with that derived from pressure distribution, But Lee got 0, 0.6 to 1.4. It must be

pointed out that the present experiment and Lee's report had a maximum Z_n / D = 20, which contributed to the higher range of coincidence for the velocity and pressure distributions.

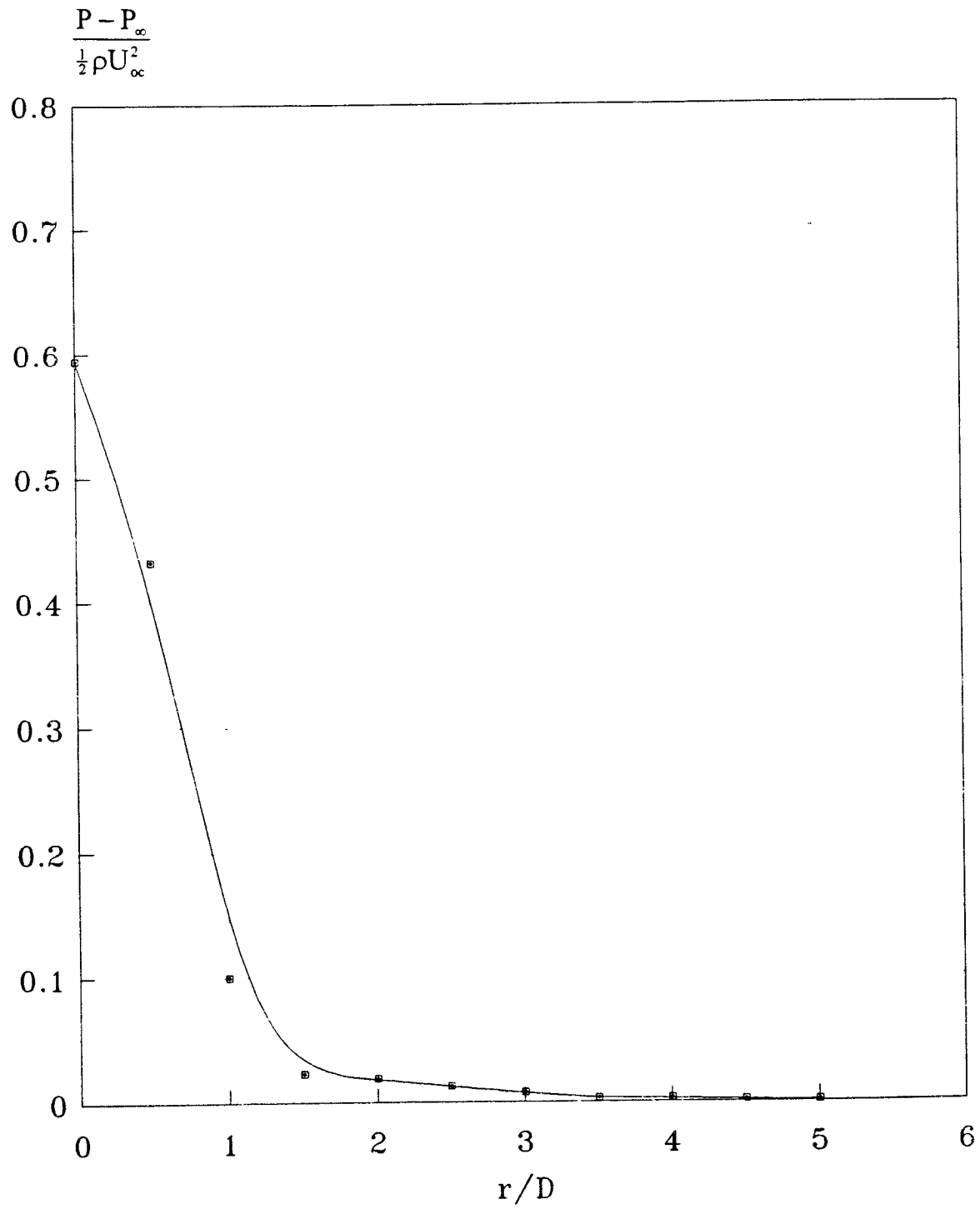

Figure 5-19 Pressure distribution along flat plate
Re_d = 64,000, Z_n / D = 4, D = 0.5 in.

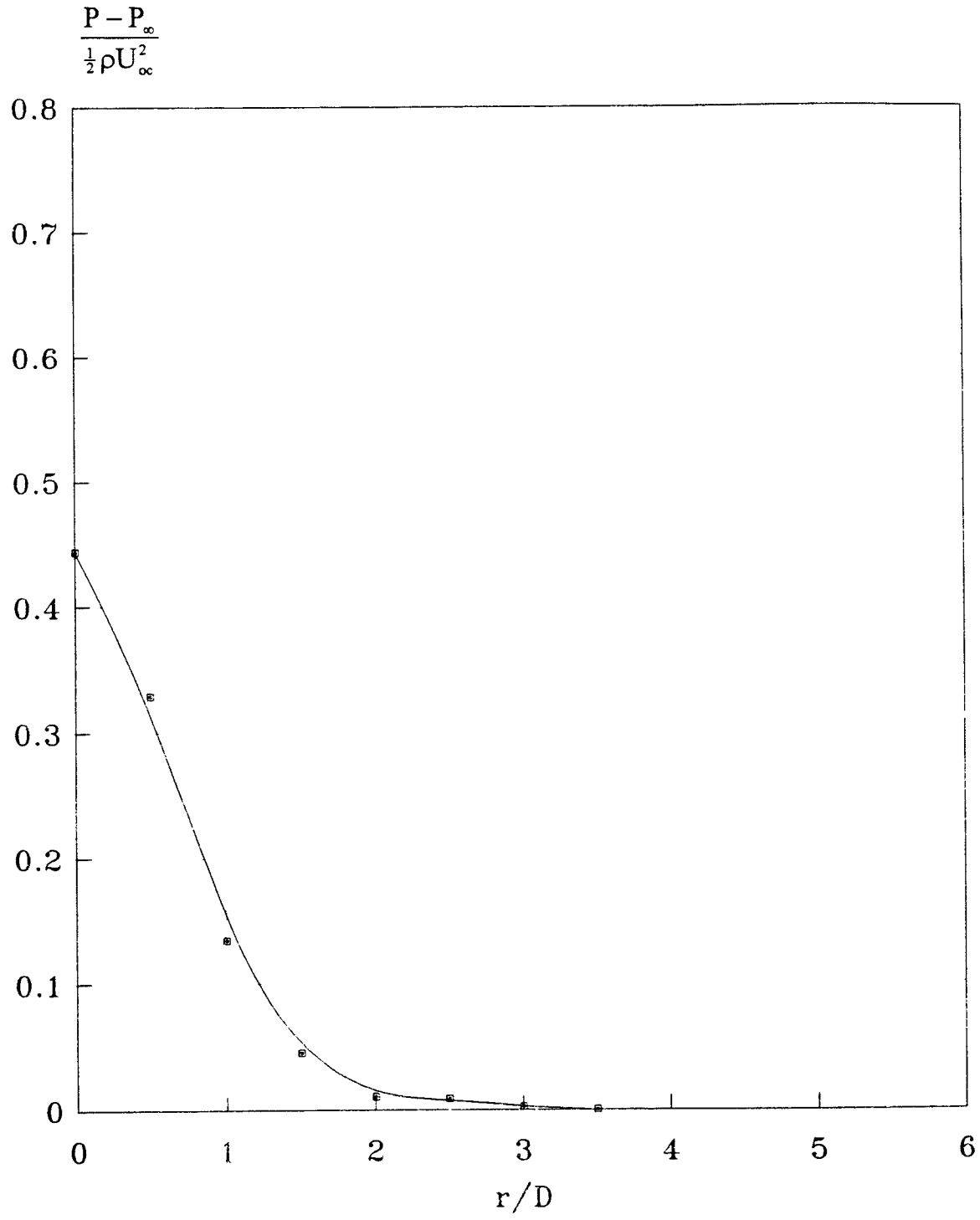

Figure 5-20 Pressure distribution along flat plate
Re_d = 44,000, Z_n / D = 7, D = 0.5 in.

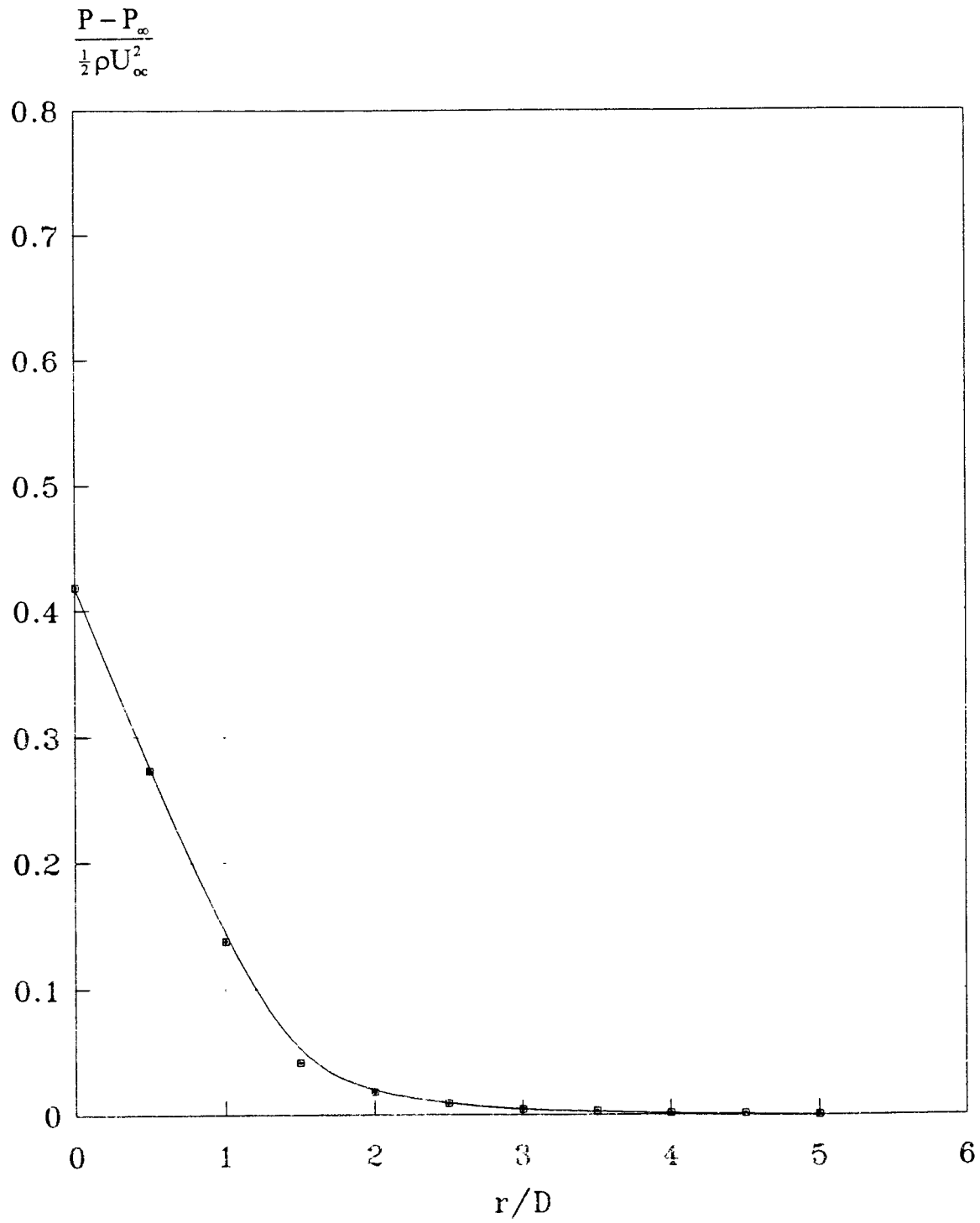

Figure 5-21 Pressure distribution along flat plate
Re_d = 67,000, Z_n / D = 7, D = 0.5 in.

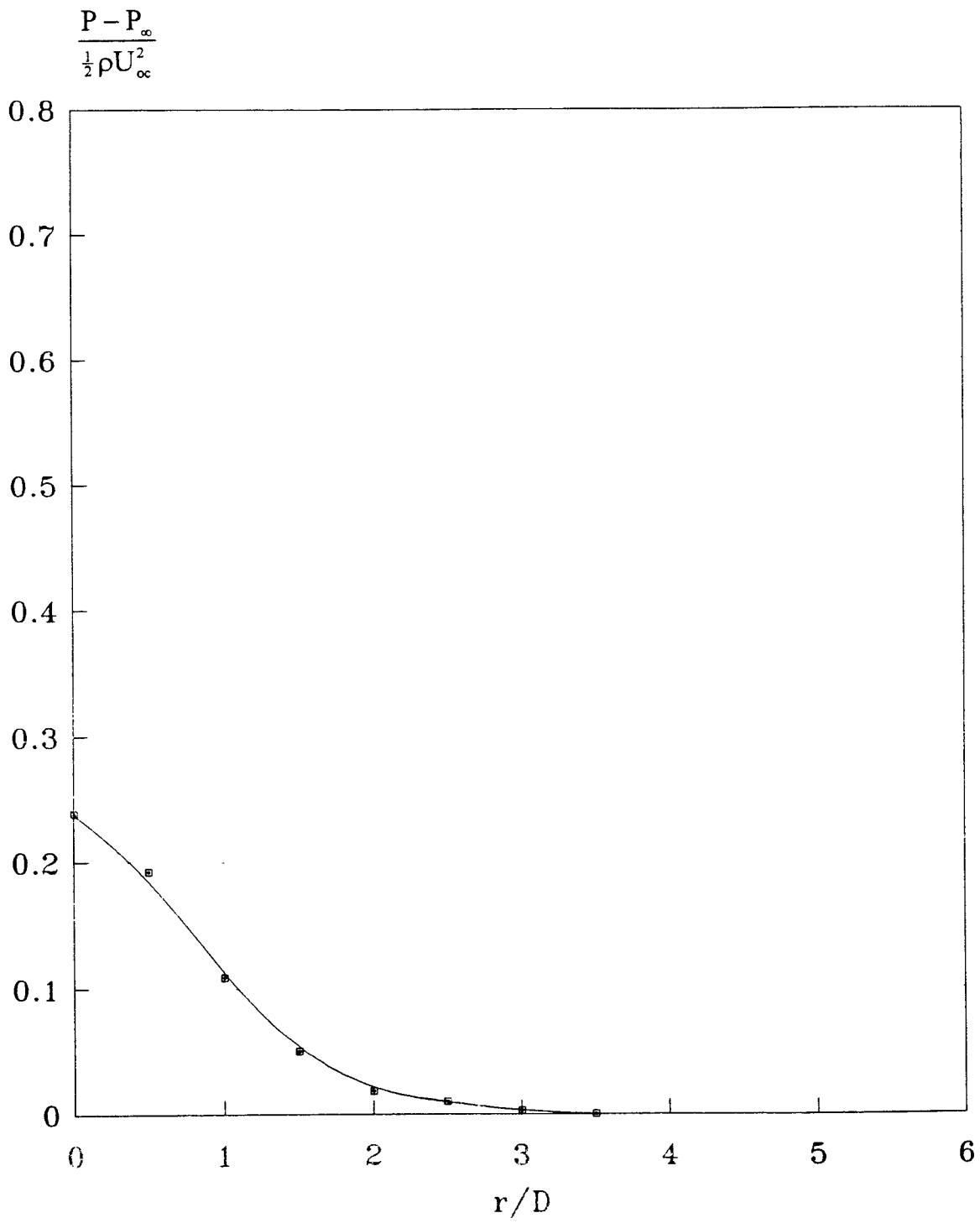

Figure 5-22 Pressure distribution along flat plate
Re_d = 48,000, Z_n / D = 10, D = 0.5 in.

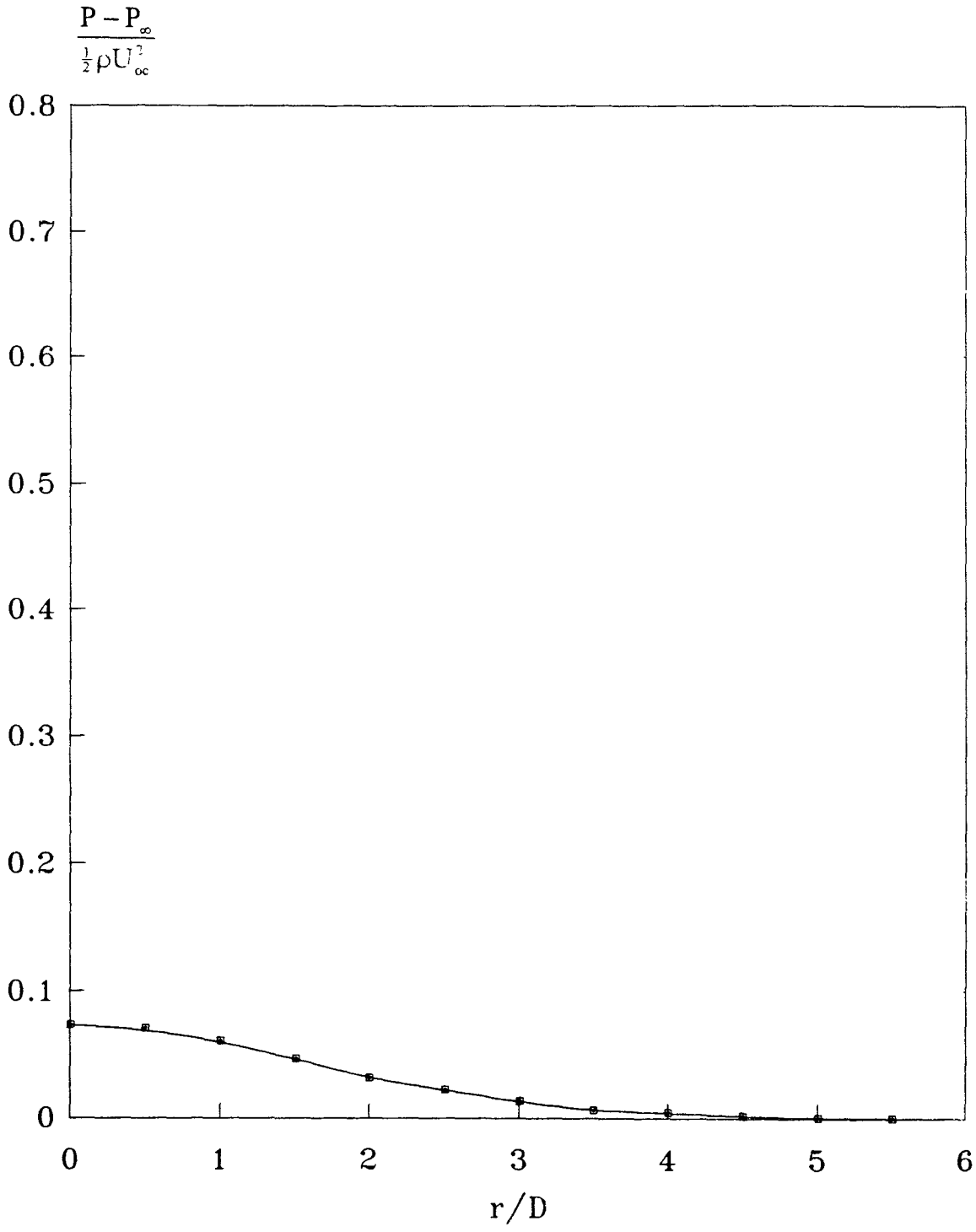

Figure 5-23 Pressure distribution along flat plate
Re_d = 60,000, Z_n / D = 20, D = 0.5 in.

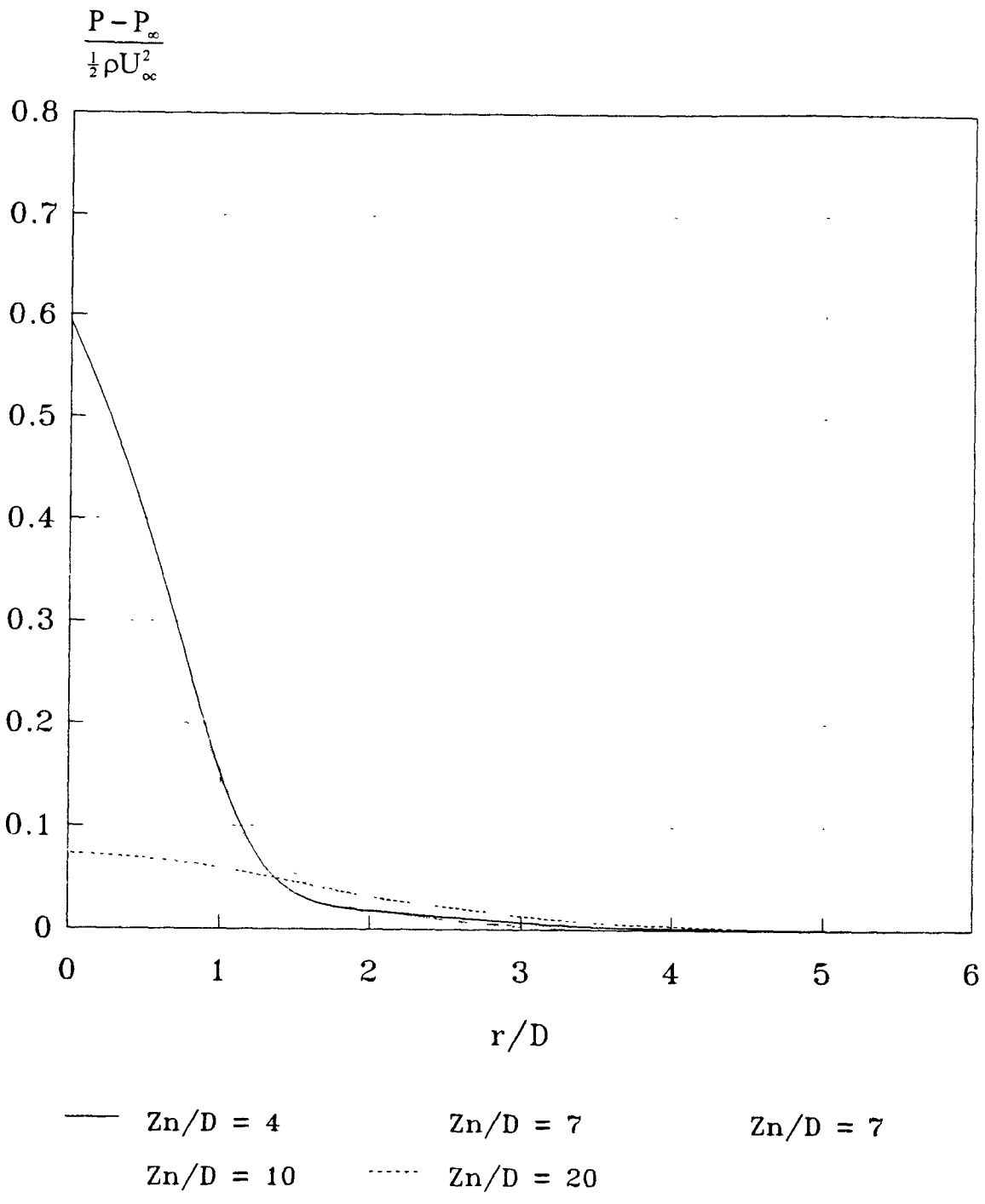

Figure 5-24 Pressure distribution along flat plate
for varied Z_n / D, D = 0.5 in.

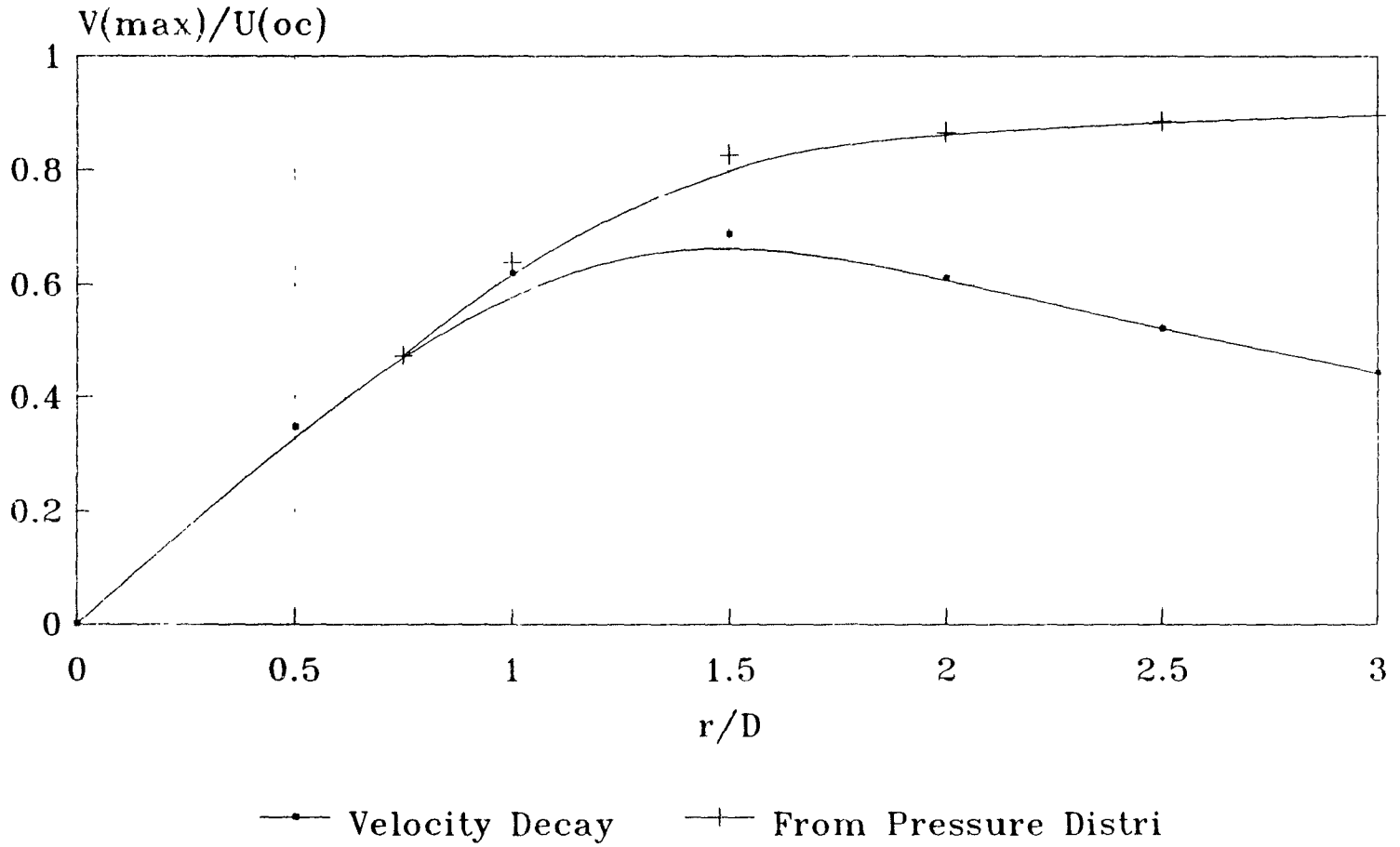

Figure 5-25 Maximum velocity decay along the flat plate for $Re_d = 40{,}000$, $Z_n / D = 4$, $D = 0.5$ in.

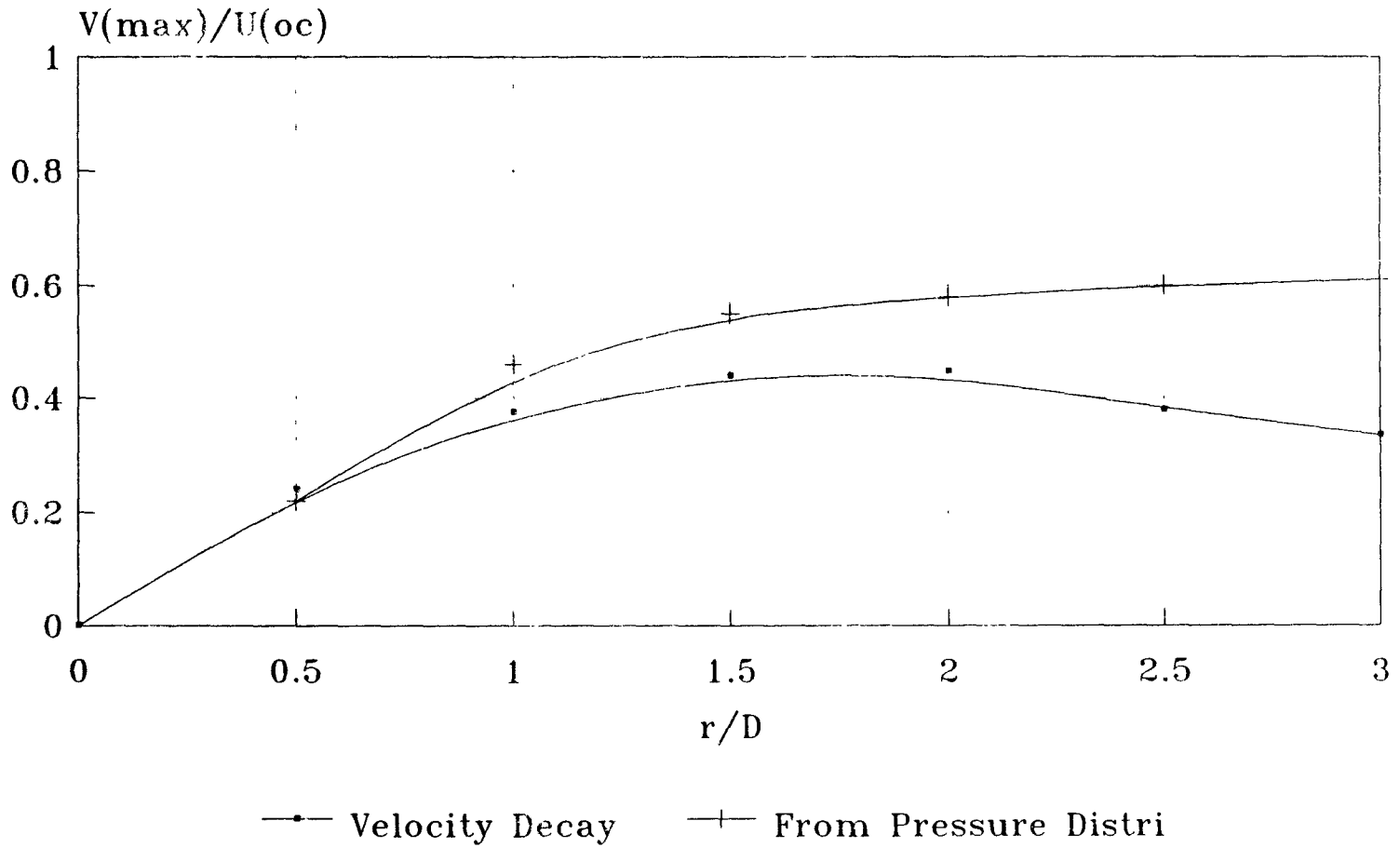

Figure 5-26 Maximum velocity decay along the flat plate for $Re_d = 44{,}000$, $Z_n / D = 7$, $D = 0.5$ in.

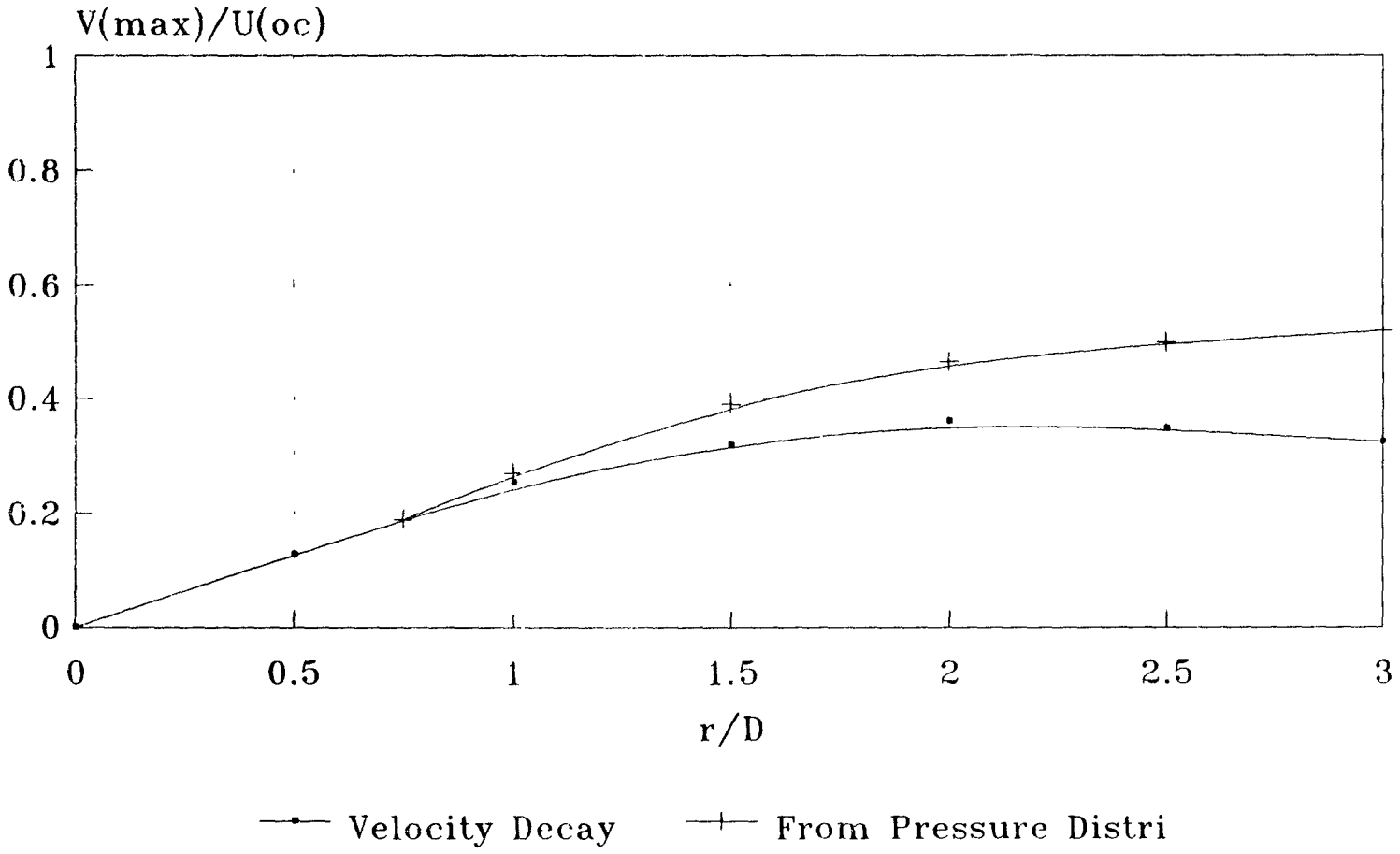

Figure 5-27 Maximum velocity decay along the flat plate for Re_d = 48,000, Z_n / D = 10, D = 0.5 in.

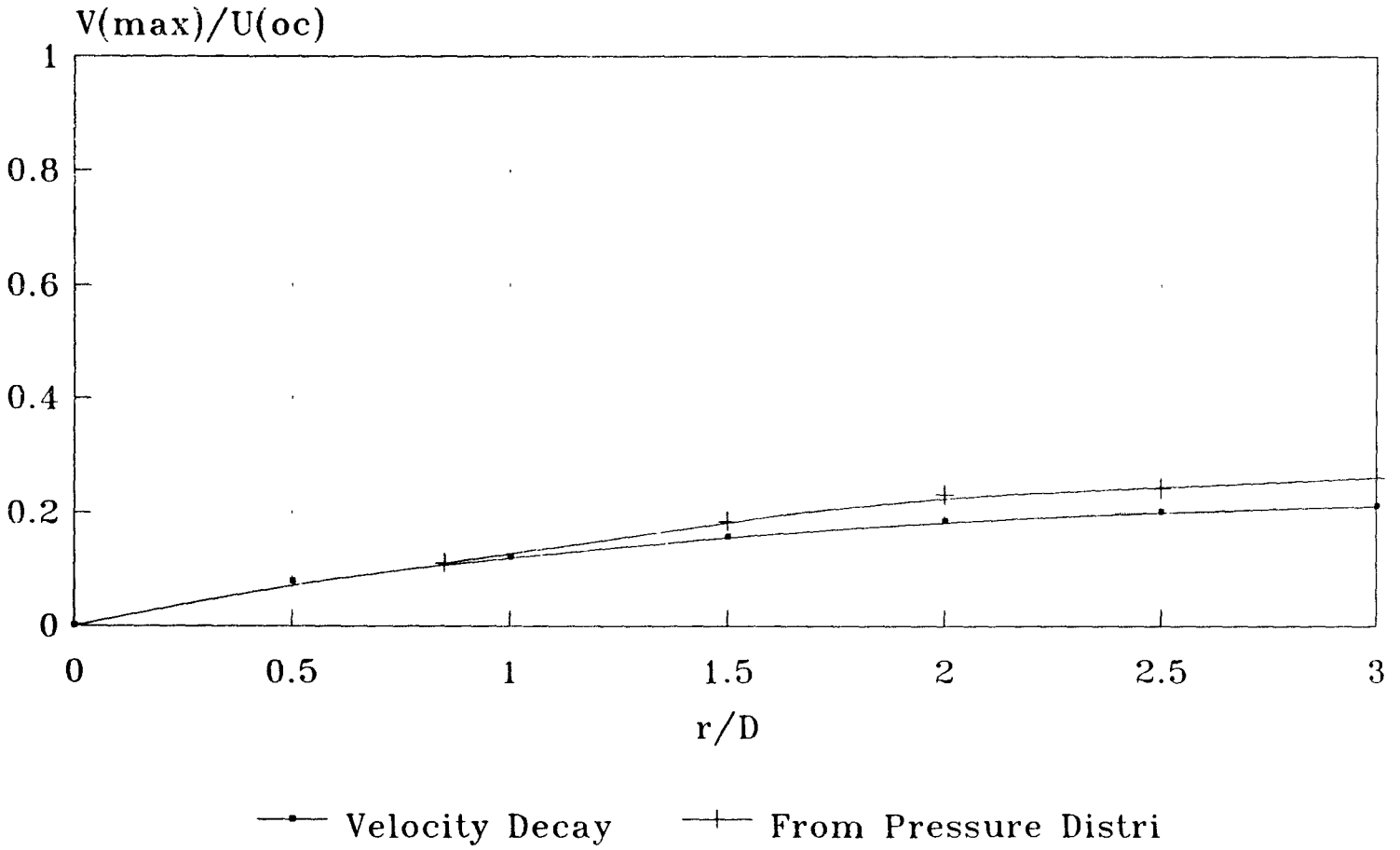

Figure 5-28 Maximum velocity decay along the flat plate for $Re_d = 60{,}000$, $Z_n / D = 20$, $D = 0.5$ in.

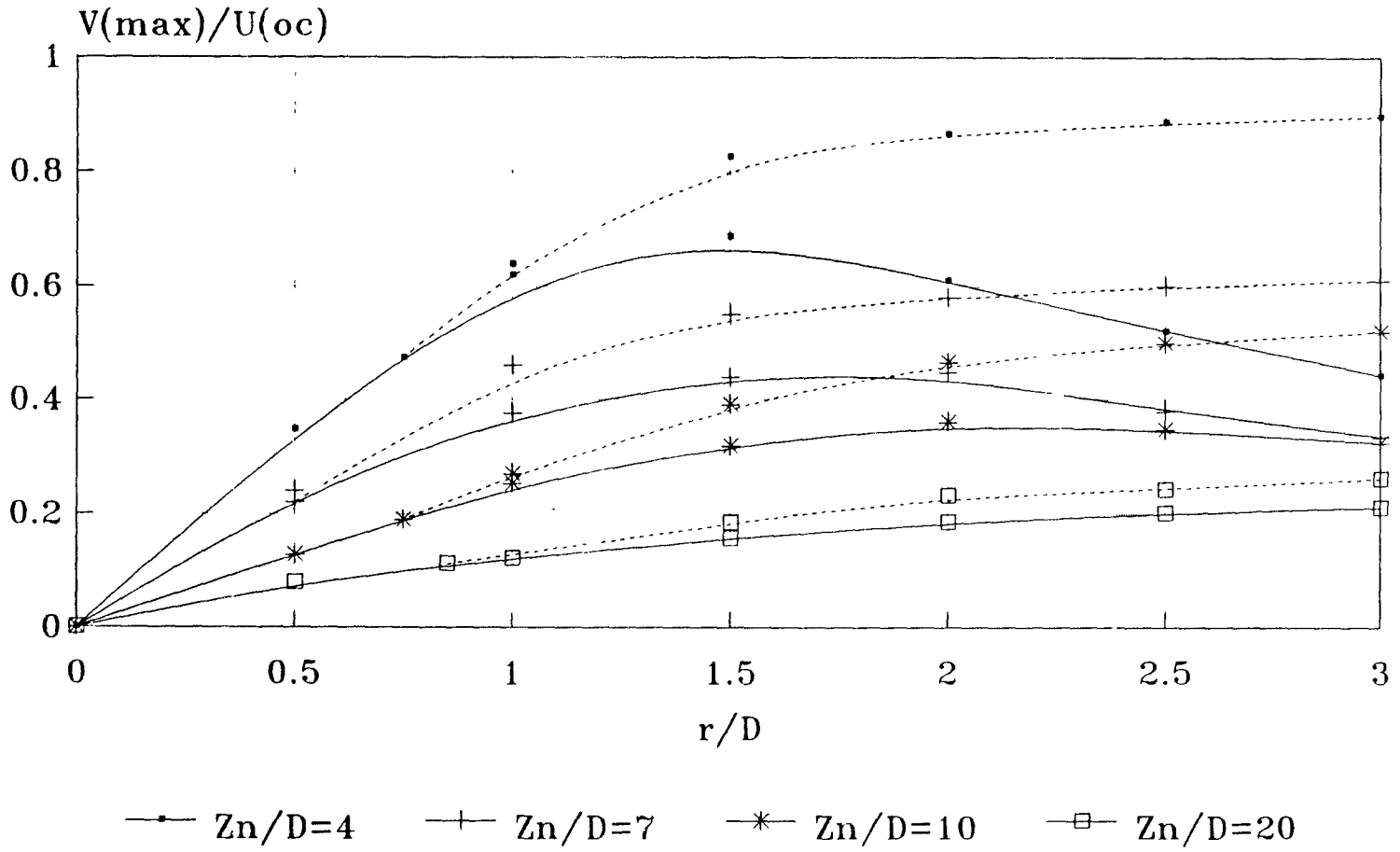

Figure 5-29 Maximum velocity decay along the flat plate for varied Z_n / D, D = 0.5 in.
dash line from pressure distribution

5.3 Wall Jet Zone

5.3.1 The Similarity of the Dimensionless Velocity Profile of the Wall Jet

The profiles of dimensionless velocity V / V_{max} are plotted with respect to $Z / Z_{\frac{1}{2}}$ ($Z_{\frac{1}{2}}$ being the Z- direction location where $V = 1/2V_{max}$) in Figures from 5-30 through 5-49. The fully developed wall jet is similar for different locations measured from the stagnation point and for different Z_n / D, but for the same surface condition. The experimental investigation also shows that as Reynolds Number increases, the velocity profile near the wall becomes more flattened. The effect of varying Reynolds Number was observed only in the portion of the boundary layer near the wall. The dimensionless velocity profile is very similar to that Bakke [2] as well as to that of Glauert [7], Lee [14], and Basu [3]. The characteristics of the velocity profile are similar to those of the turbulent free jet studied by many other previous investigators.

Figures 5-30 through 5-39 show that there exists an approximate similarity in the wall jet flow regardless of the distance between the jet nozzle and the target plate. By the particular method used of making the velocity profile dimensionless, it becomes also relatively independent of the influence of Reynolds Number, except in the boundary layer immediately at the wall. Since the boundary layer is very very thin, only rough measurements were taken in this layer with the probes available no matter what is the best we can acquired for the present investigation.

An experiment is taken this time when the plate is covered with different kinds of sand paper. It is found that the boundary layer of the sand paper is apparently thicker than of the smooth plate. Shown in Figure 5-35 and 5-39, one can find that the value of $Z / Z_{\frac{1}{2}}$ increases from around 2.1 that is of the smooth plate to 3.0 or even more depending on the roughness of the sand paper.

Figure 5-40 through 5-49 shows the plots of the velocity profile very close to the wall on log-log coordinates to observe the power of "n" in the equation,

$$\frac{V}{V_m} \propto \left(\frac{Z}{Z_{\frac{1}{2}}}\right)^{\frac{1}{n}} \tag{35}$$

"n" was found to vary between 6.986 to 10.671 for the same smooth plate and the different Z_n / D and different Reynolds Numbers. For the sand paper surface, it was interesting to observe that "n" was found to decrease to the range of 4 to 6. It is the result opposite to what Basu [3] got (from 13.57 increases to 14.62), and the author believes it is correct because in the boundary layer of a rough surface the velocity should be smaller than it is in the boundary layer of a smooth plate. This shows that as the surface roughness of the impinging target increases, "n" decreases, in other word, the rate of velocity decay near the plate increases. Lee [14] conducted experiments that produced an "n" value of about 7.5 to 14. For the smooth plate Basu got "n" from 7.97 to 13.57. It can therefor be concluded that the results given by Lee [14] and Basu [3] was a little bit different from the present experiment results. The value of "n" is listed below:

	Z_n / D	Re_d	Distance*	n
Smooth Plate	4	40,000	2.0 in.	6.986
Smooth Plate	4	64,000	3.0 in.	7.691
Smooth Plate	7	44,000	2.5 in	7.019
Smooth Plate	7	67,000	3.5 in.	7.904
Smooth Plate	10	48,000	2.5 in.	7.175
Smooth Plate	10	68,000	3.25 in.	8.232

Smooth Plate	20	60,000	3.25 in.	9.412
Smooth Plate	20	80,000	3.5 in.	10.671
#40Sandpaper	10	48,000	2.5 in.	5.248
#60Sandpaper	20	80,000	3.5 in.	4.235

* Distance = Distance from stagnation point

5.3.2 Maximum Velocity Decay along Flat Plate

The maximum velocity is located just beyond the turbulent boundary layer. It is the highest value of the wall jet velocity in the velocity profile. Figure 5-50 through 5-55 show that the maximum velocity decay is governed by the equation,

$$\frac{V_m}{U_\infty} = \frac{A}{\left(\frac{r}{D}\right)^B} \tag{36}$$

Where, A = 1.4225, B = 1.1165 (for smooth plate)

A = 1.2767, B = 1.1088 (for #40 sand paper)

Various previous investigators have obtained quite close values of the coefficient "B". Thus, the power of (r / D) was taken as 1.1 by Poreh [16], 1.14 by Brady [4], 1.12 by Bakke [2] and Lee [14]. The exact power of (r / D) is possible a weak function of Reynolds Number. The difference is very difficult to determine accurately. For rough surface, as "n" is smaller than it is for smooth plate, the coefficient "B" is also a little bit smaller.

The power of (r / D) is always larger than 1, that is to say the decay of maximum velocity along the flat plate is faster than that of a free radial jet, which decays with the power 1 of (r / D).

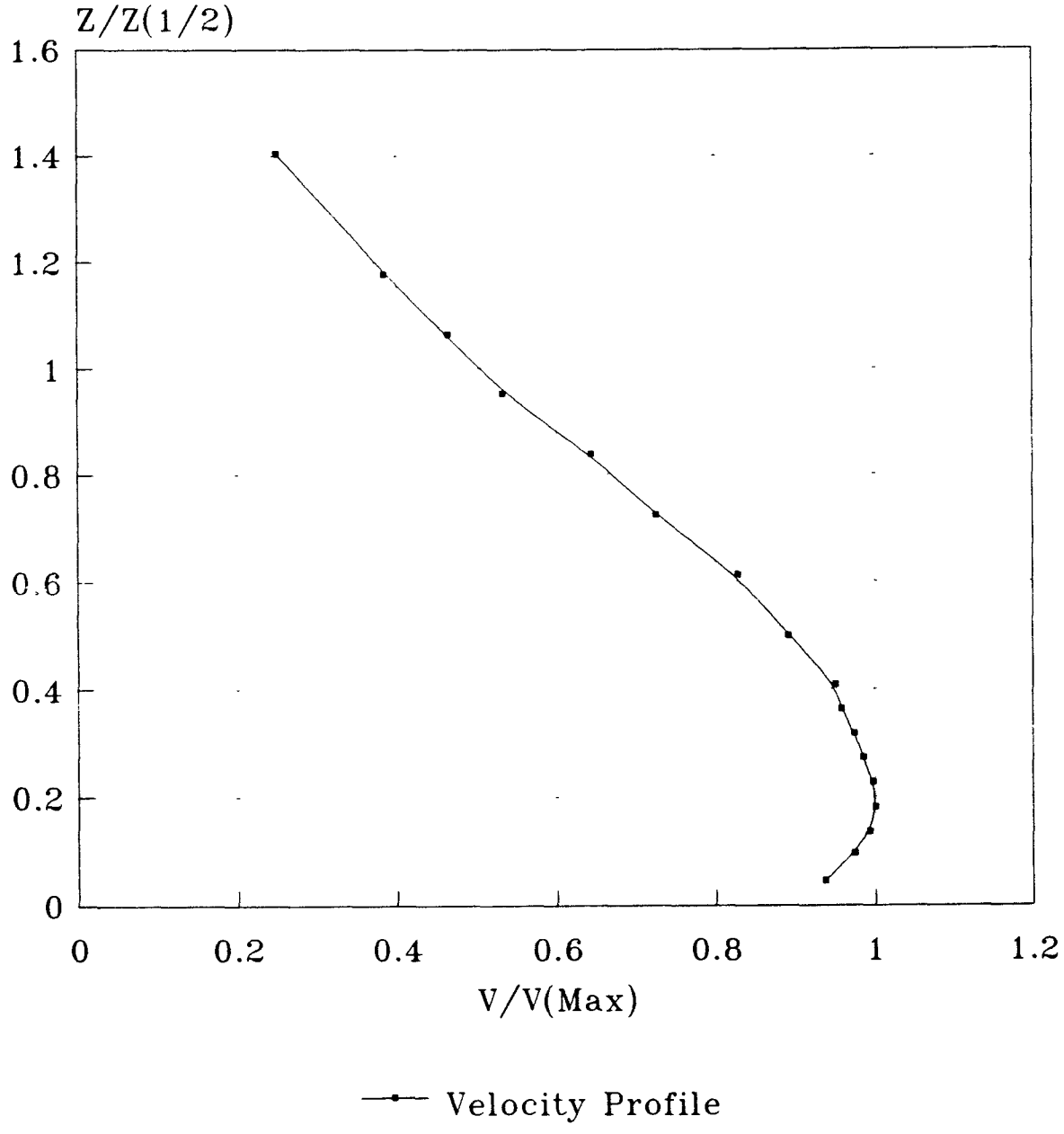

Figure 5-30 Velocity profile of wall jet
$Re_d = 40{,}000$, $Z_n / D = 4$, $D = 0.5$ in.
2.0 in. from stagnation point

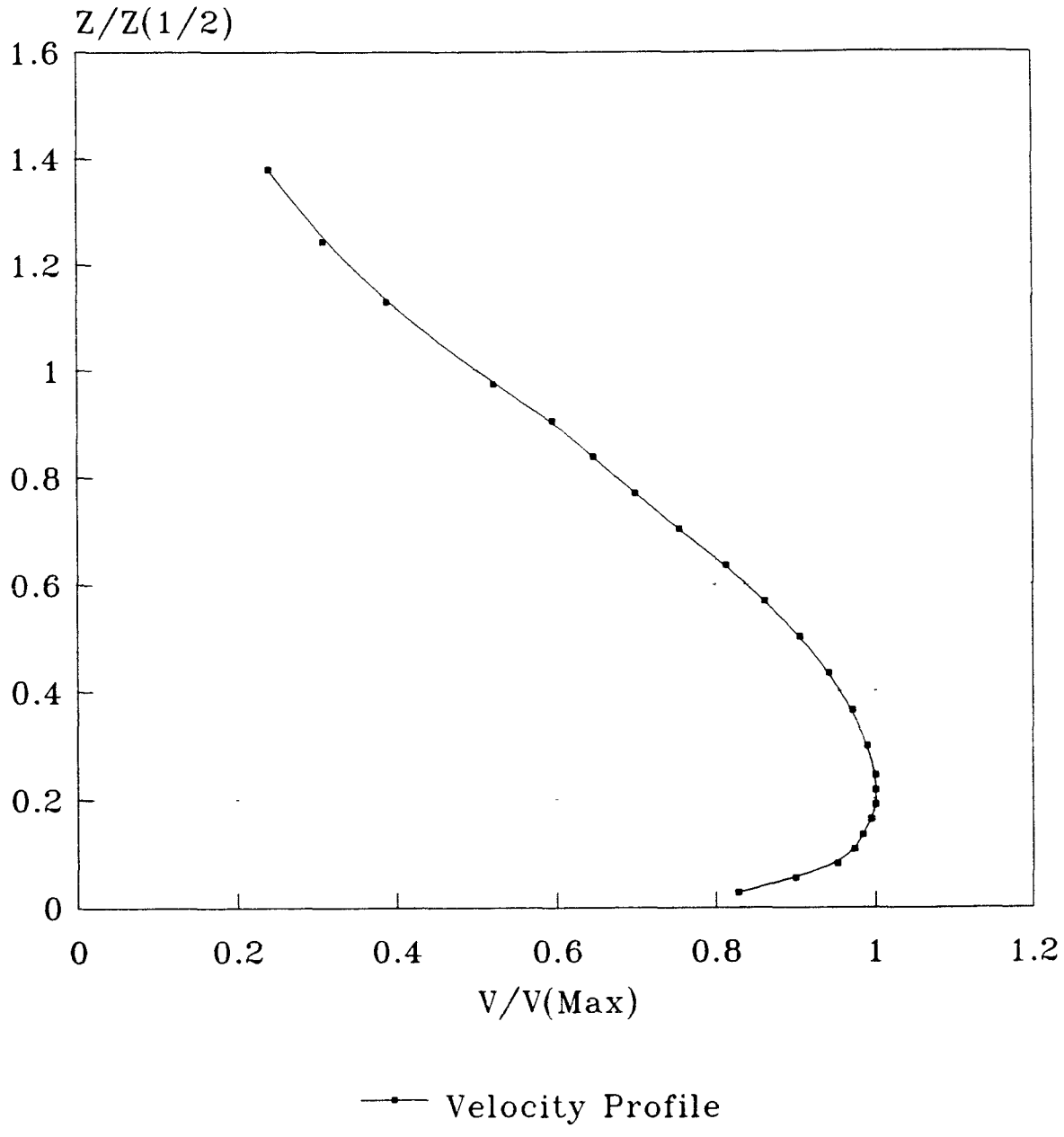

Figure 5-31 Velocity profile of wall jet
$Re_d = 64{,}000$, $Z_n / D = 4$, $D = 0.5$ in.
3.0 in. from stagnation point

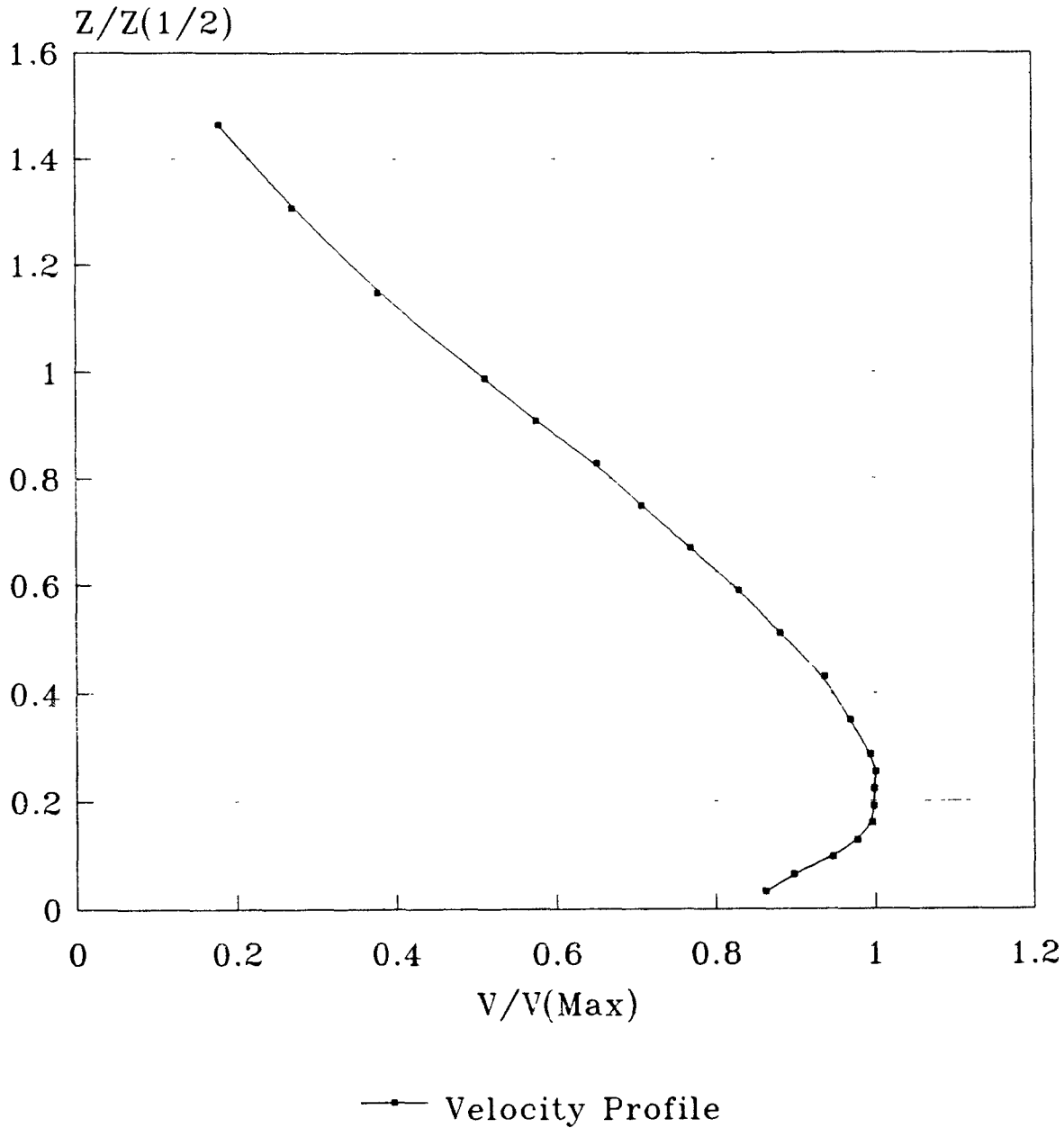

Figure 5-32 Velocity profile of wall jet
Re_d = 44,000, Z_n / D = 7, D = 0.5 in.
2.5 in. from stagnation point

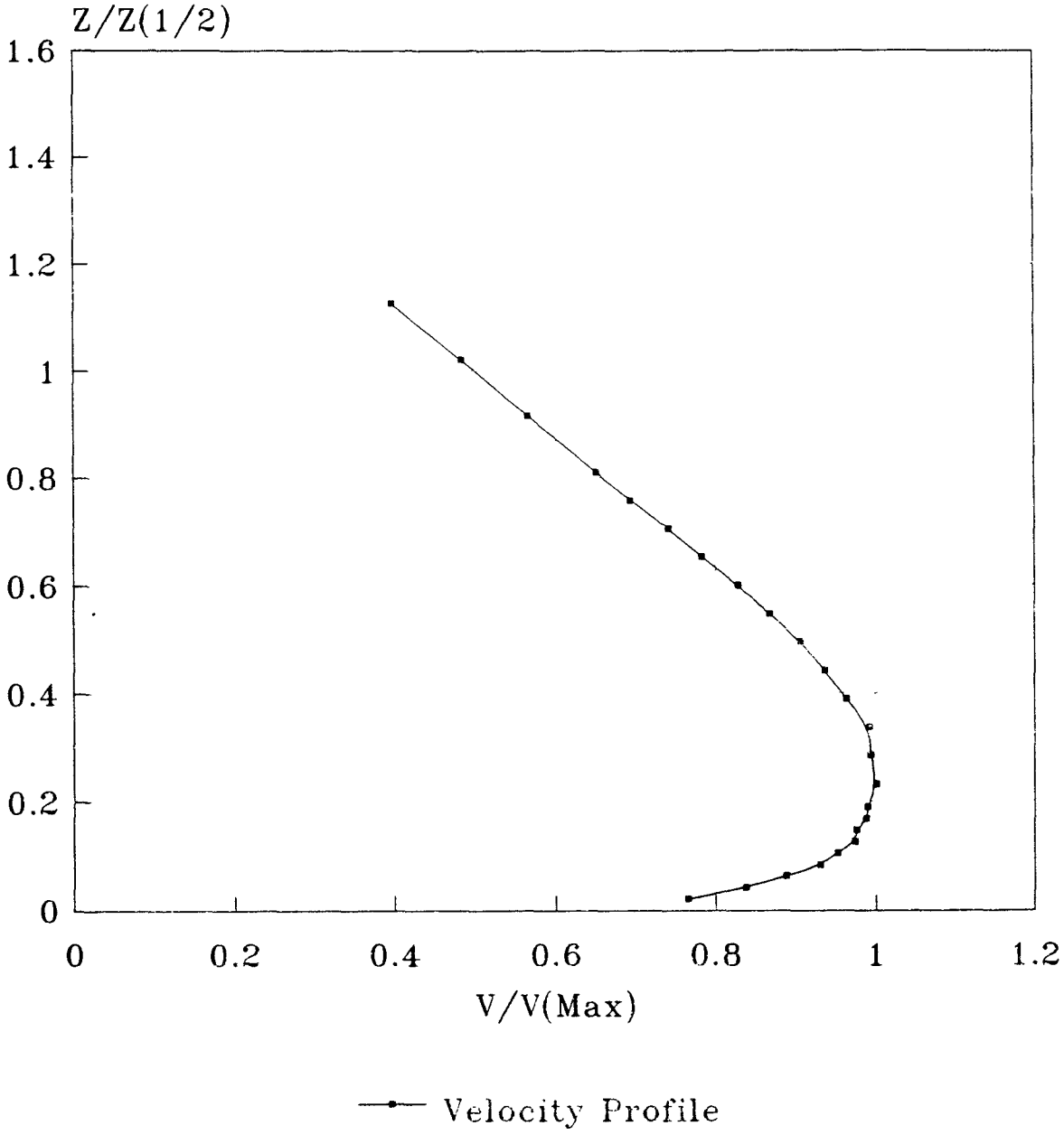

Figure 5-33 Velocity profile of wall jet
Re_d = 67,000, $Z_n / D = 7$, D = 0.5 in.
3.5 in. from stagnation point

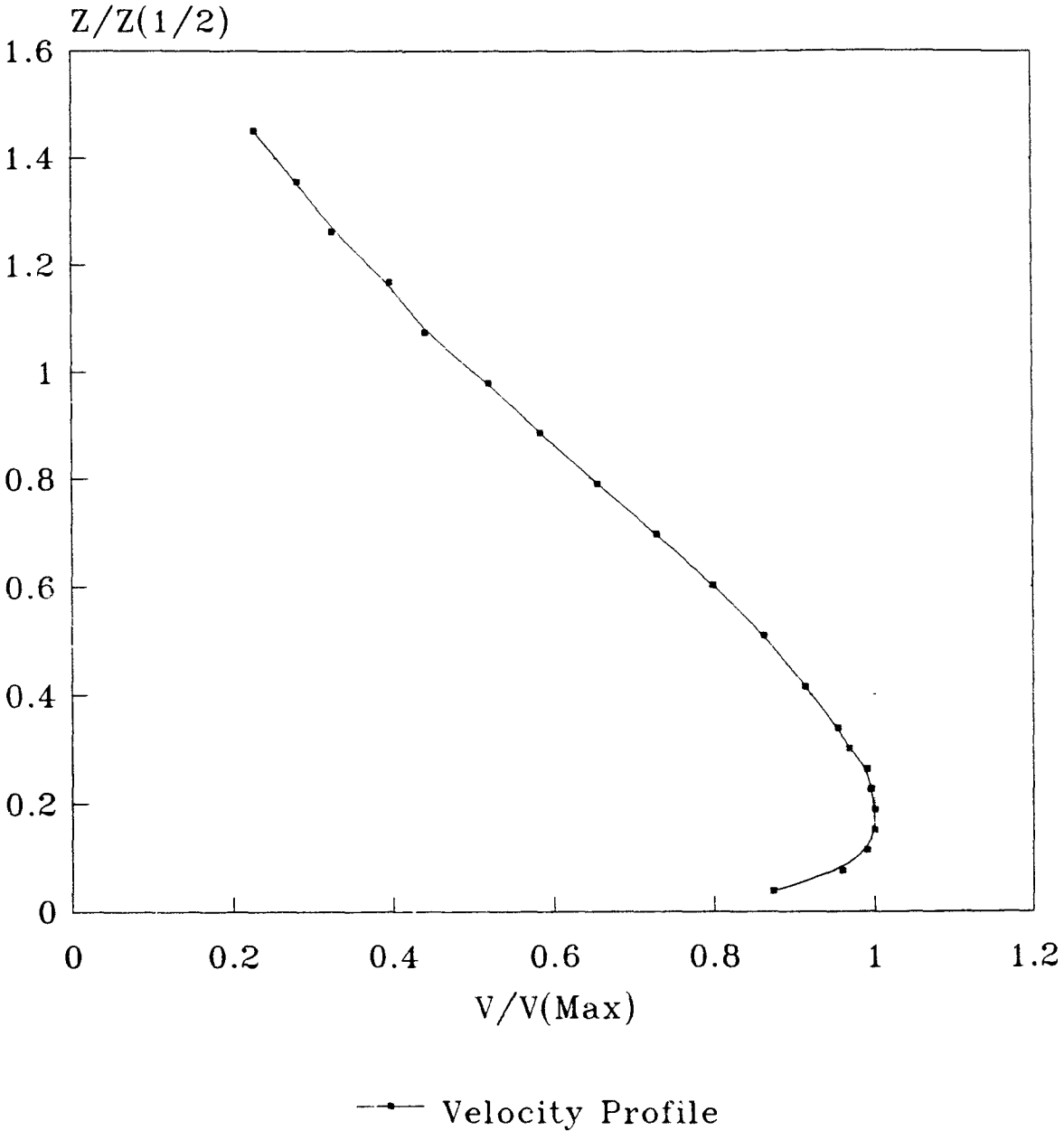

Figure 5-34 Velocity profile of wall jet
Re_d = 48,000, Z_n / D = 10, D = 0.5 in.
2.5 in. from stagnation point

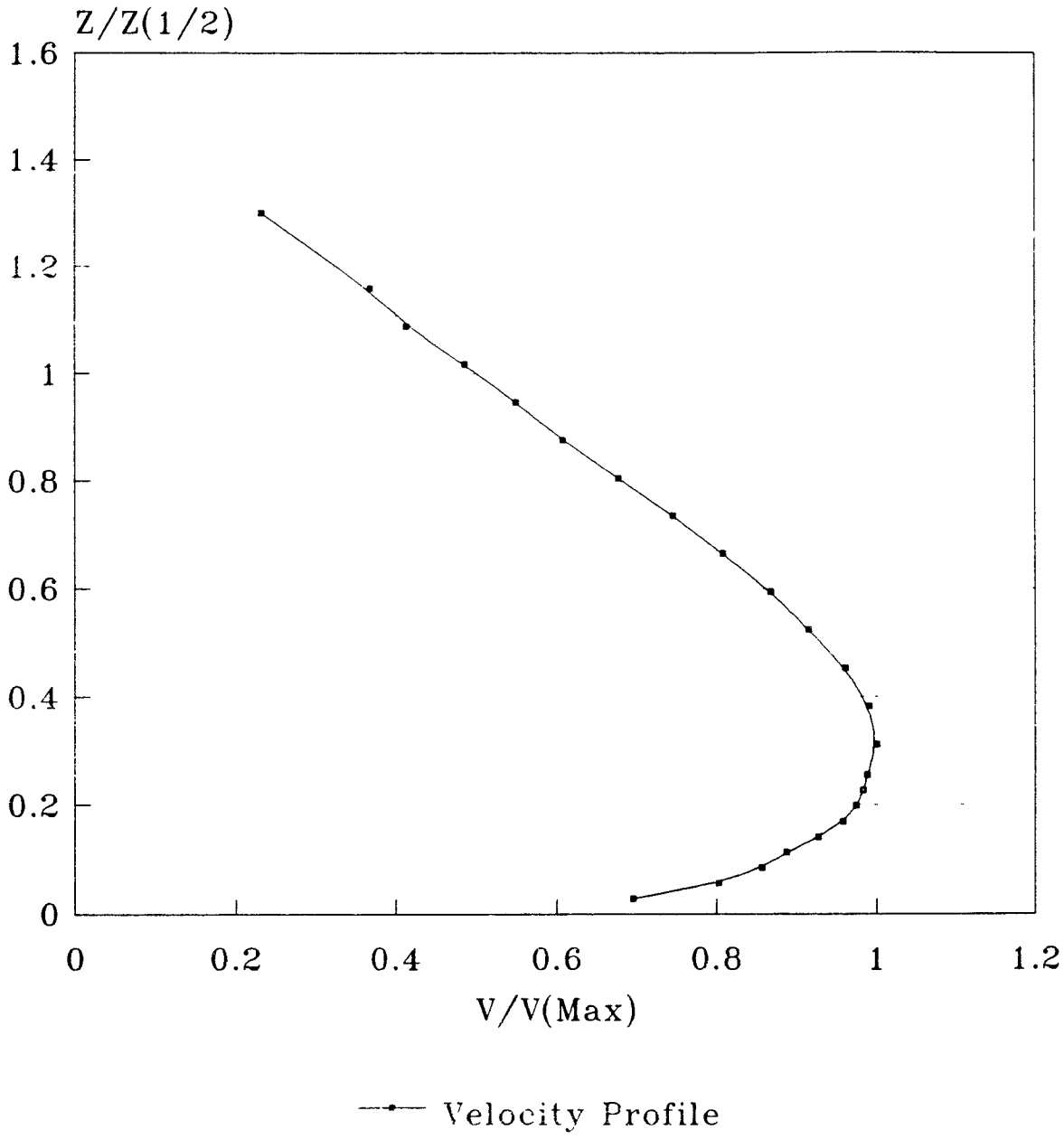

Figure 5-35 Velocity profile of wall jet
Re_d = 48,000, Z_n / D = 10, D = 0.5 in.
2.5 in. from stagnation point, #40 sand paper

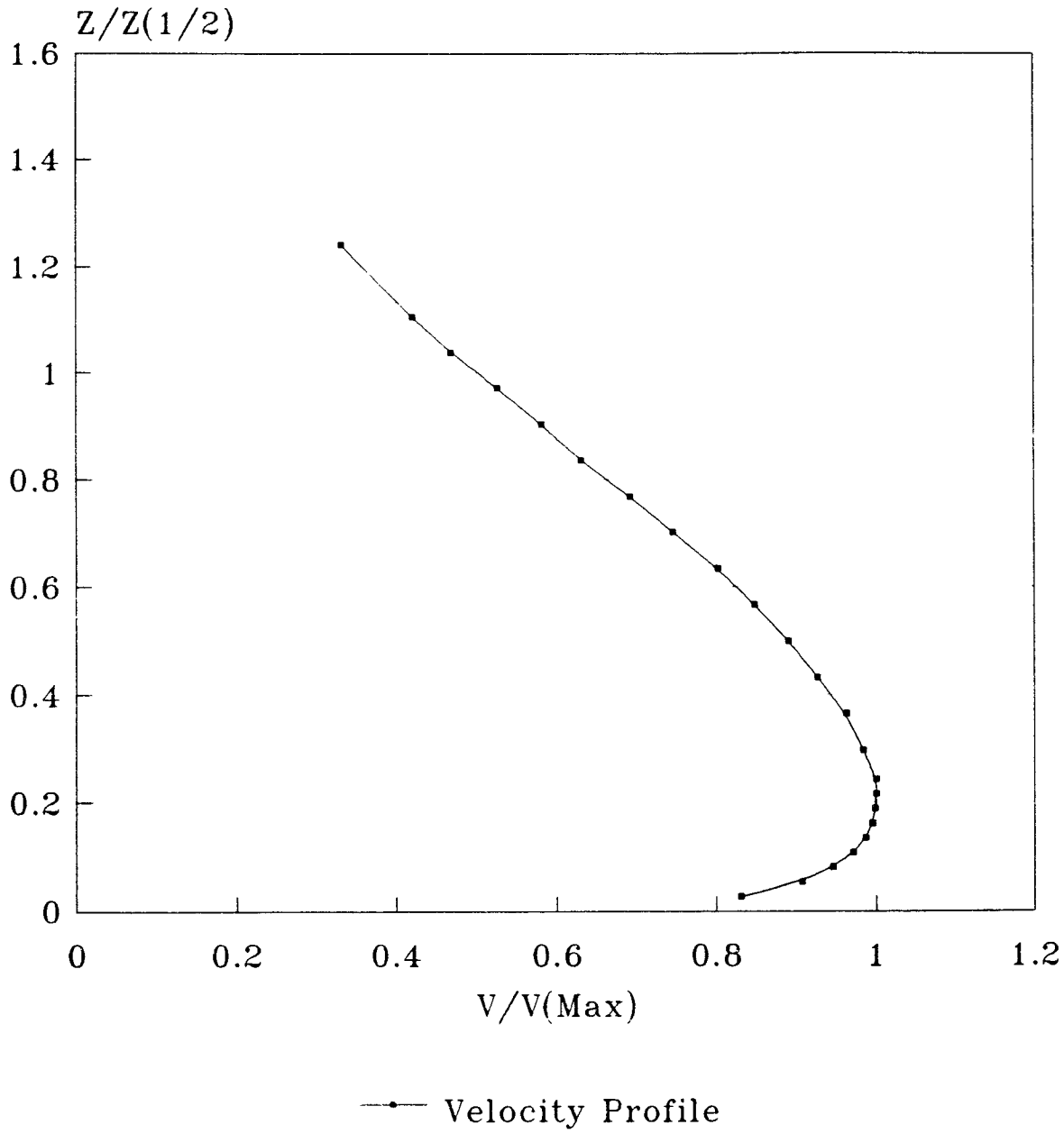

Figure 5-36 Velocity profile of wall jet
Re_d = 68,000, Z_n / D = 10, D = 0.5 in.
3.25 in. from stagnation point

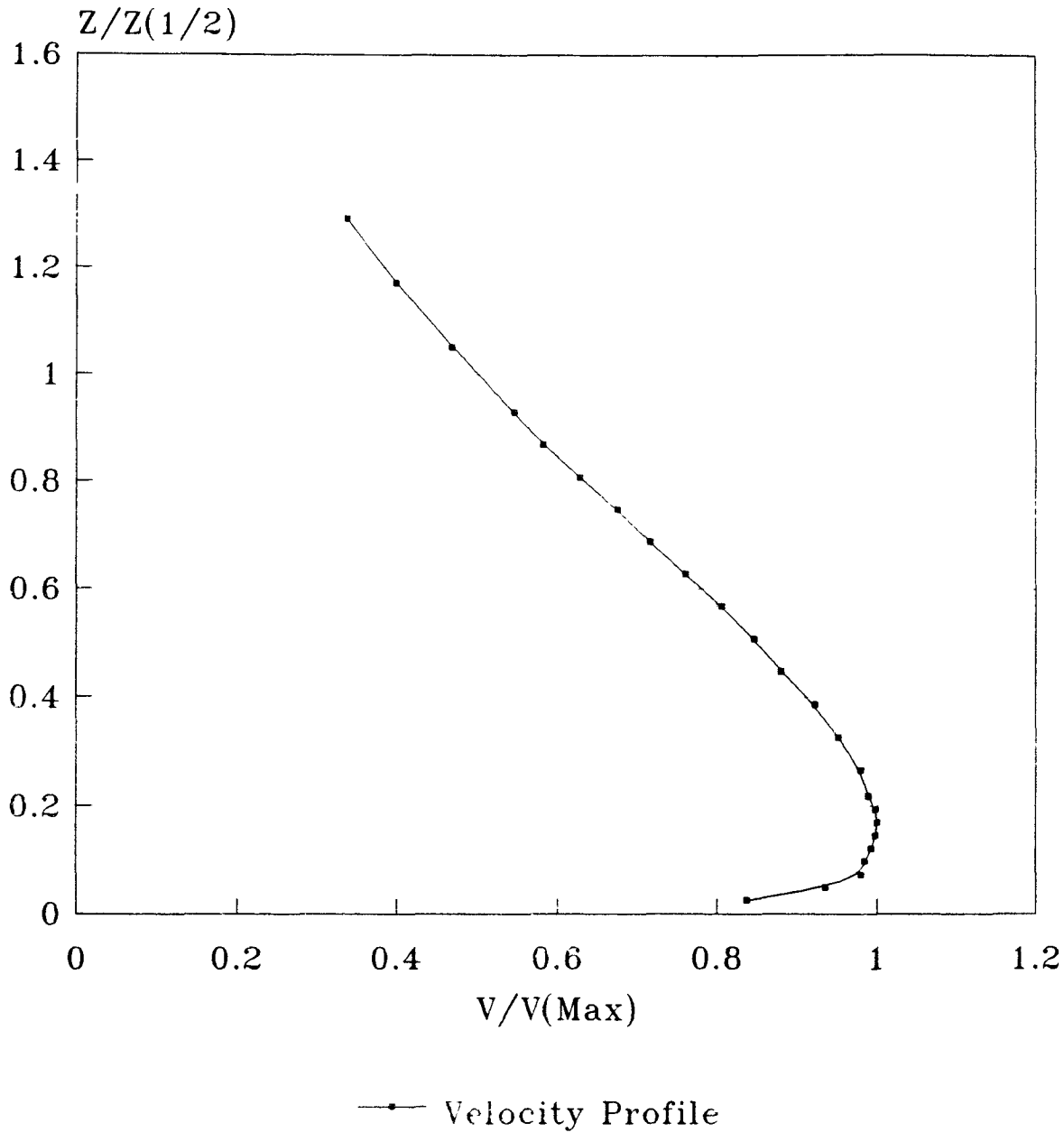

Figure 5-37 Velocity profile of wall jet
Re_d = 60,000, Z_n / D = 20, D = 0.5 in.
3.25 in. from stagnation point

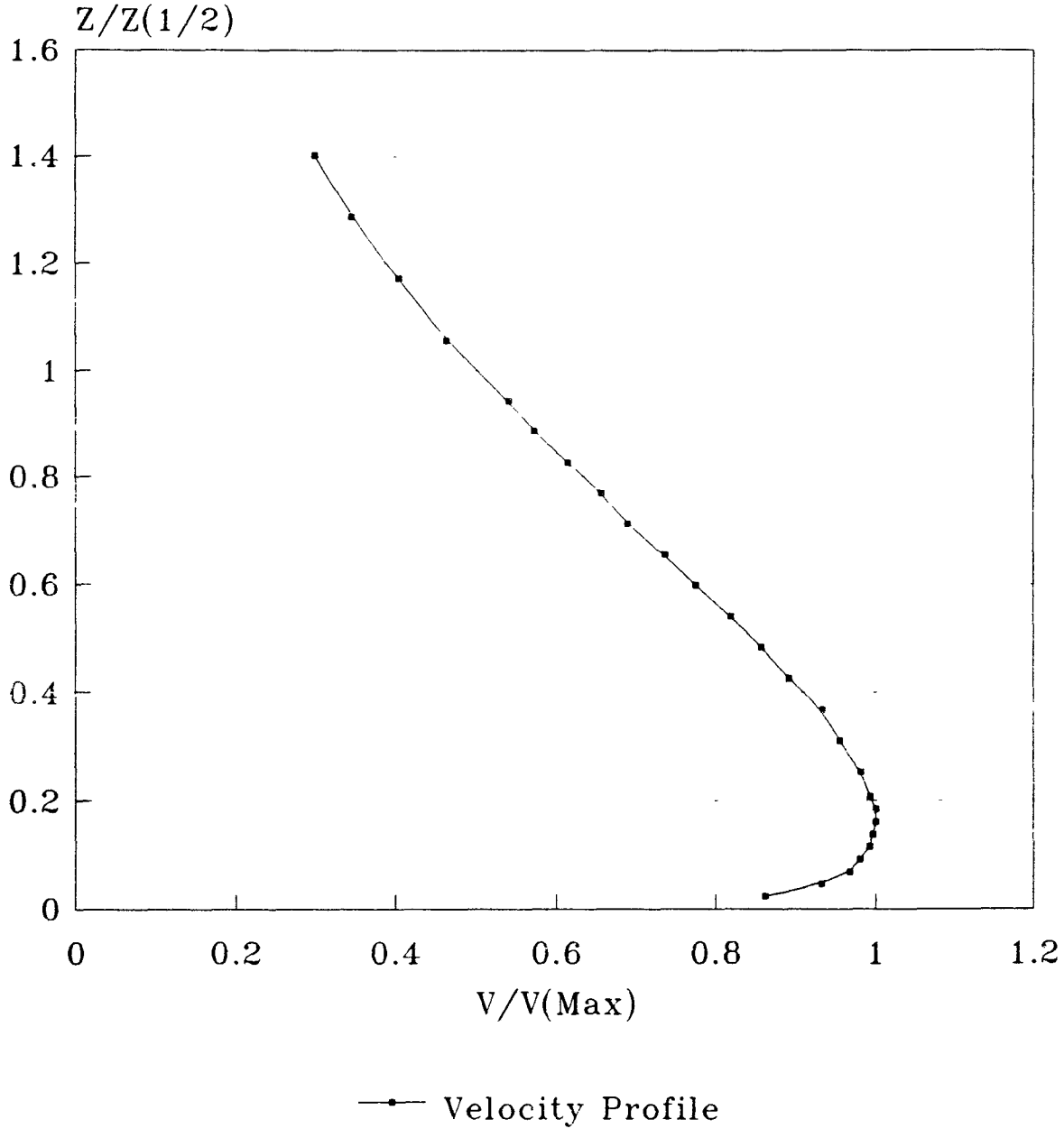

Figure 5-38 Velocity profile of wall jet
$Re_d = 80{,}000$, $Z_n / D = 20$, $D = 0.5$ in.
3.5 in. from stagnation point

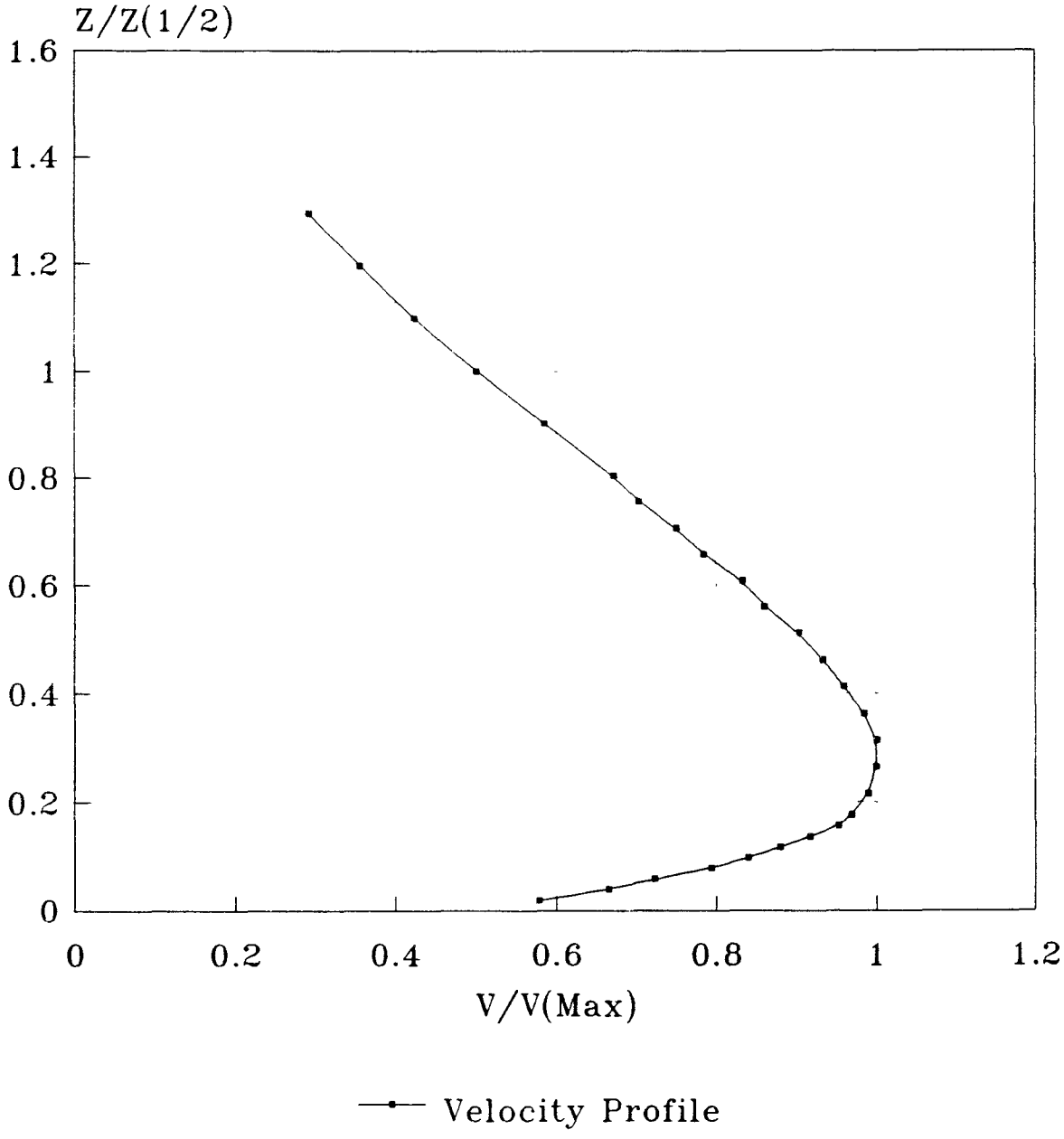

Figure 5-39 Velocity profile of wall jet
Re_d = 80,000, Z_n / D = 20, D = 0.5 in.
3.5 in. from stagnation point, #60 sand paper

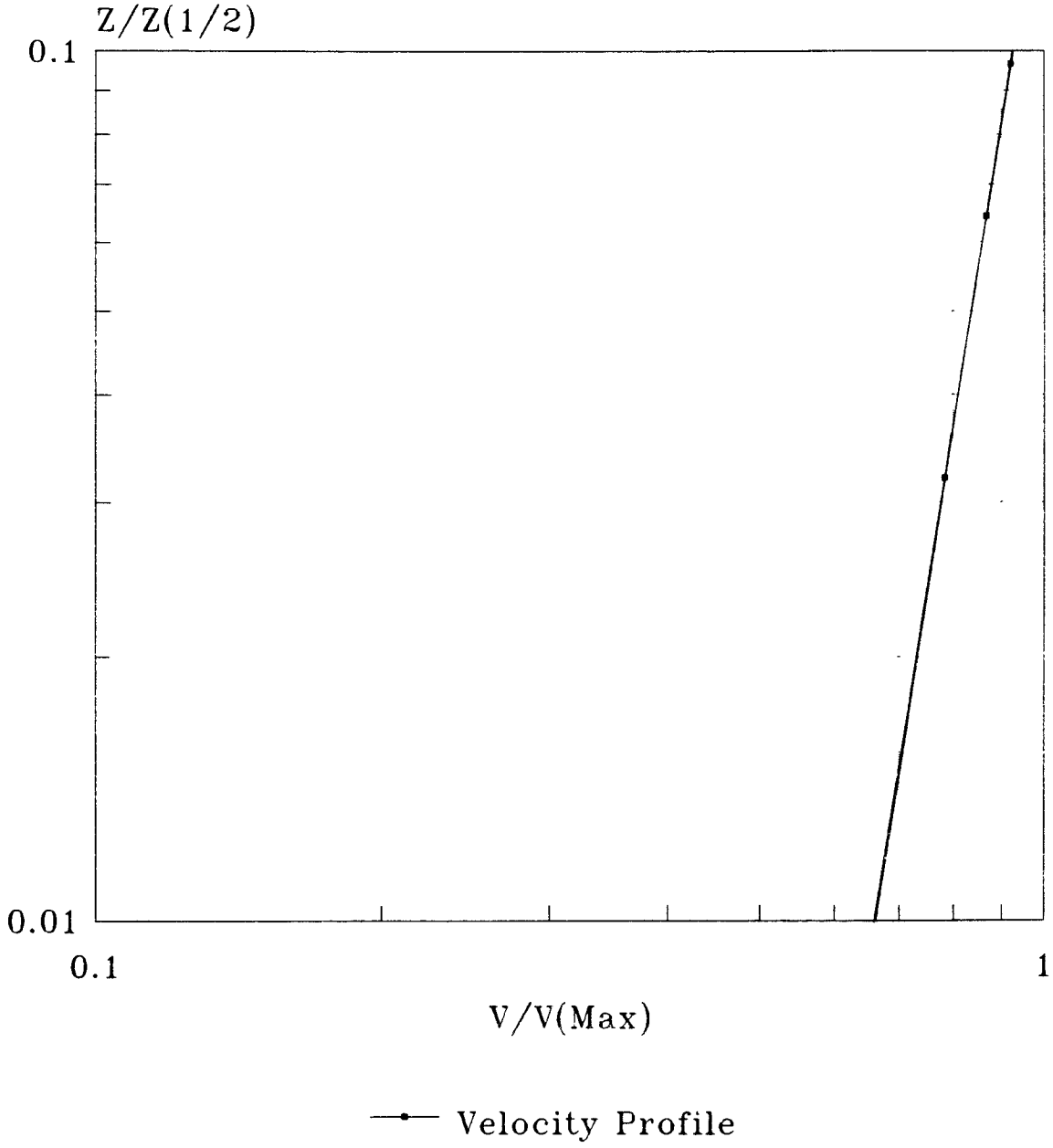

Figure 5-40 Velocity profile of wall jet
Re_d = 40,000, Z_n / D = 4, D = 0.5 in.
2.0 in. from stagnation point

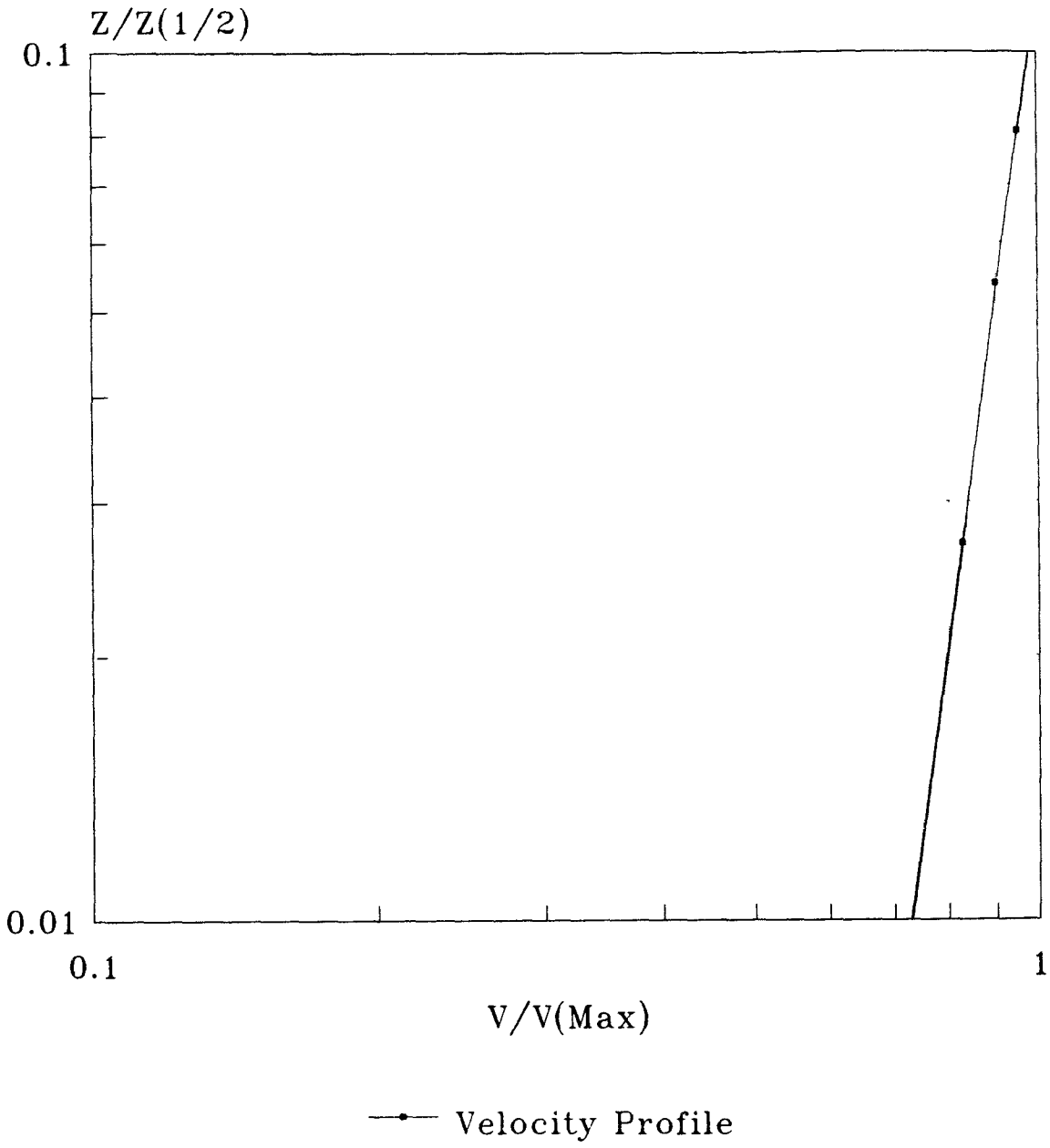

Figure 5-41 Velocity profile of wall jet
Re_d = 64,000, Z_n / D = 4, D = 0.5 in.
3.0 in. from stagnation point

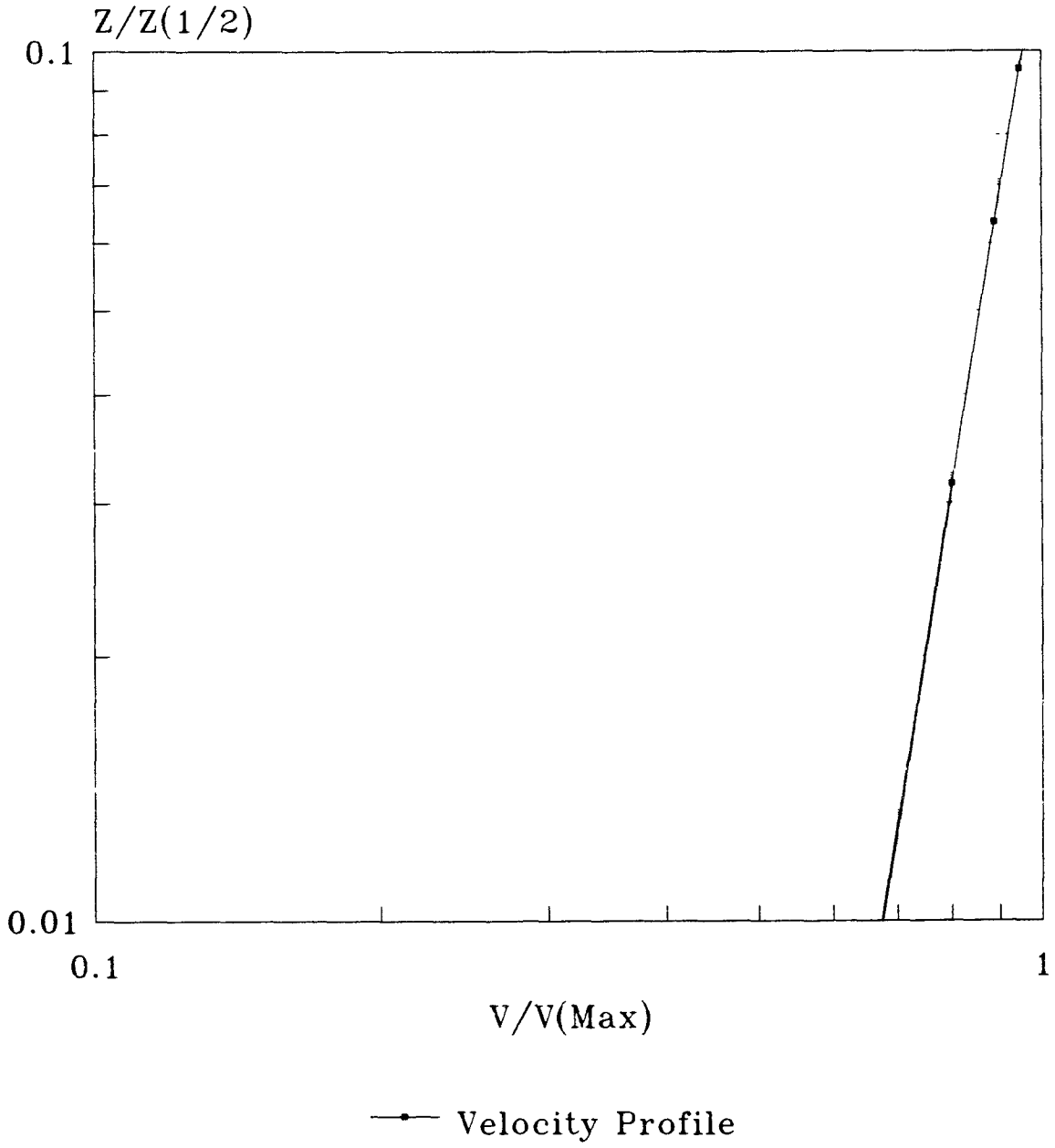

Figure 5-42 Velocity profile of wall jet
Re_d = 44,000, Z_n / D = 7, D = 0.5 in.
2.5 in. from stagnation point

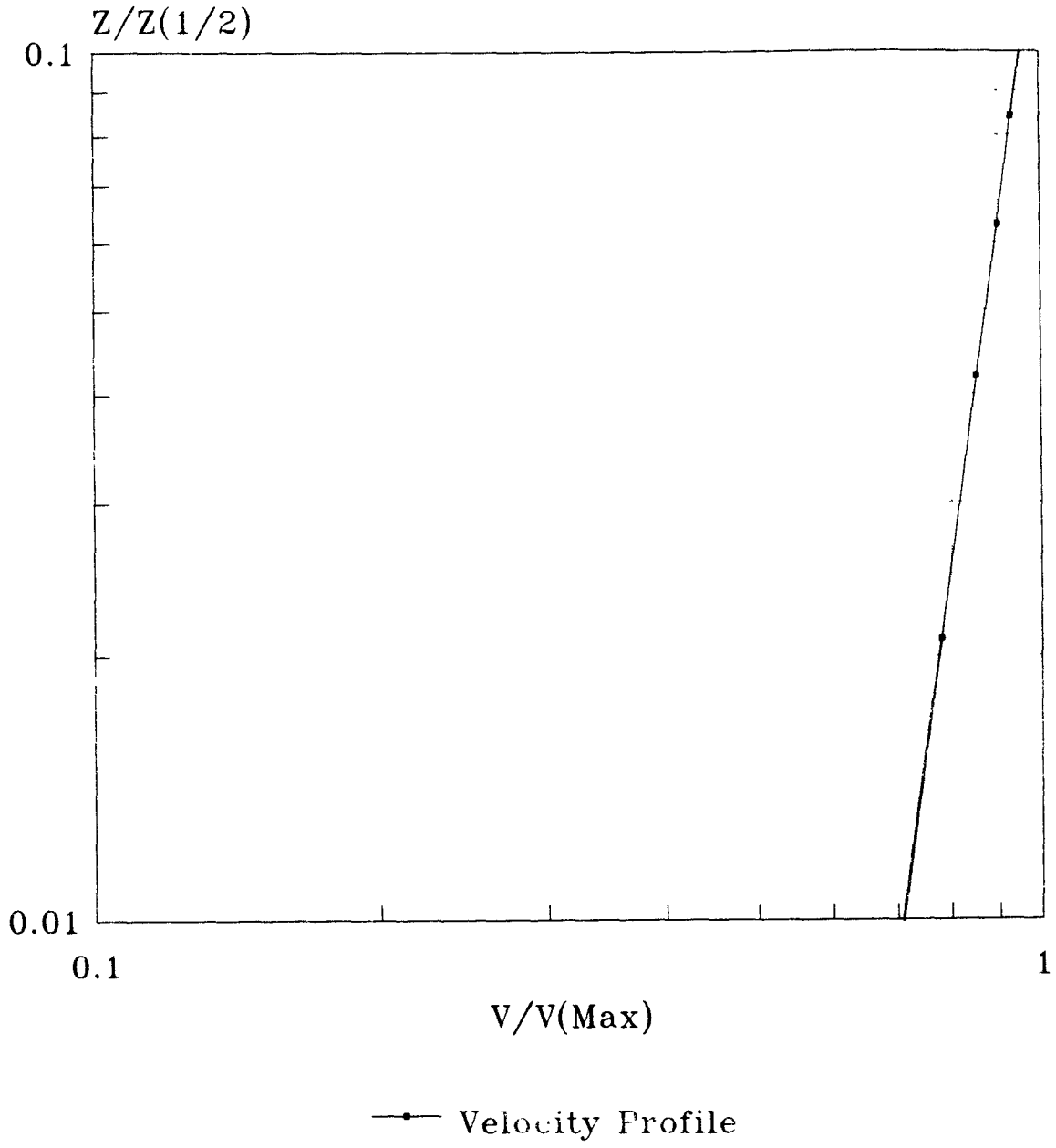

Figure 5-43 Velocity profile of wall jet
Re_d = 67,000, $Z_n / D = 7$, D = 0.5 in.
3.5 in. from stagnation point

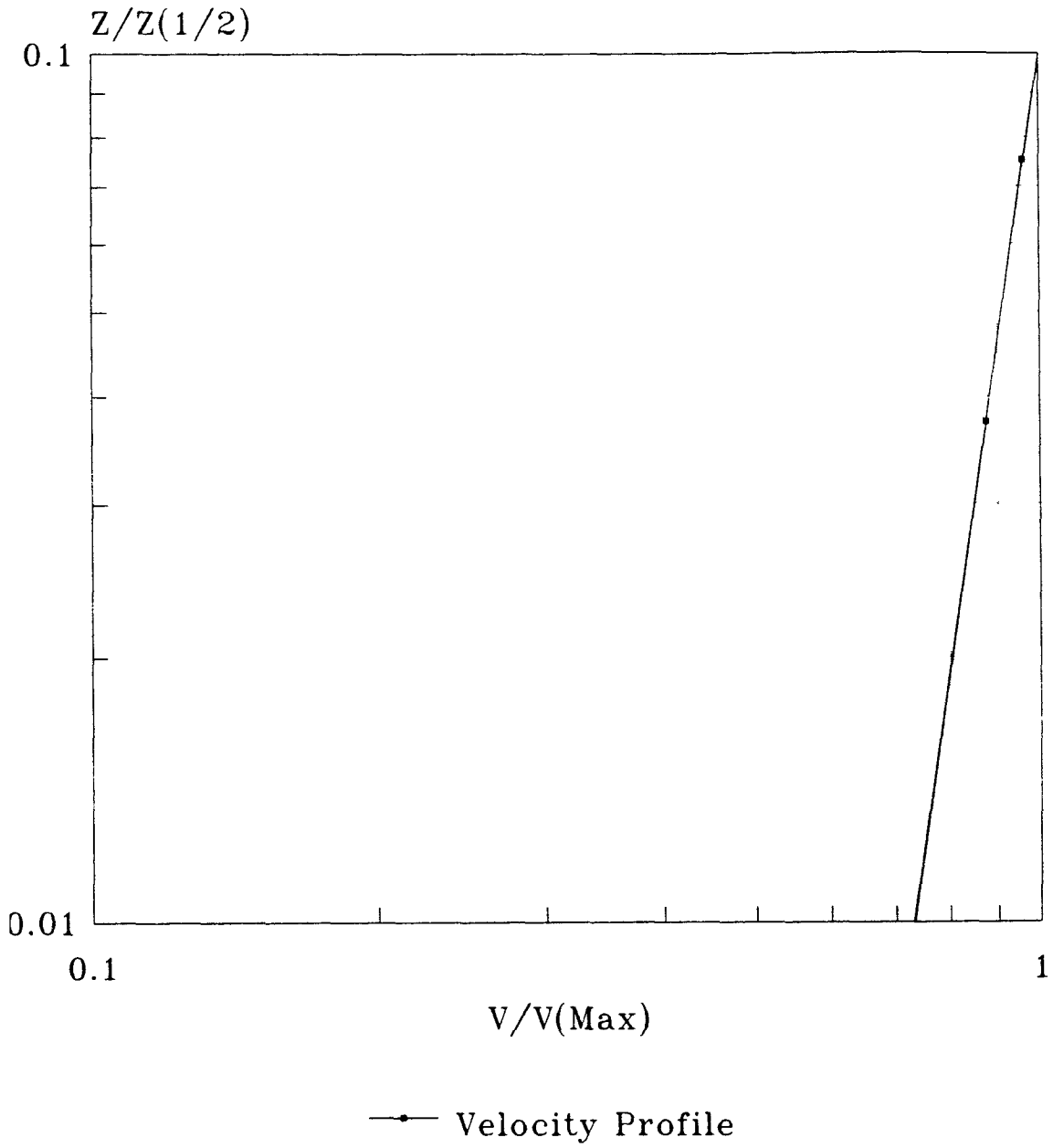

Figure 5-44 Velocity profile of wall jet
$Re_d = 48{,}000$, $Z_n / D = 10$, $D = 0.5$ in.
2.5 in. from stagnation point

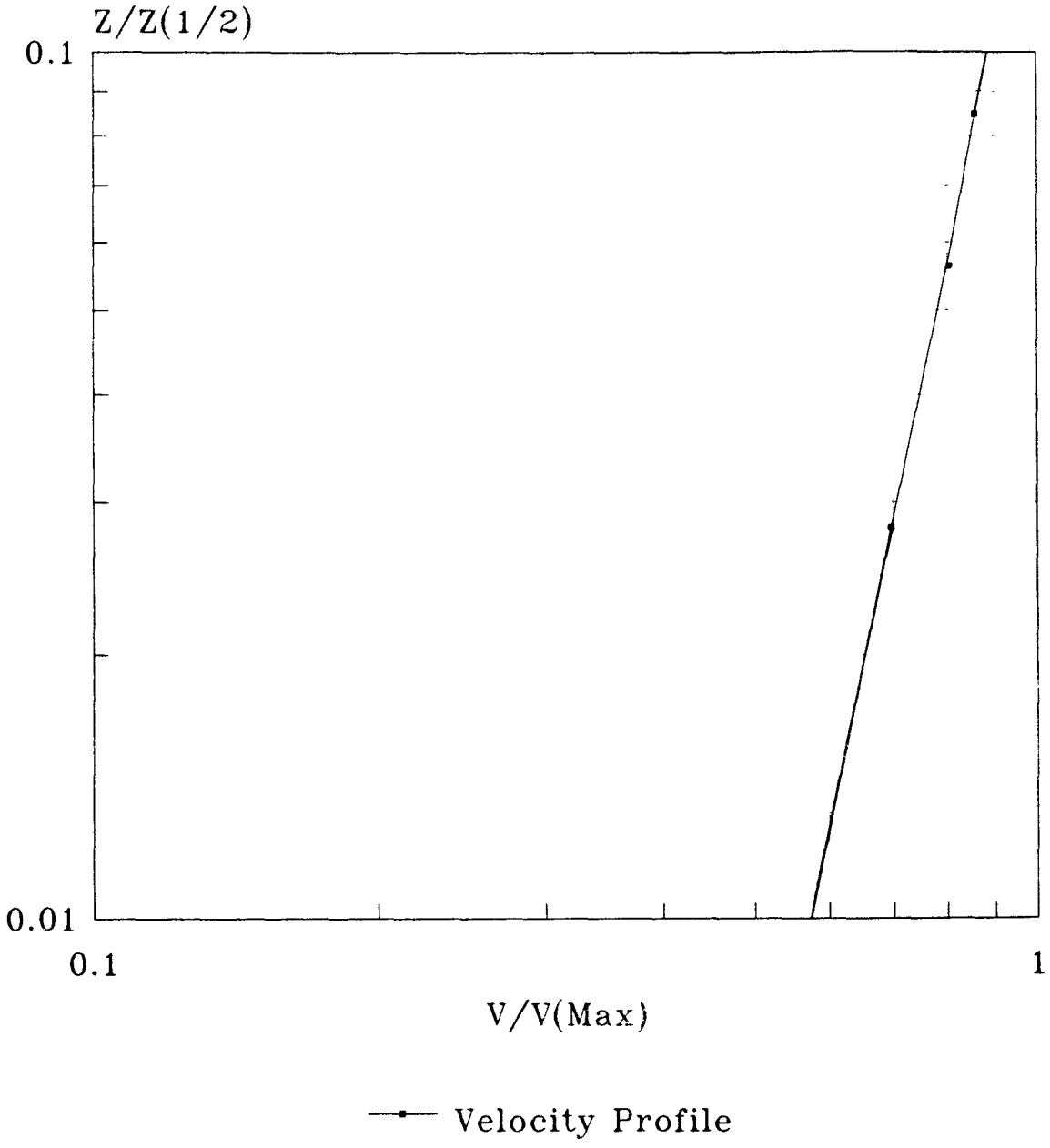

Figure 5-45 Velocity profile of wall jet
Re_d = 48,000, Z_n / D = 10, D = 0.5 in.
2 5 in. from stagnation point, #40 sand paper

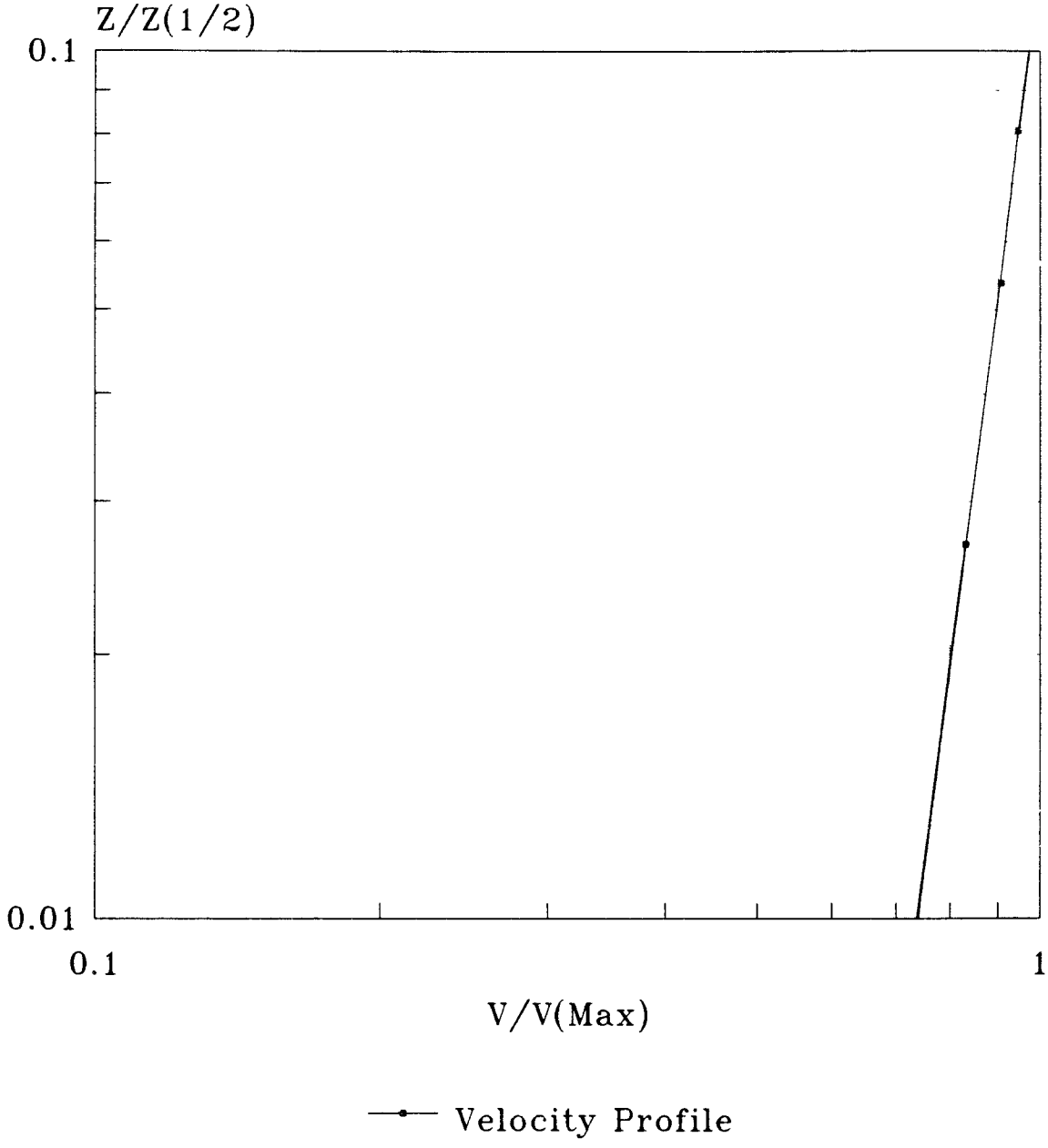

Figure 5-46 Velocity profile of wall jet
Re_d = 68,000, Z_n / D = 10, D = 0.5 in.
3.25 in. from stagnation point

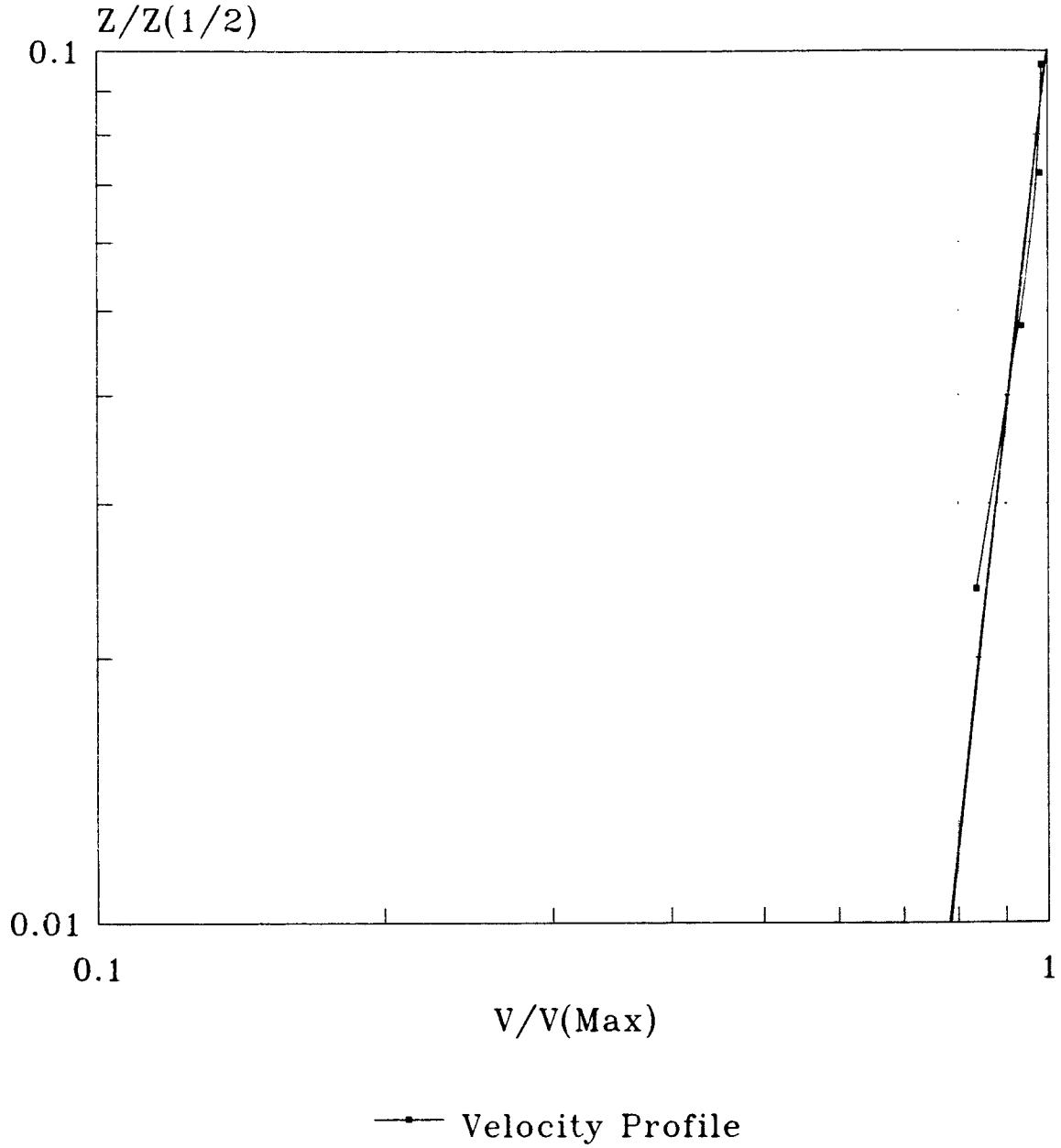

Figure 5-47 Velocity profile of wall jet
Re_d = 60,000, Z_n / D = 20, D = 0.5 in.
3.25 in from stagnation point

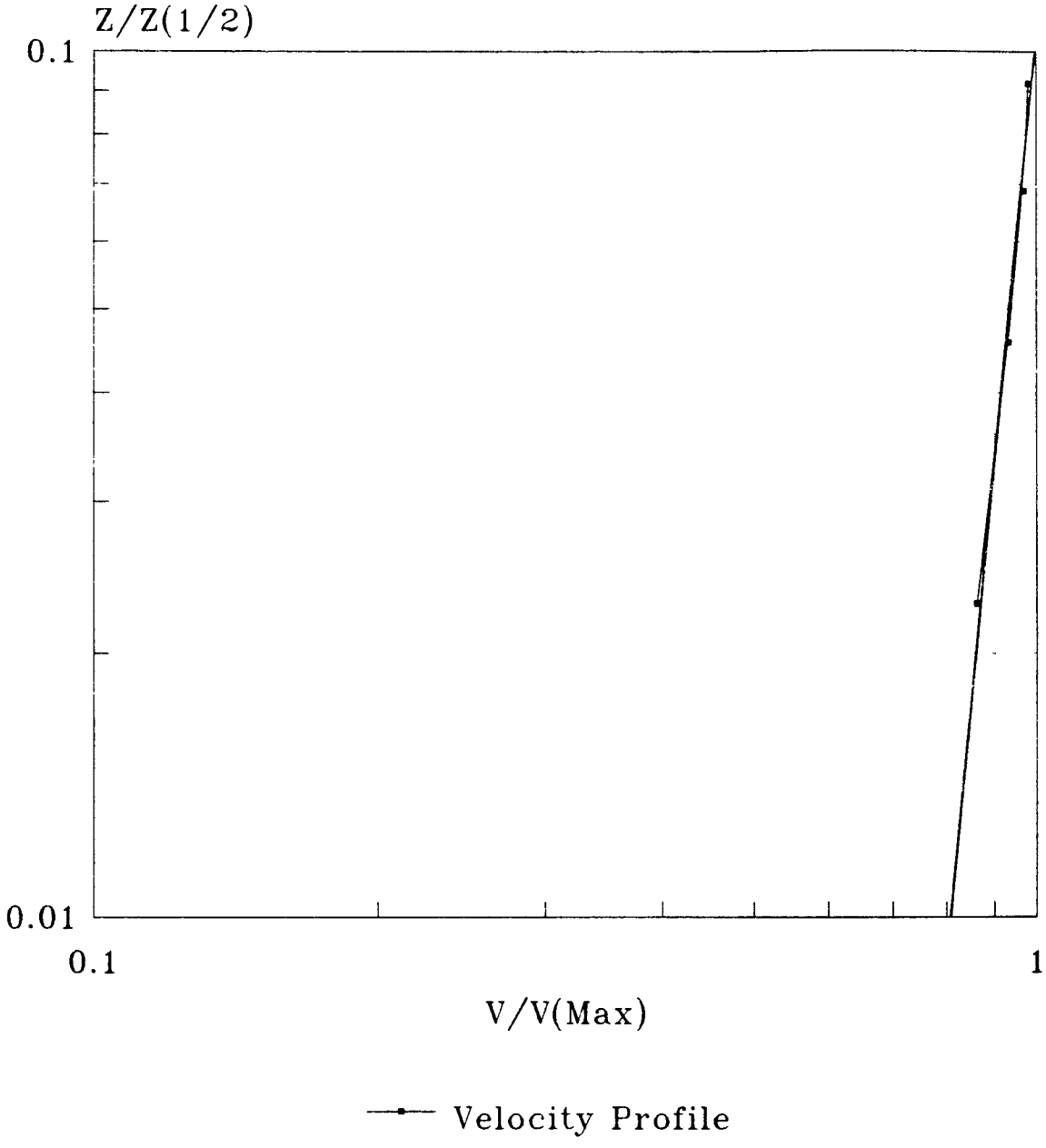

Figure 5-48 Velocity profile of wall jet
Re_d = 80,000, $Z_n / D = 20$, D = 0.5 in.
3.5 in. from stagnation point

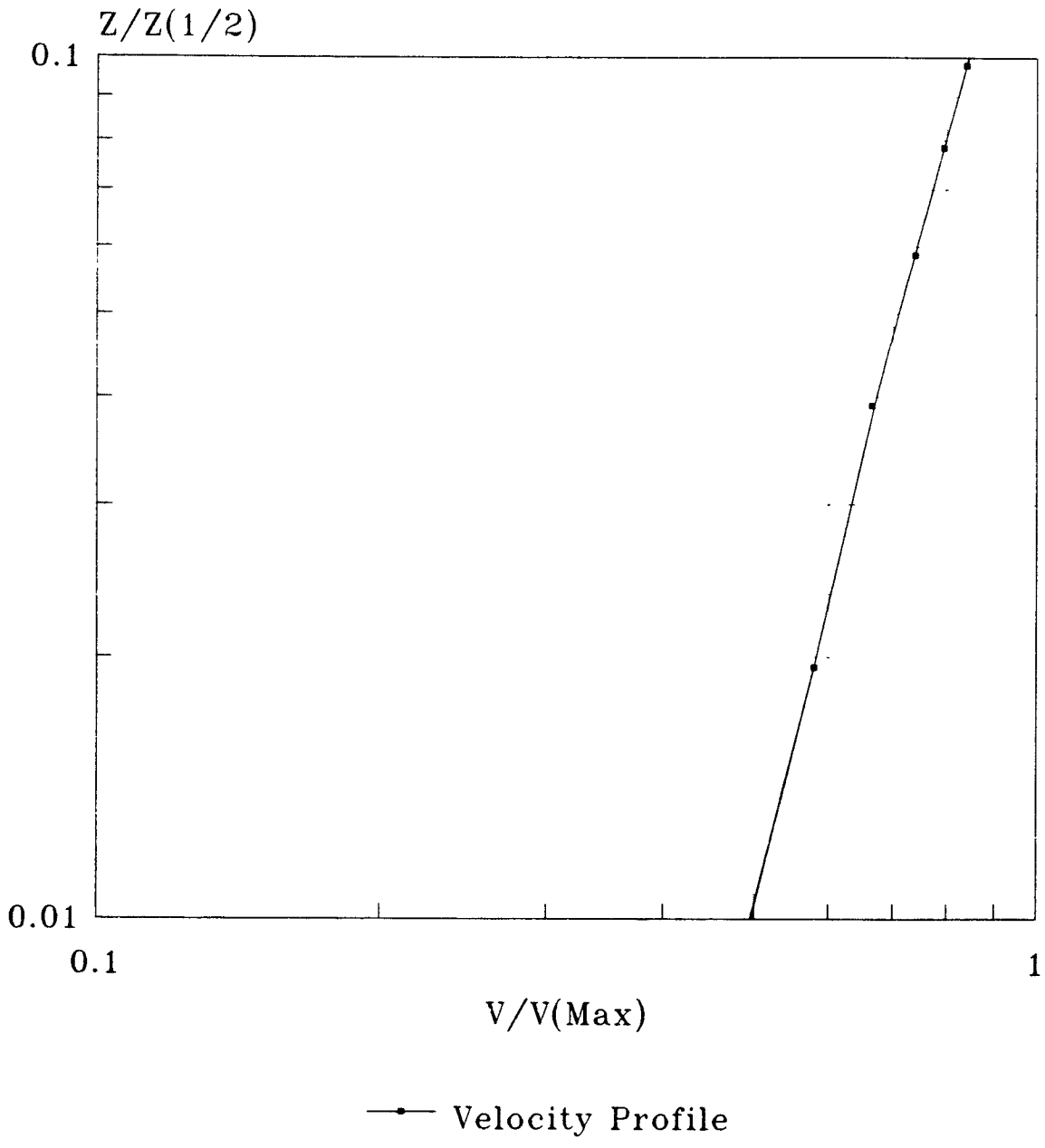

Figure 5-49 Velocity profile of wall jet
Re_d = 80.000, Z_n / D = 20, D = 0.5 in.
3.5 in. from stagnation point, #60 sand paper

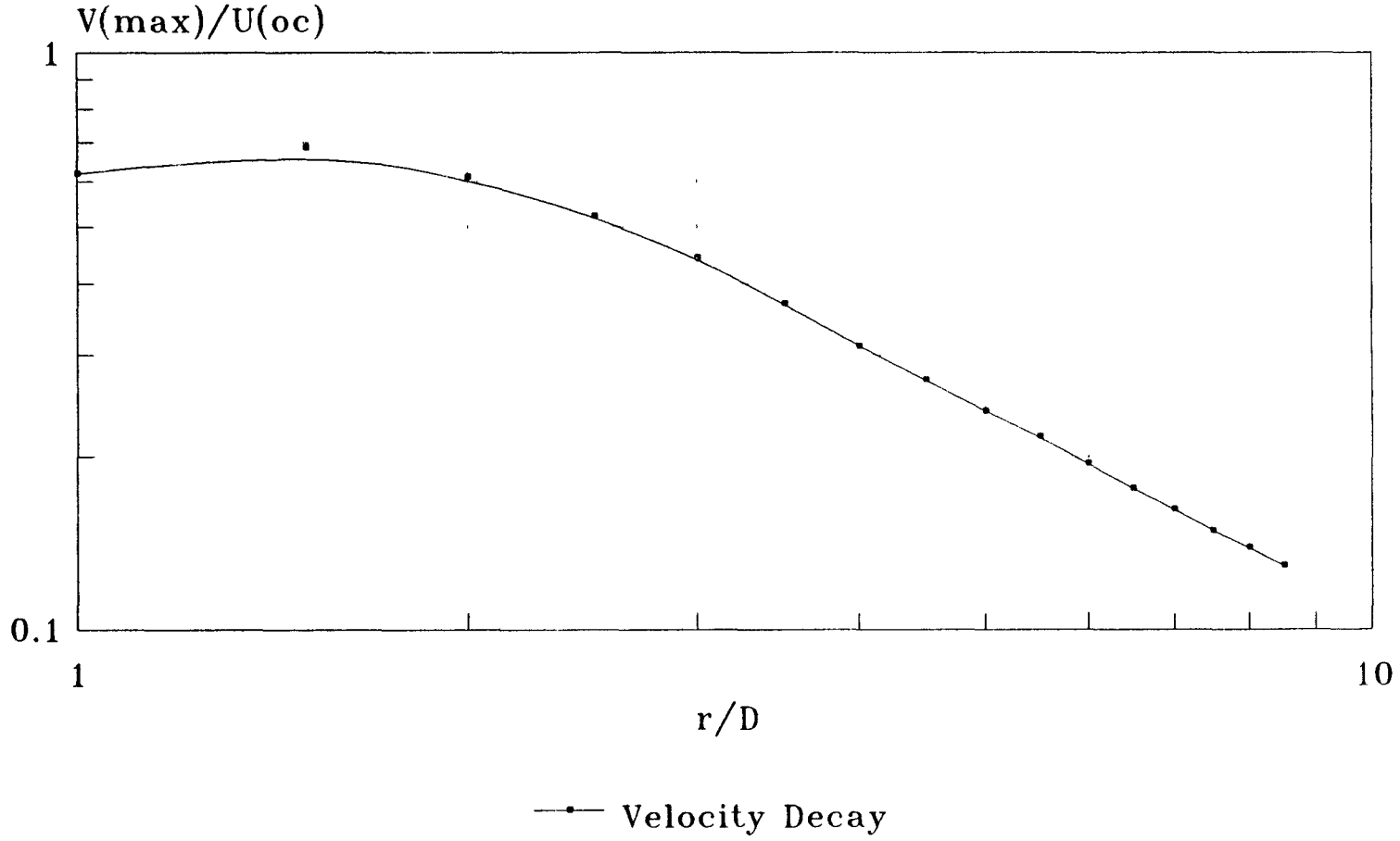

Figure 5-50 Maximum velocity decay along the flat plate for $Re_d = 40{,}000$, $Z_n / D = 4$, $D = 0.5$ in.

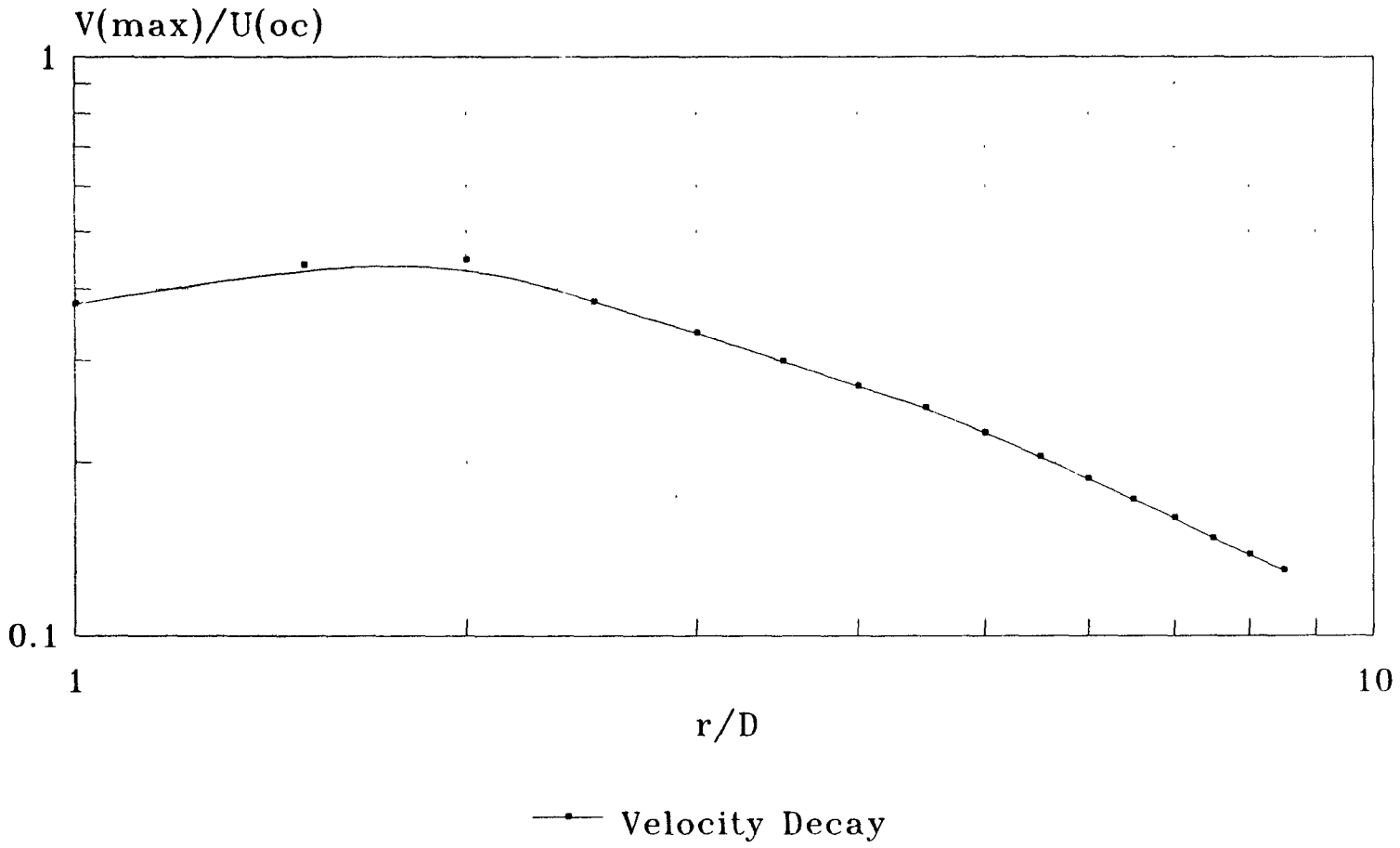

Figure 5-51 Maximum velocity decay along the flat plate for $Re_d = 44{,}000$, $Z_n / D = 7$, $D = 0.5$ in.

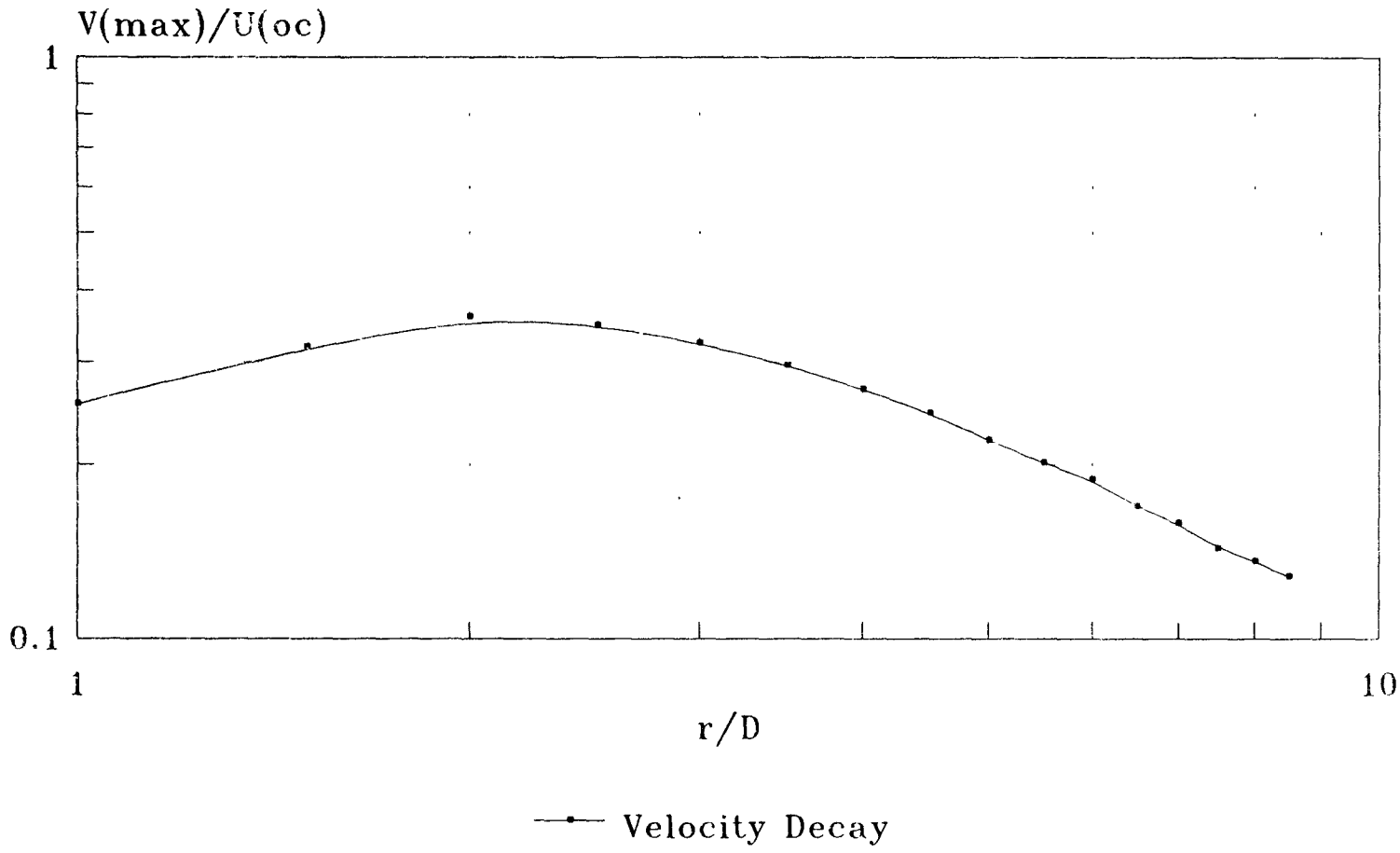

Figure 5-52 Maximum velocity decay along the flat plate for $Re_d = 48{,}000$, $Z_n / D = 10$, $D = 0.5$ in.

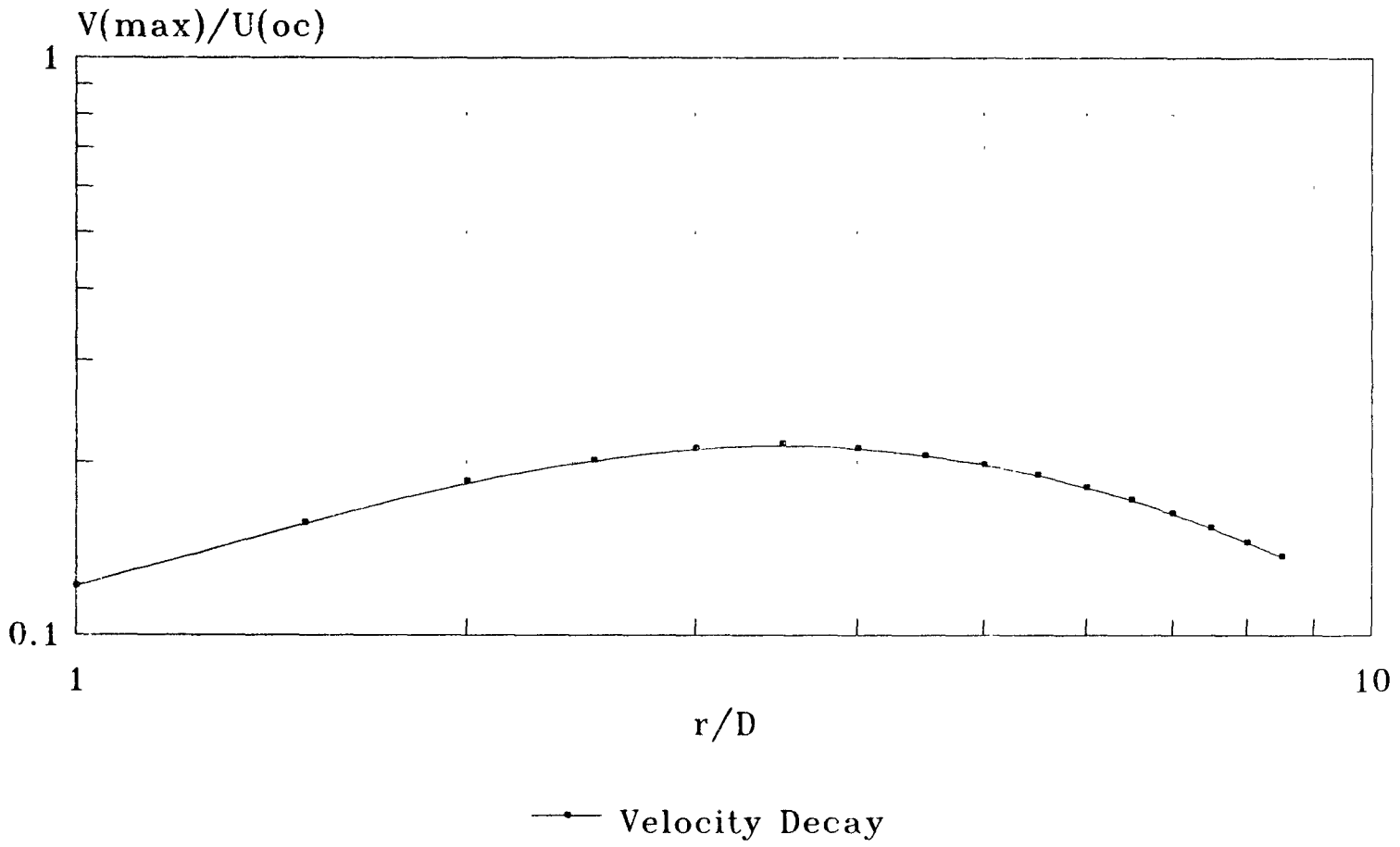

Figure 5-53 Maximum velocity decay along the flat plate for Re_d = 60,000, Z_n / D = 20, D = 0.5 in.

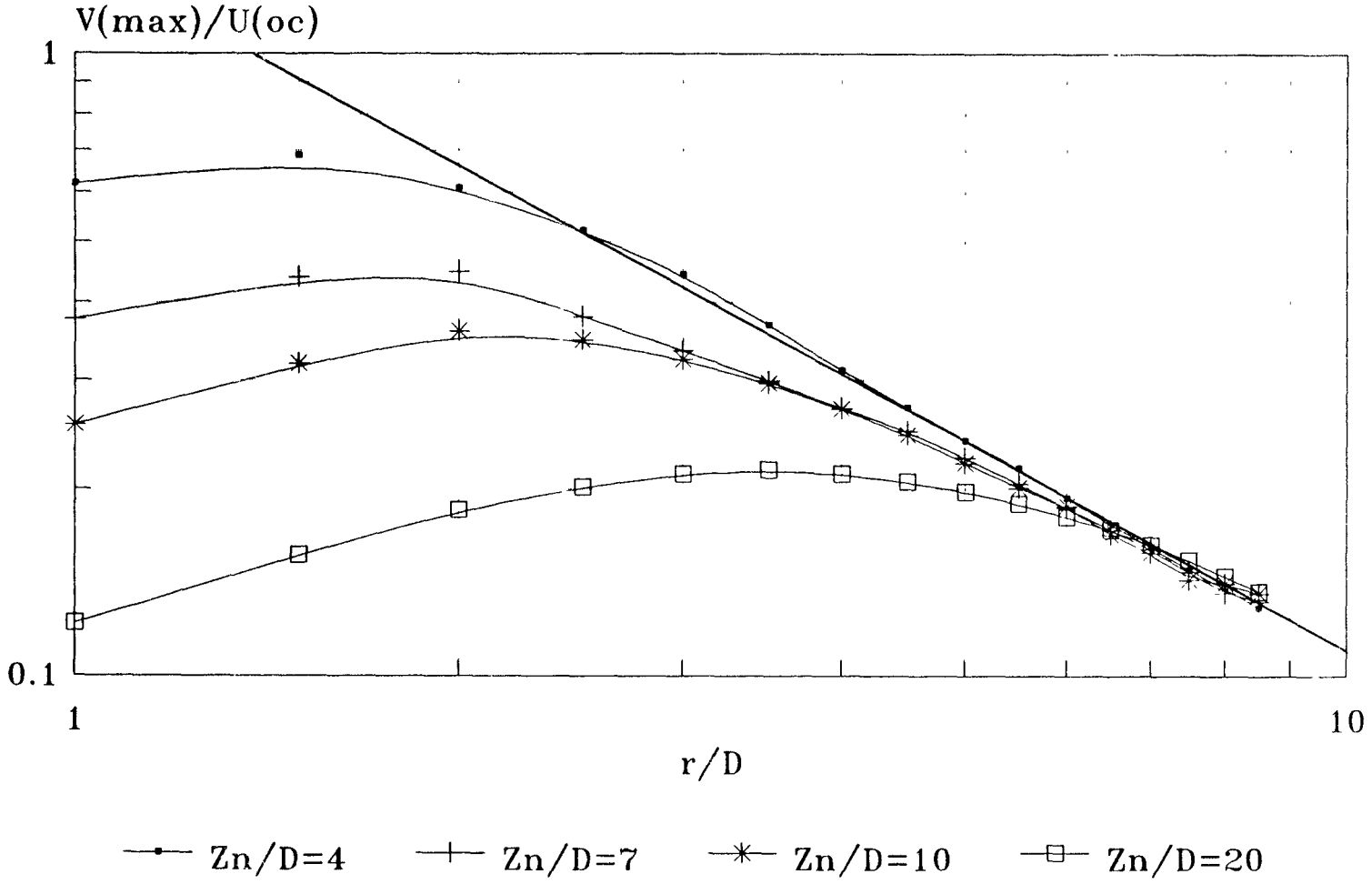

Figure 5-54 Maximum velocity decay along the flat plate for varied Z_n / D, D = 0.5 in.

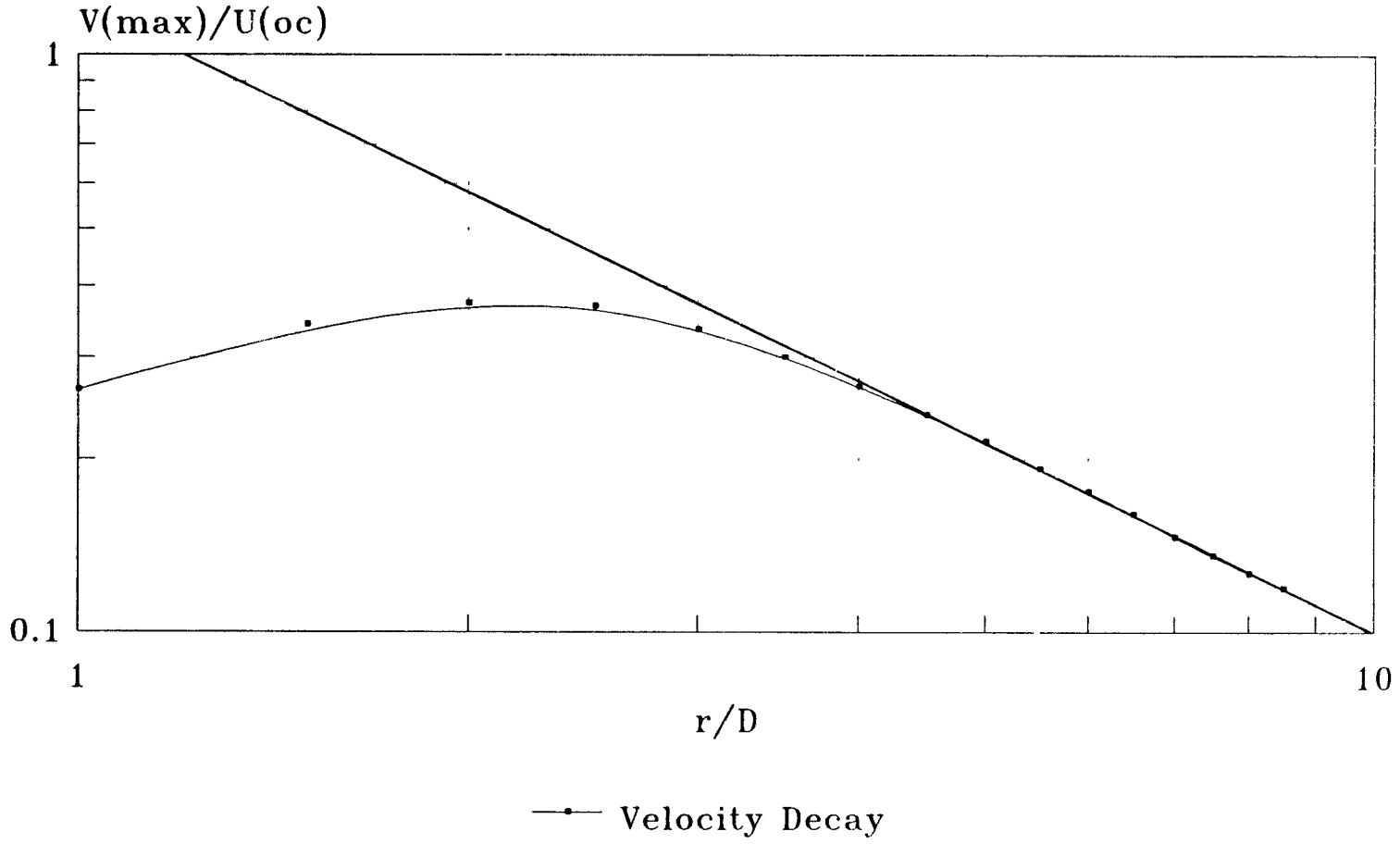

Figure 5-55 Maximum velocity decay along the flat plate for Re_d = 48,000, Z_n / D = 10, D = 0.5 in., #40 sand paper covered

5.4 Measurement of Boundary Layer Thickness Along the Flat Plate

To measure boundary layer thickness in the present experiment is quite difficult. However, the approximate variations of the boundary layer along the flat plate from the stagnation point to a further distance away had been investigated and the results are shown in Figure 5-56 through 5-60.

Theoretically, the boundary layer thickness at the stagnation point is given by,

$$\frac{\delta}{D} = \frac{1.98}{\sqrt{a^* \cdot Re_d}}$$

It is found, that in Figure 5-60, the results at the stagnation point are 20% to 45% greater than the values expected by the above equation. The boundary layer thickness is found to be constant until r / D = 1.

The boundary layer growth in the fully turbulent region away from the stagnation point, as given by Figure 5-60 is,

$$\frac{\delta}{D} = 0.0171 \cdot \left(\frac{r}{D}\right)^{0.949} \tag{37}$$

According to Lee [14], the boundary layer away from the stagnation point was given by the equation,

$$\frac{\delta}{D} = 0.0175 \cdot \left(\frac{r}{D}\right)^{0.95} \tag{38}$$

Thus, Figure 5-60 gives an accurate representation of the boundary layer growth, away from the stagnation point.

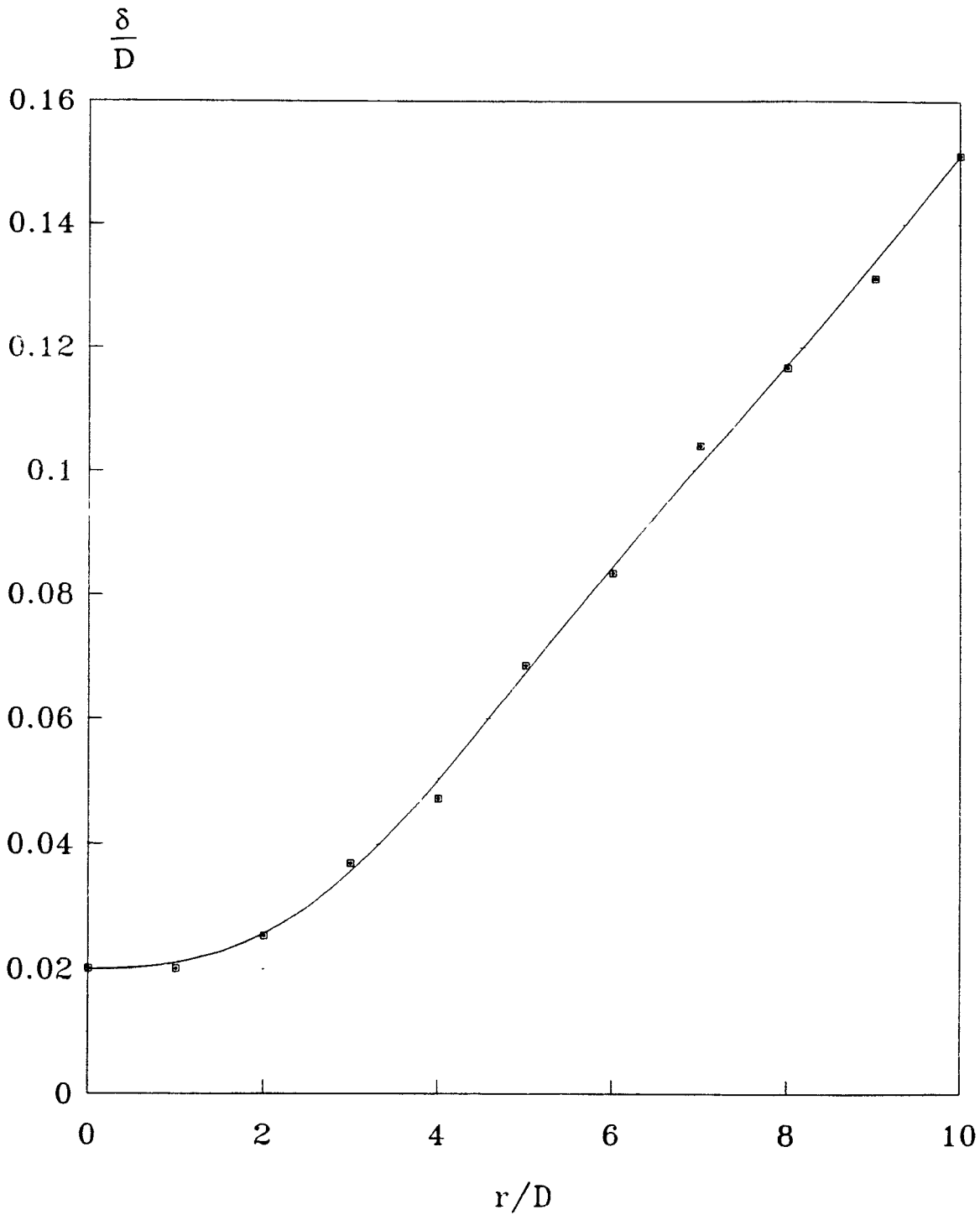

Figure 5-56 Boundary layer thickness
Re_a = 48,000, Z_n / D = 4, D = 0.5 in.

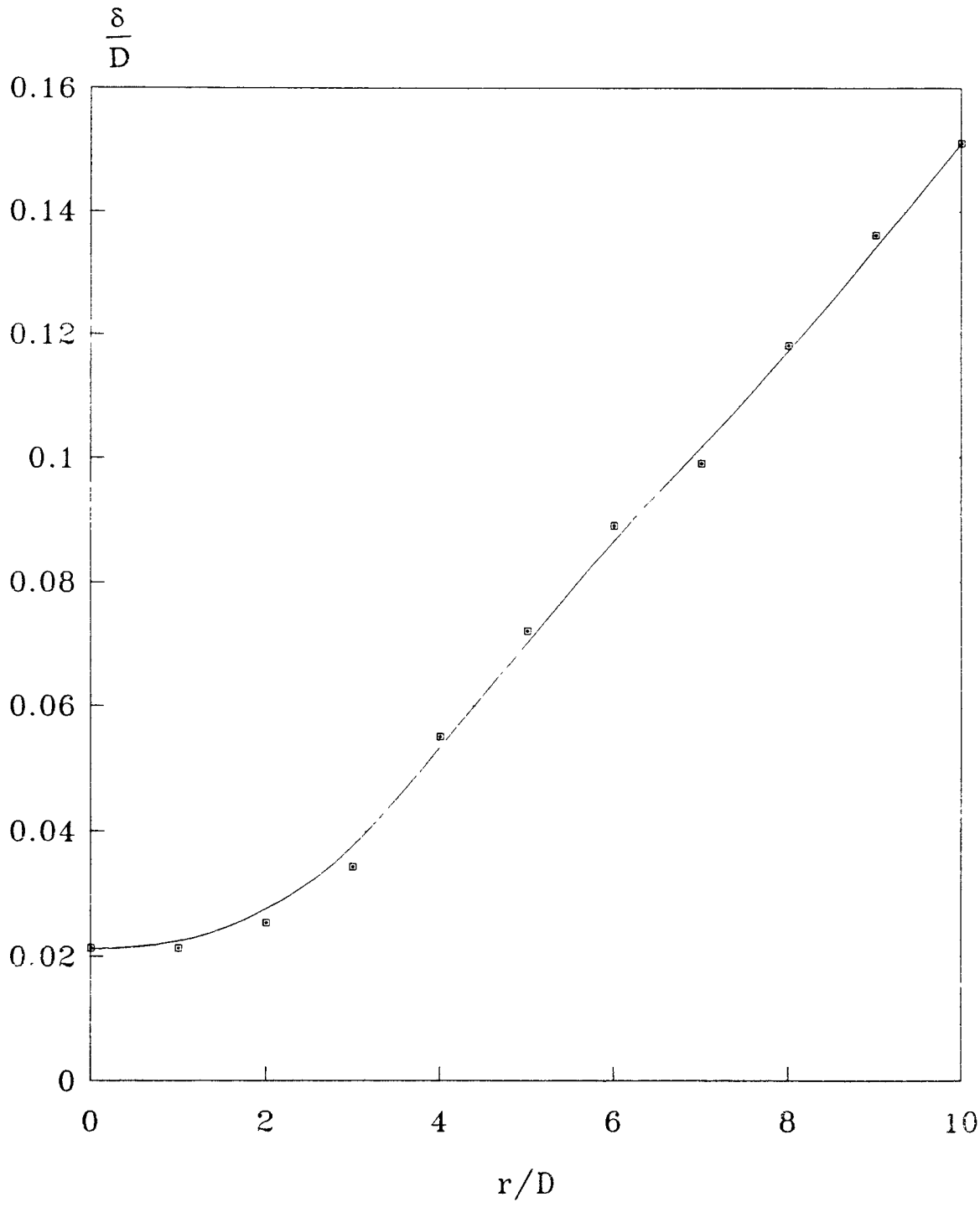

Figure 5-57 Boundary layer thickness
Re_d = 48,000, Z_n / D = 7, D = 0.5 in.

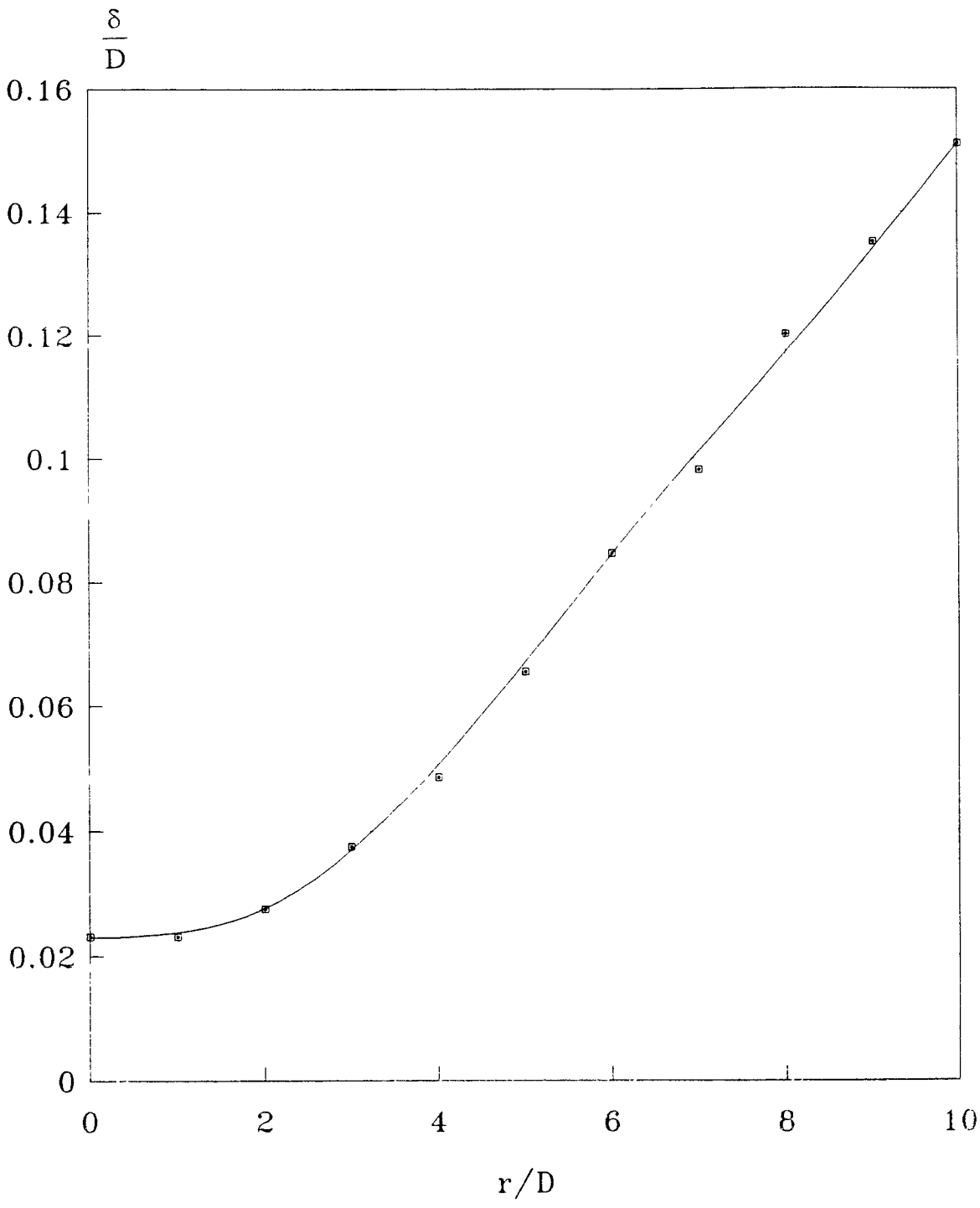

Figure 5-58 Boundary layer thickness
$Re_d = 48{,}000$, $Z_n / D = 10$, $D = 0.5$ in.

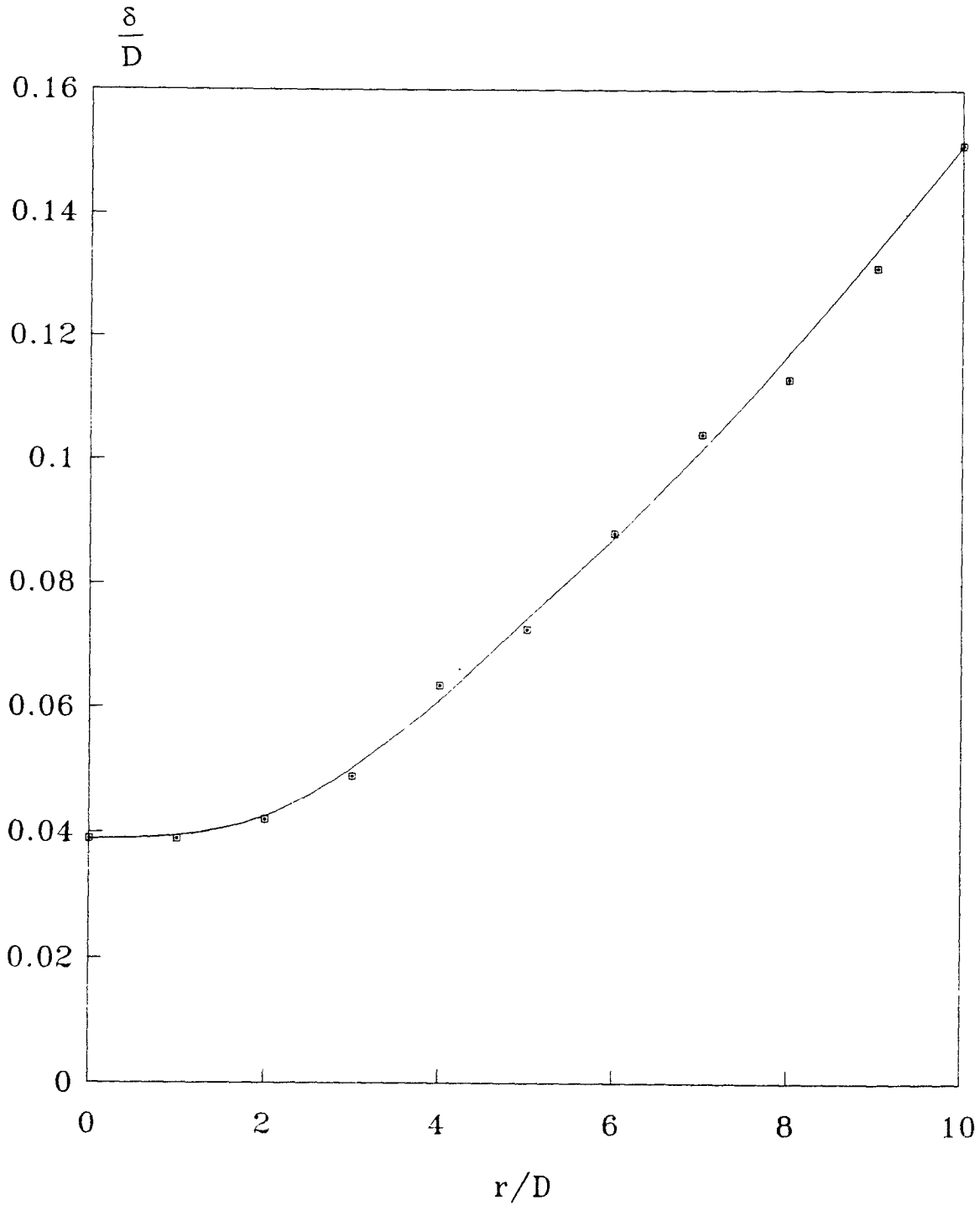

Figure 5-59 Boundary layer thickness
Re_d = 48,000, Z_n / D = 20, D = 0.5 in.

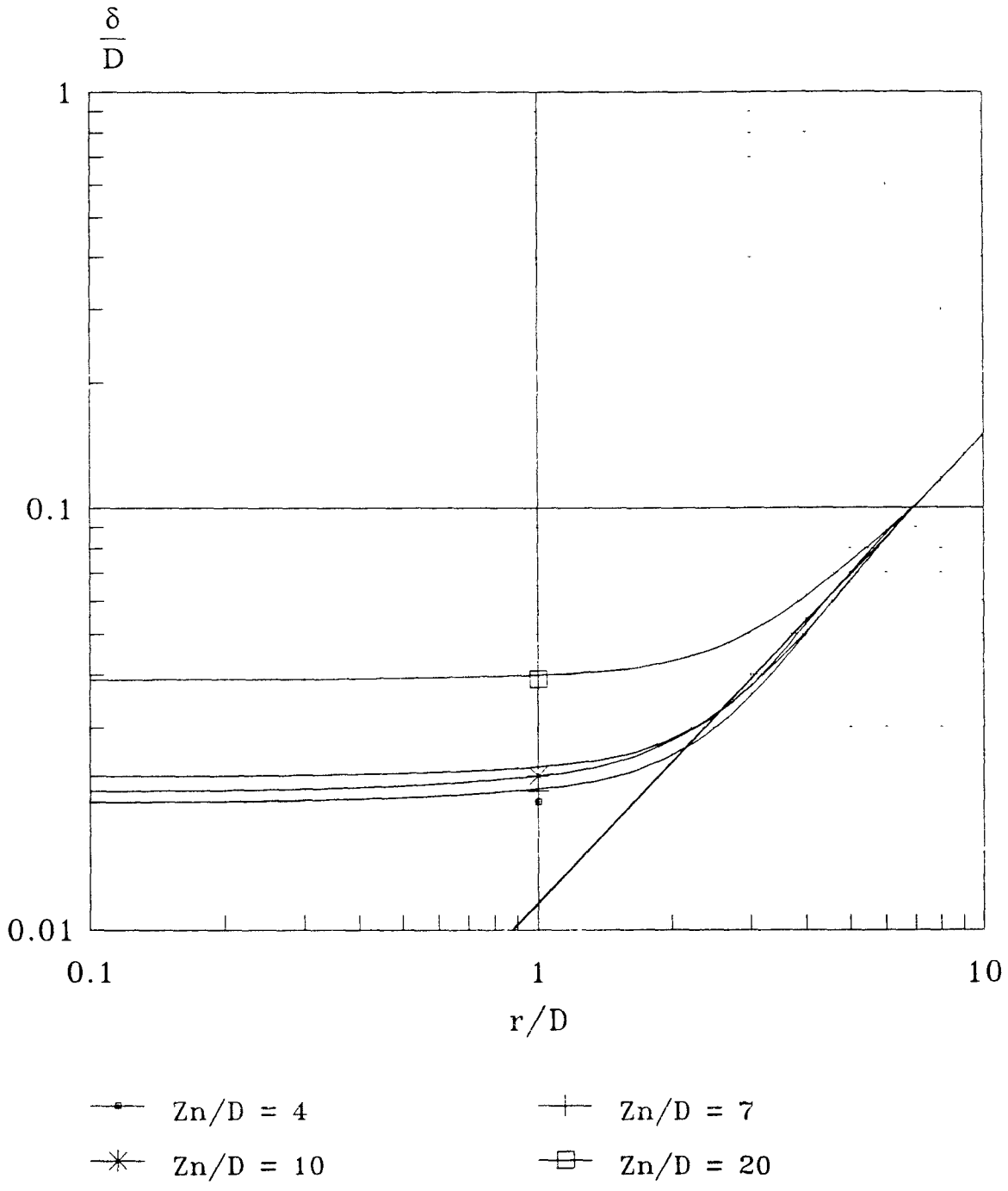

Figure 5-60 Boundary layer thickness

Re_d = 48,000, with varied Z_n / D, D = 0.5 in.

CHAPTER 6
CONCLUSIONS AND RECOMMENDATIONS

6.1 Conclusions

The characteristics of fluid flow resulting from impinging jets in all three zones (namely, Free jet zone, Deflection zone, and Wall jet zone) have been investigated thoroughly. It has been found that the dimensionless length of the potential core is a weak function of the Reynolds Number, in turbulent flow, and becomes a strong function of the Reynolds Number. According to our experimental results, the highest value of the theoretical dimensionless potential core length, C, is 6.40 and the lowest value is 6.08.

The dimensionless velocity profile of the wall jet is self similar except near the flat plate, although the deviation from a true similar profile is quite small. The velocity and pressure distributions in the free jet zone, deflection zone and wall jet zone have been studied. The Reynolds Number was found to have negligible effect on the growth of half- valued width of free jet and on the maximum velocity decay.

The boundary layer thickness at the stagnation point and some distance away from it in the wall jet region, was determined and found to be in a reasonably satisfactory agreement with the theoretical expression. Some results obtained in the present experiment were in close agreement with those produced by Lee [14] and other previous investigators. But some results, like "n" for the sandpaper surface, is opposite to the results obtained by previous investigators. Measurements at the stagnation point and determination of the boundary layer thickness near the stagnation point were carried out cursorily since the limitation of the experimental equipment on hand. The author suggests to use advanced

experimental instruments to repeat this kind of experiments and surely can get more information from the experiment to develop the theory more completely.

6.2 Recommendations

1. The present experimental result shows that the "theoretical dimensionless length of the potential core" C is a function of Reynolds Number and nozzle diameter. The author believes that the accurate effect of diameter D on the coefficient C can be found by using more nozzles of different sizes, such as 0.75 inch, 0.875 inch in diameter.

2. It seems better to use large diameter nozzle to repeat this experiment since the flow in a large diameter nozzle is more steady than it is in a smaller one that can result in easier and more accurate measurements and results of this experiment. It is so recommended to investigate the flow properties within the deflection zone.

3. Since in the present experiment, the Reynolds Number is limited in the range that is less than 10^5, it is more extensively to investigate the impinging jet in large Reynolds Number, such as 10^5 to 10^6.

4. Use more kinds of sand paper as the impinging target to measure the velocity profile, the boundary layer thickness and finally to get "n". Use larger plate to investigate the flow far from the stagnation point.

5. Use better and sensitive instruments that can help determine the accurate position of the measuring points to repeat this experiment, i. e., we can put the experimental frame (the plate) on a transversing carriage so that the plate

can be moved in all three dimensions smoothly. This will result in finding the stagnation point easily and more accurate.

REFERENCES

1. Abramovich, G. N., 1963. *The Theory of Turbulent Jets.* MIT Press, Cambridge, Mass.

2. Bakke, P., 1957. "An Experimental Investigation of a Wall Jet." *J. Fluid Mech., Vol. 12*: 467-472.

3. Basu, Saibal, 1983. "Experimental Investigation of an Axisymmeric Air Jet Imping on a Flat Plate" *Master Thesis, New Jersey Institute of Technology, Newark, New Jersey.*

4. Brady, W. G. and Ludwig, G., 1963. "Theoretical and Experimental Studies of Impinging Uniform Jets." *Journal of American Helicopter Society*: 8: 2: 1 - 13.

5. Clauser, F. H., 1954-2. "Turbulent Boundary Layers in Adverse Pressure Gradients." *Journal of Aeron. Science, Vol. 21*:91.

6. Dudek, J. A.., 1973. "A Calibration Procedure for Pressure Probes in Three-Dimensional Subsonic Flows." *ASME Publication*: 1-8.

7. Glauert, M. B., 1956. "The Wall Jet." *Journal of Fluid Mechanics, Vol. 1*: 625-643.

8. Goertler, H., 1942. "Berechung von Aufgaben der freien Turbulenz auf Grund eines neuen Naherungsansatzes." *ZAMM, Vol. 22*: 244-254.

9. Homann, F., 1936. "Der Einfluss grosser Zahigkeit bei der Stromung um den Zylinder und um die Kugel." *ZAMM*: 153-164.

10. Hrycak, Peter, 1968. "Heat Transfer from Impinging Jets." *A Literature Review, Prepared under Grant NGR-31-009-004, Newark College of Engineering*

11. Hrycak, Peter, "Heat Transfer from a Row of Impinging Jets to Concave Cylindrical Surfaces." *Int. Jl. of Heat and Mass Transfer, Vol. 24*: 407-419.

12. Hrycak, P., Lee, D. T., Gauntner, J. W. and Livingood, J. N. B., 1970. "Experimental Flow Characteristics of a Single Turbulent Jet Impinging on a Flat Plate." *NASA TND - 5690.*

13. Jachna, Stefan, 1978. "Axisymmetric Air Jet Impinging on a Hemispherical Concave Plate." *PhD Dissertation, New Jersey Institute of Technology, Newark, New Jersey.*

14. Lee, David T. H., 1969. "Experimental Investigation of Submerged Incompressible Turbulent Impinging Jets." *Master Thesis, Newark College of Engineering, Newark, New Jersey.*

15. Leister, Peter, 1977. "Experimental Investigation on the Turbulence Structure of an Impinging, Pulsating Jet" *Symposium on Turbulent Shear Flows, Vol. 1*:3.25-3.44.

16. Poreh, M., Tsuei, Y. G. and Cermak, J. E., 1959. "Flow Characteristics of a Circular Submerged Jet Impinging Normally on a Smooth Boundary." *Proc. 6th Midw. Conf. on Fluid Mech.*: 198.

17. Reichardt, H., 1942. "Gesetzmassigkeiten der freien Turbulenz." *VDI - Forschunsheft*: 414.

18. Schach, W., 1935. "Deflection of a Circular Fluid Jet by a Flat Plate Perpendicular to the Flow Direction." *Ing. Archiv, Vol. 6*: 51-59.

19. Schlichting, H., 1968. *Boundary Layer Theory.* 6th Edition, McGraw Hill Book Company, New York.

20. Snedeker, R. S. and Donaldson, C. du P., 1964. "Experiments on Free and Impinging Underexpanded Jets from a Convergent Nozzle." *Ad 461622.*

21. Strand, T., 1964. "On the Theory of Normal Ground Impingement of Axisymmetric Jets in Inviscid Incompressible Flow." *AIAA Paper 64-424.*

22. Tanaka, T. and Tanaka, E., 1977. "Experimental Studies of a Radial Turbulent Jet." *Bulletin of the JSME, Vol. 20, No. 140*: 209.

23. Tani, I. and Komatsu,Y., 1964. "Impingement of a Round Jet on a Flat Surface." *Proc. XI Intl. Cong. of Appl. Mech.*: 672-676.